NMR studies of carbon nanotubes and derivatives

Christophe Goze-Bac

ACADEMIE DE MONTPELLIER

UNIVERSITÉ MONTPELLIER SUD DE FRANCE

SCIENCES ET TECHNIQUES DU LANGUEDOC

Habilitation à diriger des recherches

présentée par

Christophe Goze-Bac

qui sera soutenue le 5 Décembre 2008

devant le jury composé de :

Launois Pascale	Université Paris-Sud, Orsay	Examinatrice
Massiot Dominique	CEMHTTI CNRS, Orléans	Examinateur
Mauri Francesco	Université Pierre Marie Curie, Paris	Rapporteur
Neveu André	Université Montpellier 2	Examinateur
Sundqvist Bertil	University of Umeå, Suéde	Rapporteur
Zanca Michel	CHU Gui de Chauliac & Université Montpellier 2	Président du Jury
Zettl Alex	University of Berkeley, CA USA	Rapporteur

Contents

Curriculum vitæ

Christophe Goze-Bac
Born : 06-06-1970
Perpignan, France
Married to Isabelle, one child Noé
CNRS Tenured Researcher
von Humboldt Fellow

Nationality French
2 rue du cormier des oiseaux
34660 Cournonterral
France
Phone : +33 467143479
goze@univ-montp2.fr

Education

- June 1988, High School Diploma in Physics-Biology, Lycée Arago Perpignan
- June 1990, Associate Degree in Physics-Mathematics, University Perpignan
- June 1992, Bachelor in Physics, University Montpellier 2
- June 1993, Master Degree in Theoretical Physics, University of Montpellier 2
- March 1996, PhD in Physics, Condensed Matter University of Montpellier 2

  Contribution to the study of fullerene : NMR and ESR investigations

Work experience

- April 1996 , Postdoctoral position, Alexander von Humboldt Fellow : Pr. Michael Mehring, University of Stuttgart, Germany

  Magnetic and electronic properties of intercalated C_{60} compounds

- July 1997, Postdoctoral position, EU Fellow, Pr. Angel Rubio, University of Valladolid, Spain *Mechanical properties of carbon nanotubes*
- November 1997, CNRS Tenured Researcher UMR5581, University of Montpellier 2
    1. *Electronic, magnetic and dynamical properties of carbon nanostructures*
    2. *NMR studies of confined liquid crystal*
- February 2004, Researcher at University of Berkeley, Californie USA. 6 months visiting Pr. Alex Zettl et Pr. Alex Pines : *High resolution NMR techniques applied to carbon nanostructures*
- Since September 2004, CNRS Tenured Researcher UMR5587, University of Montpellier 2
    1. *Electronic, magnetic and dynamical properties of carbon nanostructures*
    2. *Near field NMR and MRI applied to living sciences*

Research activities

- Since 1993, Synthesis of fullerene and nanotubes : isotopic engineering, purification, functionalization, intercalation, encapsulation ...
- Since 1993, Structural, electronic, magnetic and dynamical properties of fullerenes and derivatives : NMR and ESR studies
- Since 1997, Modelization of mechanical properties of carbon nanotubes
- Since 1998, Structural, electronic, magnetic and dynamical properties of carbon nanostructures : NMR studies vs temperature
- Since 1999, Confined liquid crystal : NMR studies
- Since 2007, Near field NMR and MRI developments. Application to living sciences: biology and agronomy

PhD supervising

1. Laetitia Vaccarini, PhD University Montpellier 2 (2000)
   Propriétés mécaniques des nanotubes de carbone
   co-direction with Patrick Bernier

2. Sylvain Latil, PhD University Montpellier 2 (2001)
   Magnétisme des nanotubes de carbone
   co-direction with Patrick Bernier

3. Carlos Fehr, PhD University Montpellier 2 (2002)
   Propriétés des cristaux liquides en géométrie confinée
   co-direction with Eric Anglaret

4. Michael Schmid, PhD University Stuttgart (2005)
   NMR investigations of intercalated carbon nanotubes
   co-direction with Pr. Michael Mehring

5. Edy Abou-Hamad Ater, PhD University Montpellier 2 (2008)
   Etude RMN des nanotubes de carbone et dérivés
   Supervisor : Christophe Goze-Bac

6. Chadi Massoud, PhD University Montpellier 2 (2010)
   Développements IRM pour l'étude de la filtration glomérulaire
   co-direction with Pr. Michel Zanca (CHU)

PhD Commitee

1. Sylvain Latil, PhD University Montpellier 2
   Magnétisme des nanotubes de carbone
   Supervisor : Patrick Bernier
   19 september 2001

2. Carlos Fehr, PhD University Montpellier 2

   Propriétés des cristaux liquides en géométrie confinée

   Supervisor : Eric Anglaret

   18 december 2002

3. Mayeul D'Avezac, PhD University Pierre Marie Curie, Paris

   Etude Ab initio des spectroscopies par résonance magnétique

   Supervisor : Pr. Francesco Mauri

   3 october 2005

4. Younghyun Kim, PhD University Philadelphia PA, USA

   Nuclear Magnetic Resonance studies of local magnetic, electronic and dynamic properties in filled single wall carbon nanotubes

   Supervisor : Pr. David Luzzi

   19 novembre 2007

5. Joëlle Beyrouthy, PhD University Pierre Marie Curie, Paris

   Réduction dimensionelle d'un modèle viscoélastique en grandes déformations. Analyse théorique et simulation numérique

   Supervisor : Pr. Hervé Le Dret

   26 september 2008

Post doctoral fellows

1. Juan Primera (Ater Polytech) : *Intercalation compounds of nanotubes with iodine* , June 2003

2. Thomas Wågberg (Uni Umeå): *NMR studies of fullerenes and nanotubes* , 2003-2005

3. Joëlle Beyrouthy (Ater University Montpellier 2 / Postdoc CNRS) : *Modelization of nanotubes as radio-frequency antenna*, 2008-2009

Graduate students

1. Jean Christian Colombier, *Etude par Résonance Magnétique Nucléaire des nanotubes de carbone intercalés au Rubidium*, stage de l'IUP Génie des Matériaux 2ème année, Faculté des Sciences et Techniques de St Jérôme, Académie d'Aix-Marseille, june-july 2002.

2. Sylvian Cadars, *Etude par Résonance Magnétique Nucléaire des nanotubes de carbone intercalés au Baryum*, stage de 3ème année de Magistère de l'Université Joseph Fourier de Grenoble, Mention Chimie, july 2003.

3. Samer Kourhy-Hanna, *Développements RMN en champ proche*, Master 1 Biologie Université Montpellier 2, march-july 2008

4. Mohmmed Halidi, *Développements électroniques de la RMN en champ proche transportable*, Master 2 Informatique Electronique Système, Ecole Doctorale I2S Université Montpellier 2, may-novembre 2009

Invited Professors / Researchers

- Pr. Angel Rubio, Univeristy San Sebastian, Spain : 1 month in 2006
  Magnetic interactions in carbon nanostructures, University Montpellier 2

- Dr. Luc Henrard, University Namur, Belgium : 2 months in 2007
  Intercalation compounds of nanotubes, University Montpellier 2

- Dr. Paul Stein, University Odense, Danemark : 1 year in 2008/2009
  Near field NMR and MRI, Région LR/CNRS

- Dr. Thomas Wågberg, University Umeå: 1 month 2009
  NMR on encapsulated molecules inside nanotubes, University Montpellier 2

Research Administration

- Elected at the Laboratory council UMR5581 1999-2003

- Member of the council of NMR facility users, University Montpellier 2 1999-2002
- Member of the council of the Physics department 2000-2004
- Responsible of the NMR facility users of the Physics department, since 2003
- Member of the council of the Department Mathématiques Informatique Physique Systèmes, University Montpellier 2, since 2007
- Elected at the board directors of the University of Montpellier 2, since 2008
- Head of the group "nanoNMRI" of the CNRS/UM2 laboratory LCVN UMR5587

Contracts Managing and Financial Supports

1. EU Contract FUNCARS, 2000-2003 (co-responsible) [25 000€]
   Fonctionalization of carbon nanotubes
2. Contrat Stryker Howmedica, 2006-2007 [25 000€]
   ESR studies of biocompatible materials
3. ACI NANO NACEP, 2004-2006 [47 000€]
   Electrochemical functionalization of carbon nanotubes
4. Molecular Foundry, Berkeley CA, USA, 2005-2007 [User Facility]
   Magnetic interactions in carbon nanostructures
5. Equipment Région Languedoc-Roussillon, 2006 [40 000€]
   NMR and MRI spectrometer
6. Invited Professor University Montpellier 2 [8 000€]
   Angel Rubio University San Sebastian Spain, 1 month in 2006/2007
7. Equipment CNRS, 2007 [50 000€]
   NMR and MRI spectrometer

8. Invited Professor University Montpellier 2 [16 000€]
   Luc Henrard University Namur Belgium, 2 months in 2007/2008

9. Equipment BQR University Montpellier 2, [10 000 €]
   NMR and MRI spectrometer

10. Project CNRS, 2008 [40 000 €]
    Near field NMR and MRI : applications to living sciences

11. Projet Agropolis RTRA, 2008 (co-responsible) [45 000 € + 3 years postdoc]
    INRA Avignon *Virtual fruit, NMR and MRI on plants*

12. Région Languedoc-Roussillon ARPE, 2008 [30 000 €]
    Near field NMR and MRI : applications to living sciences

13. Financial support CIFRE Siemens Medical (co-responsible) [86 400€]
    salary Chadi Massoud, 2007-2010 CHU Gui de Chauliac et Lapeyronie *New MRI techniques*

14. Invited Reseacher CNRS [37 200€]
    Paul Stein University Odense Danmark, 6 months in 2008/2009

15. ATER University Montpellier 2 [52 800€]
    salaries Edy Abou-Hamad and Joëlle Beyrouthy 2008-2009

16. Invited Professor University Montpellier 2 [8 000€]
    Thomas Wågberg Univerity Umeå, 1 month in 2009

Patent

Nanotubes for optical limiting, n° 98 15820

Conference organizing commitee

- Physique en herbe, Montpellier, University Montpellier 2 1994

- ICSM'98, Corum Montpellier
- FUNCARS, final meeting 20-21 march 2003, CNRS Montpellier
- NT'08, Corum Montpellier

Teaching

- Polytech Montpellier

  School of Engineering FQSC

  Physics : *Interaction Onde/Matière (15h)*

  Promotion : 2002/2005, 2003/2006, 2004/2007 et 2005/2008

- Polytech Montpellier

  School of Engineering FQSC

  Physics : *Structures et Vibrations (15h)*

  Promotion : 2004/2007, 2005/2008, 2006/2009 et 2007/2010

- University Montpellier 2

  Master Nanostructures

  RMN du solide dans les nanomatériaux (4h)

  Promotion : 2005, 2006, 2007 et 2008

Science fair

- Fête de la Science et Village des Sciences : 2005, 2006 et 2007

  Les nanotechnologies et les nanotubes, stand en centre-ville de Montpellier

  Article dans le Midi-Libre, 10-11 october 2007

- Caravanes de la science en Lozère *Atelier Nanotubes* : october 2005

- Exposition Sciences : july 2005

  Atelier nanotubes, Palais des Congrès de Perpignan

- Présentation des "nanotubes de carbone" à l'Association des Professeurs de Physique et de Chimie, Section académique de Montpellier, 7 june 2006

- Interventions dans les Collèges et Lycées de l'agglomération de Montpellier, Année Mondiale de la Physique 2005, 2006, 2007 et 2008 : $\approx$ 30 presentations

- Portes Ouvertes Université Montpellier 2, april 2007 and 2008

- Accueil niveau collège, dans le laboratoire pour stage d'une semaine (2008)
  Synthèse de nanotube de carbone multi feuillets

Publications and Communications

International Journals

1. High Resolution 13C NMR in alkali intercalated C_{60}, F. Rachdi, I. Lukyanchuk, J. Reichenbach, C. Goze et al. Physica C 235 767 (1994)

2. F. Rachdi, C. Goze, C. Reichenbach et al., Alkali intercalated C_{60} : NMR and magnetic susceptibility studies, Acta Polonica A 87 861 (1995)

3. I. Lukyanchuk, N. Kirova, F. Rachdi, C. Goze, P. Molinié M. Mehring, Electronic localization in Rb_4C_{60} from bulk magnetic measurements, Phys. Rev. B, 51, 3978-3980 (1995).

4. M. Apostol, C. Goze, F. Rachdi et M. Mehring, Off-center sites in doped alkali fullerides, Solid State Commun., 96, 253-257 (1995).

5. Zimmer, C. Goze, M. Mehring F. Rachdi, Rotational dynamics of C_{60} and activated electronic processes in Rb_4C_{60}, Phys. Rev. B, 52, 13300-13305 (1995).

6. C. Goze, M. Apostol, F. Rachdi et M. Mehring, Off-center sites some lightly-doped alkali fullerides, Phys. Rev. B, 52, 15031-15034 (1995).

7. R. Kerkoud, P. Auban-Senzier, D. Jérome, S. Brazovskii, I. Lukyanchuk, N. Kirova, F. Rachdi C. Goze, Insulator-metal transion in Rb_4C_{60} under pressure from ^{13}C NMR, J. Phys. Chem. Solids, 5 7, 143-152 (1996).

8. C. Goze, F. Rachdi, M. Mehring, High Resolution ^{13}C NMR in Cs_4C_{60}, Phys. Rev. B, 54, 5164(1996).

9. T. Yildirim, L. Barbedette, J. E. Fischer, G. Bendele, P. W. Stephens, C. L. Lin, C. Goze, F. Rachdi, J. Robert, P. Petit et T. T. M. Palstra, Synthesis and properties of Mixed Alkali-Alkaline Earth Fullerides, Phys. Rev. B, 54, 11981 (1996).

10. F. Rachdi, L. Hajji, C. Goze, D. J. Jones, P. Maireless-Torres, J. Rozière, J. M. Jan et P. Seta, Quantum size effects induced by confinement of C_{60} in MCM41, Solid State Commun., 100, 237-240 (1996).

11. D. Bormann, J. L. Sauvajol, C. Goze, F. Rachdi, A. Moreac, A. Girard, L. Forro et O. Chauvet, Raman Study of the polymerized state of the RbC_{60} and CsC_{60} Phys. Rev. B, 54, 14139-14145 (1996).

12. C. Goze, F. Rachdi, L. Hajji, M. Nunez-Regueiro, L. Marques, J.-L. Hodeau M. Mehring, High-Resolution ^{13}C NMR of high-pressure-polymerized C_{60} : Evidence for the [2+2] cycloaddion structure in the rhombohedral two-dimensional C_{60} polymer, Phys. Rev. B, 54, R3676-R3678 (1996).

13. .L. Hajji, F. Rachdi, C. Goze, M. Mehring J. E. Fischer High Resolution ^{13}C NMR investigations A_6C_{60} (A=Cs, Rb, Cs) and Ba_3C_{60} , Solid State Commun., 100, 493 (1996).

14. F. Rachdi, C. Goze, L. Hajji, K. F. Thier, G. Zimmer, M. Mehring, M. Nunez-Regueiro, L. Marques et J.-L. Hodeau High Resolution ^{13}C NMR studies of One and Two Dimensional Polymerized C_{60} , Appl. Phys. A, 64, 295 (1997).

15. E.Hernandez, C.Goze, P.Bernier et A.Rubio Elastic properties of C and $B_xC_yN_z$ composite nanotubes Phys. Rev. Lett. 80, 4502-5 (1998)

16. F.Rachdi, L.Hajji, H.Dollt, M.Ribet, T.Yildirim, J.E.Fischer, C.Goze, M.Mehring, A.Hirsch, B.Nuber NMR investigation of the azafullerene $(C_{59}N)_2$ and the alk fullerides Na_xC_{60} with x = 2, 4 and 6 Carbon, 36, 607 (1998)

17. L.Vivien, E.Anglaret, D.Riehl, F.Bacou, C.Journet, C.Goze, M.Andrieux, M.Brunet, F.Lafonta, P.Bernier et F.Hache Single wall carbon nanotubes for optical limiting Chem. Phys. Lette. 307, 317 (1999) and Erratum, ibid 312, 617 (1999)

18. E.Hernandez, C.Goze, P.Bernier et A.Rubio Elastic properties of single wall nanotubes Applied Physics A, 68, 287-292 (1999)

19. K.Thier, C.Goze, M.Mehring, F.Rachdi, T.Yildirim et J.E.Fischer Metallic properties of ternary fulleride ABa_2C_{60} Phys. Rev. B, Condens. Matter Mater. Phys., vol. 59, 16, pp. 10536-10540 (1999)

20. L.Vaccarini, C.Goze, R.Aznar, V.Micholet, C.Journet, P.Bernier, K.Metenier, F.Beguin, J.Gavillet, A.Loiseau Production and Purification des nanotubes de carbone monofeuillets C.R. Acad. Sci. Paris 327 (1999) 925-31

21. J.L. Sauvajol, E. Anglaret, S. Rols, C. Journet, C. Goze et P. Bernier, W.K. Maser, E. Munoz, A.M. Benito, M.T. Martinez, G. Coddens, A.J. Dianoux, Structure and vibrational properties of single wall carbon nanotubes, Synthetic Metals, 103, 2536 (1999).

22. C. Goze, L. Vaccarini, L. Henrard, P. Bernier, E. Hernandez and A. Rubio, Elastic and mechanical properties of carbon nanotubes, Synthetic Metals, 103, 2500 (1999).

23. L.Vivien, E.Anglaret, D.Riehl, F.Hache, F.Bacou, M.Andrieux, F.Lafonta, C.Journet, C.Goze, M.Brunet, P.Bernier Optical limiting properties of singlewall carbon nanotubes Optics Communications, vol. 174, n¡ 1-4, pp. 271-275 (2000)

24. L. Vaccarini, C. Goze, L. Henrard, E. Hernandez, P. Bernier et A. Rubio, Mechanical and electronic properties of carbon and boron-nitride nanotubes, Carbon 38, 1681 (2000)

25. C. Goze-Bac, S. Latil, L. Vaccarini, P. Bernier, P. Gaveau, S. Tahir, V. Micholet, R. Aznar, A. Rubio, K. Metenier et F. Beguin, ^{13}C NMR evidence for dynamics of nanotubes in ropes, Phys. Rev. B 63, 100302 (2001)

26. C. Goze-Bac, R. Paredes, C. Vásquez, E. Medina, and A. Hasmy, Three-dimensional rotational Langevin dynamics and the Lebwohl-Lasher model Phys. Rev. E 63, 042701 (2001)

27. S. Latil, L. Henrard, C. Goze-Bac, P. Bernier et A. Rubio, ^{13}C NMR Chemical Shift of Single-Wall Carbon Nanotubes,Phys. Rev. Lett. , 86, 3160 (2001)

28. S. Fiorito, C. Goze-Bac, J. Adrey, L. Magrini, D. Goalard et P. Bernier, Free radicals increase on UHMWPE Hip prostheses components due to inflamed synovial cells products, Journal of biomedical materials research 57 35 (2001)

29. C. Goze-Bac, P. Bernier, S. Latil, V. Jourdain, A. Rubio, SH. Jhang, Y. Park, M. Holzinger, A. Hirsch ^{13}C investigations of carbon nanotubes and derivatives, Current Applied Physics, 1, 149 (2001)

30. C. Goze-Bac, S. Latil, P. Lauginie, V. Jourdain, J. Conard, L. Duclaux, A. Rubio et P. Bernier, Magnetic interactions in carbon nanotubes, Carbon 40 1825-1852 (2002)

31. L. Duclaux, J. Salvetat, P. Lauginie, T. Cacciaguera, A. Faugère, C. Goze-Bac et P. Bernier, Synthesis and characterization of SWNT heavy alkali metal intercalation coupounds, J. Phys. Chem. of Solids, 64 571 (2003)

32. M. Schmid , S. Kramer, C. Goze-Bac, M. Mehring, S. Roth et P. Bernier, NMR investigations of hydrogen in carbon nanotubes, Synthetic Metals 135 727 (2003)

33. M. Schmid, C. Goze-Bac, S. Kramer, M. Mehring, P. Petit and C. Mathis, Metallic properties of Li-intercalated carbon nanotubes, Phys. Rev. B 74 073416 (2006)

34. C. Fehr, C. Goze-Bac, E. Anglaret, C. Benoit et A. Hasmy, Orientational order and dynamics of a nematic liquid crystal in porous media Europhys. Lett., 73, 553-559 (2006)

35. J. Steinmetz, S. Kwon, H.J. Lee, E. Abou-Hamad, R. Almairac, C. Goze-Bac H. Kim, YW. Park Polymerization of conducting polymers inside carbon nanotubes,

Chemical Physics Letters, 431, 139-144 (2006)

36. J. Steimetz, H.J. Lee, S. Kwon, D.S. Lee, C. Goze-Bac, E. Abou-Hamad, H. Kim, Y.W. Park, Routes to the synthesis of carbon nanotube-polyacetylene composites by Ziegler-Natta polymerization of acetylene inside carbon nanotubes, Current Applied Physics, 7, 39-41, (2007)

37. Y. Kim, O. Torrens, J. Kikkawa, E. Abou-Hamad, C. Goze-Bac et D. Luzzi High-purity diamagnetic single-wall carbon nanotube buckypaper, Chemistry of materials. 19, 2982 (2007)

38. B. Jousselme, G. Bidan, M. Billon, C. Goyer, Y. Kervella, S. Guillerez, E. Abou Hamad, C. Goze-Bac, J-Y. Mevellec, S. Lefrant, One-step electrochemical modification of carbon nanotubes by ruthenium complexes via new diazonium salts, Journal of Electroanalytical Chemistry, Volume 621, Issue 2, 15 (2008)

Chapter in Books

1. S. Latil, J.C. Charlier, A. Rubio and C. Goze-Bac, Application of the electronic properties of carbon nanotubes : computation of the magnetic properties and the ^{13}C NMR shifts, Frontiers of Multifunctional Integrated Nanosystems E. Buzneva & P. Schraff, Berlin (2004).

2. C. Goze-Bac, Chapter : Introduction to carbon nanotubes, Carbon nanotubes : Angel or Daemons ? by S. Fiorito, World Scientific (2008)

Proceedings of international conferences

1. F. Rachdi, L. Hajji, T. Yildirim, J.E. Fischer, C. Goze. M. Mehring, NMR studies of sodium fullerides, Wolrd Scientific 270 (1998)

2. E. Hernandez, C. Goze et A. Rubio, Tight Binding calculations of elastic properties of single wall nanotubes, World Scientific IWEPNM98 (1998)

3. C. Goze, K.F. Thier, M. Mehring, F. Rachdi, T. Yildirim et J.E. Fischer, Metallic Behavior of ABa_2C_{60} (A=K,Rb,Cs) compounds, World Scientific IWEPNM98 266 (1998)

4. L.Vaccarini, C.Goze, R.Aznar, V.Micholet et P.Bernier Purification procedure of carbon nanotube ICSM98, Synthetic Metals, vol 103, 1-3, pp. 2492-2493 (1999)

5. C.Goze, L.Vacarrini, P.Bernier, E.Hernandez et A.Rubio Elastic and mechanical properties of nanotubes ICSM98, Synthetic Metals, vol. 103, 1-3, pp. 2500-2501 (1999)

6. L. Vaccarini, G. Désarmot, R. Almairac, S. Tahir, C. Goze et P. Bernier, Reinforcement of an Epoxy resin by single wall nanotubes, AIP 544, IWEPN Kirchberg, 521 (2000)

7. C. Goze-Bac, M. Holzinger, V. Jourdain, S. Latil, R. Aznar, P. Bernier et A. Hirsch, ^{13}C NMR study of functionalized nanotubes, AIP MRS Boston A11.2 (2000)

8. S. Latil, C. Goze-Bac, P. Bernier, L. Henrard et A. Rubio, NMR chemical shift of single wall carbon nanotubes, AIP MRS Boston A14.13 (2000)

9. C. Fehr, P. Dieudonne, C. Goze-Bac, P. Gaveau, JL. Sauvajol, E. Anglaret, Spectroscopic studies of liquid crystals confined in sol-gel matrices, AIP MRS Boston (2000)

10. M. Schmid, C. Goze-Bac, S. Kramer, M. Mehring, S. Roth et P. Bernier, NMR investigations of hydrogen in carbon nanotubes, AIP conference proceedings 633 (2002) M. Schmid, C. Goze-Bac, M. Mehring, S. Roth et P. Bernier ^{13}C NMR investigations of the metallic state of Li intercalated carbon nanotubes Electronic Properties of Novel Materials: XVIIth International Winterschool, Ed. H. Kuzmany, J. Fink, M. Mehring and S. Roth, World Scientific, 131 (2003)

11. T. Wågberg, C. Goze-Bac, R. Röding, B. Sundqvist, D. Johnels, H. Kataura, and P. Bernier ^{13}C NMR on intercalated 2D-polymerised C_{60} and modified peapod Electronic Properties of Novel Materials: XVIIth International Winterschool, Ed. H. Kuzmany, J. Fink, M. Mehring and S. Roth, World Scientific, 723, 238 (2004)

12. M. Schmid, C. Goze-Bac, M. Mehring, S. Roth, P. Bernier ^{13}C NMR studies of intercalated carbon nanotubes, Electronic Properties of Novel Materials: XVIIth International Winterschool, Ed. H. Kuzmany, J. Fink, M. Mehring and S. Roth, World Scientific, 723, 181 (2004)

13. M. Schmid, C. Goze-Bac, M. Mehring and S. Roth 7Li NMR on Li intercalated carbon nanotubes, AIP conference proceedings 786 202 (2005)

Invited speaker to international conferences

1. C. Goze, "^{13}C NMR investigations of carbon nanotubes", Kirchberg: XIIIth IWEPNM99, march 1999.

2. C. Goze-Bac, "NMR investigations of functionalized carbon nanotubes", Materials Research Society fall meeting, Boston USA, november 2000

3. C. Goze-Bac, "NMR studies of carbon nanotubes and some of their derivatives" IWEPN2001, Kirchberg meeting, Austria, march 2001

4. C. Goze-Bac, "Nuclear Magnetic Resonance on materials based on carbon nanotubes", International Winterschool Euroconference on Electronic Properties of Novel Materials, Kirchberg Austria, march 9 2003

5. C. Goze-Bac, "Nuclear Magnetic Resonance investigations of carbon nanotubes based materials", Materials Research Society spring meeeting, San Francisco USA, april 22 2003

Oral contributions

1. C. Goze, NMR investigations of alkali intercalated C_{60}, Physique en herbe 94, Montpellier, july 1994.

2. C. Goze, Résonance Magnétique Nucléaire des composés du C_{60} insérés aux métaux alcalins, Groupe de Dynamique de Recherche GDR1019, Chemiry and Biochemistry of fullerene, Ecole Normale Supérieure, Paris, december 1994.

3. C. Goze, Etude RMN des composés du insérés aux métaux alcalins, Journées RMN du solide de Montpellier, february 1995

4. C. Goze, NMR studies of alkali fullerides, European Materials Research Society, Sumposium K, Strasbourg, may 1995.

5. C. Goze, Rapport final d'activité Groupe de Dynamique de Recherche GDR1019, Composés de la famille du C_{60} Intercalation du C_{60} : structures et propriétés électroniques, CNRS Campus Michel-Ange, Paris, september 1995.

6. C. Goze, Production, purification et propriétés des nanotubes monofeuillets : un bilan", GDR nanotube, Onera, january 1999.

7. C. Goze, "NMR investigations of carbon nanotubes and some derivatives", Fullerene'99, Workshop on nanotubes and fullerene chemistry, Bonas, september 1999.

8. C. Goze, Etude RMN des nanotubes de carbone GDR Nanotube, Strasbourg december 1999.

9. C. Goze-Bac, NMR in carbon nanostructures, Funcars meeting, Erlangen october 2000

10. C. Goze-Bac, Functionalized carbon nanotubes, Funcars meeting, Montpellier october 2001

11. C. Goze-Bac, Etude RMN des nanotubes de carbone, Comité d'évaluation de l'UMR5581, 6 march 2002, Montpellier

12. C. Goze-Bac, Résonance Magnétique Nucléaire, séminaire du GDPC, 28 march 2002, Montpellier

13. C. Goze-Bac, NMR and Raman investigations of carbon nanotubes, European Network Funcars, University of Friburg, 29 june 2002, Friburg

14. C. Goze-Bac, Synthèses et propriétés des nanotubes de carbone, European Network Cardecom, 30 september 2002, CRIF Belgique

15. C. Goze-Bac, Nanotubes de carbone et dérivés : étude RMN, GDR Nanotube, 15 october 2002, La grande Motte ù

16. C. Goze-Bac, NMR investigations of carbon nanotubes based materials, University of Carlifornia at Berkeley, Pr. Alex Pines, 25 april 2003, Berkeley USA

17. C. Goze-Bac, HRNMR MAT of carbon nanotubes, University of Carlifornia at Berkeley, groupe Pr. Alex Pines, july 2004, Berkeley USA

18. C. Goze-Bac, NMR on carbon based materials, University of Carlifornia at Berkeley, Pr. Alex Zettl, july 2004, Berkeley USA

19. C. Goze-Bac, Propriétés électroniques et magnétiques des nanotubes et dérivés, réunion RMN du Grand Bassin Parisien, 21 january 2005, Paris

20. C. Goze-Bac, Magnetic Interaction in carbon nanotubes based materials, 18 february 2005, Physics Department, University Umea, Sweden

21. C. Goze-Bac, NMR investigations of functionalized carbon nanotubes, workshop NACEP, 2006, Nantes

22. C. Goze-Bac, NMR investigations of carbon nanotubes salts, workshop TRICOTRA 2007, Montpellier

23. C. Goze-Bac, NMR and carbon nanotubes : 9 years later , seminar UMR5587, 2008, Montpellier

Chapter 1

Introduction to carbon nanotubes

Brief history of the nanotubes

The experiments on the synthesis of new carbon clusters during the mid-1980 by Harry Kroto and Richard Smalley are the prelude to the story of nanotubes. From the vaporization of graphite and its expected condensation in carbon clusters of different sizes, particular structures containing precisely 60 and 70 carbons appear to be much more stable. These unexpected results brought into the spotlight the now famous C_{60} and its closed shell similar to a soccer ball, as presented in Figure 1.1. The family of the fullerene is discovered and published in Nature in 1985[1]. Five years later, the success in the synthesis of C_{60} in bulk quantity by Wolfgang Kratschmer and Donald Huffman [2] gave to the community, the opportunity to study the properties of this new form of carbon. During 15 years an impressive number of publications and extraordinary results appeared on the bucky ball and its derivatives.[3, 4]

During this time in the early-1990, Sumio Iijima was investigating by electron microscopy technique the carbon soot and deposit produced by a Kratschmer-Huffman's machine. From his findings, he concluded to the existence of novel graphitic structures, another new form of carbon similar to tiny tubules of graphite presumably closed at each ends[5]. The Figure 1.2 shows a high resolution transmission microscopy image of one multiwalled carbon nanotubes produced by the electric arc method very similar to the hollow carbon

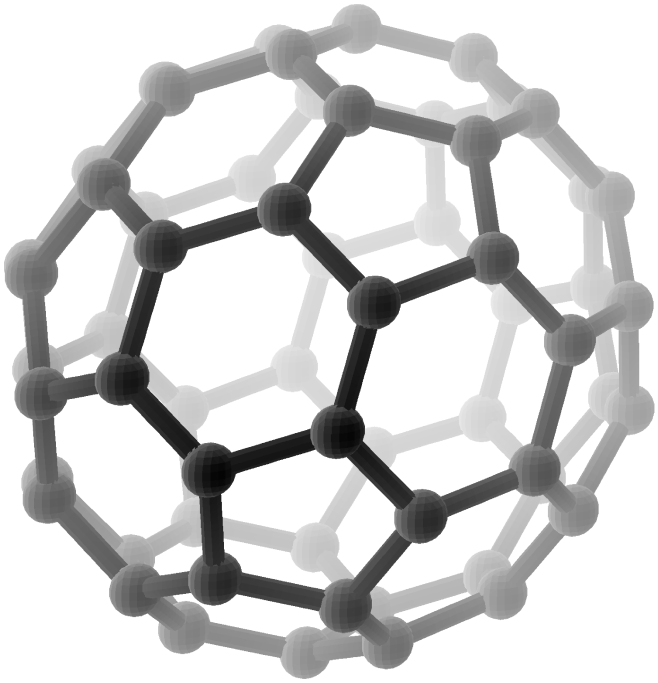

Figure 1.1: The C_{60} molecule : the bucky ball

cylinders observed in 1991. From historical point of view, if the anterior existence of nanotubes is well established[6, 7, 8], S. Iijima's work pointed out the exceptional properties and potential applications of these nanostructures. An important step was accomplished in 1992, by improving the method of synthesis and the capacity of production with gram quantities[9]. In 1993, another key point is the successful synthesis of single walled carbon nanotubes which appeared to be the ideal nanotubes with a very single layer[10, 11, 12]. Diameter appeared to be amazingly small compared to multi walled carbon nanotubes, as it can be seen between Figures 1.2 and 1.3. In 1997, high yields of single walled nanotubes were achieved by electric arc techniques with the help of optimized conditions[13]. This definitely extends the possibilities of investigations of single and multi walled carbon nanotubes.

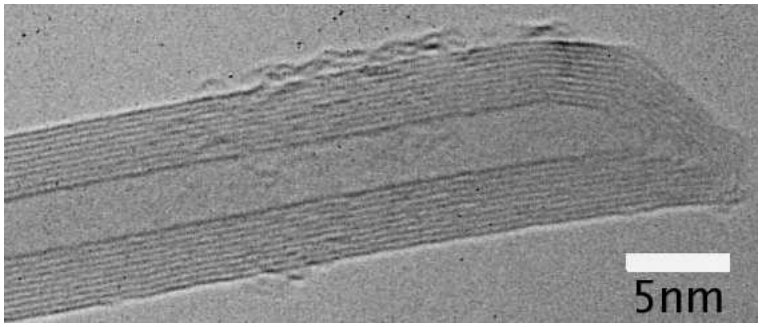

Figure 1.2: High resolution transmission microscopy of MWNT produced by the electric arc method

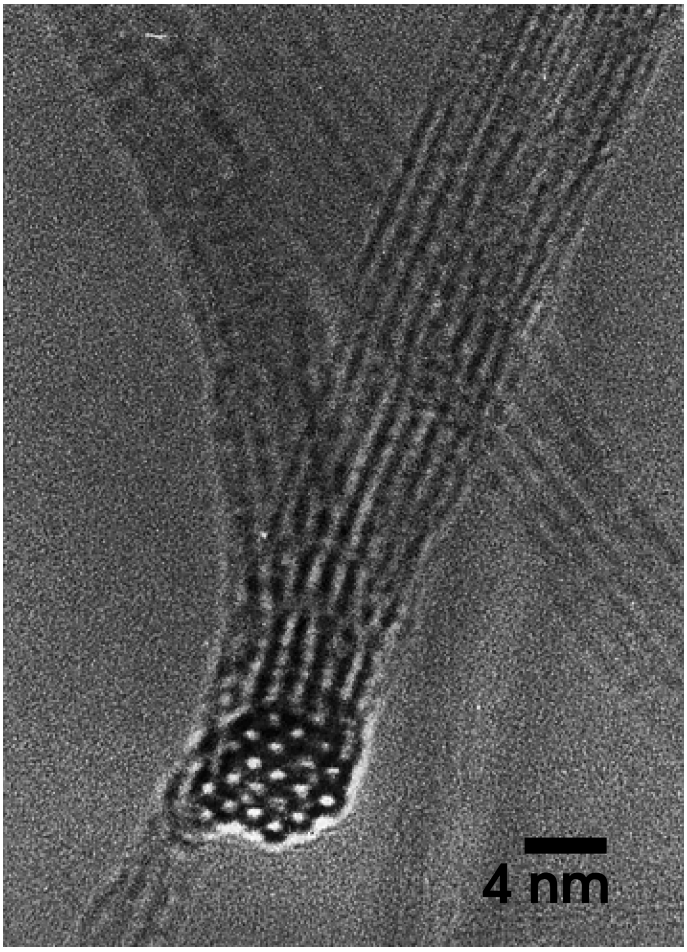

Figure 1.3: High resolution transmission microscopy image of one bundle of single walled nanotubes[13].

Size and shape of nanotubes

Downsized 10.000 times a human air, you will get the size and shape of a typical nanotube.

These molecules are few nanometers in diameter and several microns in length. Single

carbon nanotubes come often as tightly bundles of single walled nanotubes entangled as curly locks, see Figure 1.4. The packing of the nanotubes inside a bundle is more or less triangular with an intertube distance about 3.14Å[14, 15], as shown in Figure 1.3. Here, the bundle is about 20 nanotubes but can be made of hundreds of individuals. This assembly of nanotubes is stabilized by van der Waals interactions. If the distribution of nanotube diameters is quite narrow within a bundle, it has been shown that the arrangement of the carbon atoms is diverse[16, 17].

In the case of multiwalled nanotubes, at least two concentric nanotubes of different diameters are encapsulated like Matrioschka Russian doll[5]. Their lengths are from hundreds of nanometers to tens of micrometers, with diameter of few to hundreds of nanometers.

Synthesis of nanotubes

A wide variety of processes is now available to produce carbon nanotubes. They can be classified, first into high temperature methods like the electric arc[2, 5, 9, 13], laser ablation[12] and solar beam [18] based on the sublimation of a graphitic rod in inert atmosphere and second into process working at moderate temperature like the catalytic chemical vapor deposition which produces nanotubes from the pyrolysis of hydrocarbons[19, 20]. Originally, the electric arc discharge setup developed by Kratschmer-Huffamn was invented for fullerene production. Such electric arc chamber is presented in Figure 1.4 a). In a helium or argon atmosphere a DC current (100Amps 27 Volts) is applied through two high purity graphite electrodes. In these conditions, the temperature can reach 6000K which is high enough to sublimate continuously the graphite from the rod of the anode. At the cathode where the temperature is lower, a deposit and soot are produced. Fullerene like C_{60} and C_{70} are generally found in large quantities in the soot whereas nanotubes are present in the deposit and its vicinity. Later, this apparatus was successfully used by different groups to grow in a very simple and cheap way single walled nanotubes with the help of suitable catalyst like Ni, Co, Pt, Rh, Fe ... incorporated inside the anode[13]. In addition, it was rapidly shown that the characteristics of the nanotubes could be eas-

ily change by playing with the current, the pressure, the nature of the catalyst. This finding was a breakthrough and allowed the community to investigate the properties of carbon nanotubes to a very large extend. The picture of the electric chamber open in air presented in Figure 1.4 a), is taken after running one synthesis. The reactor contains a lot of black soot, carbon filaments and the deposit. The material to be collected which contains a high density of carbon nanotubes is in the central part of the collaret and looks like webs. High temperature routes are known to produce high quality materials which mean higher graphitization of the nanotubes. They can be used also to produce large quantities of single walled carbon nanotubes. The as-produced nanotubes are presented at different magnifications in Figure 1.4 b), c) and d) using Scanning electron microscopy images. The inset shows a high resolution transmission electron microscopy image of one bundle containing about 20 single walled nanotubes. We turn now to the Chemical

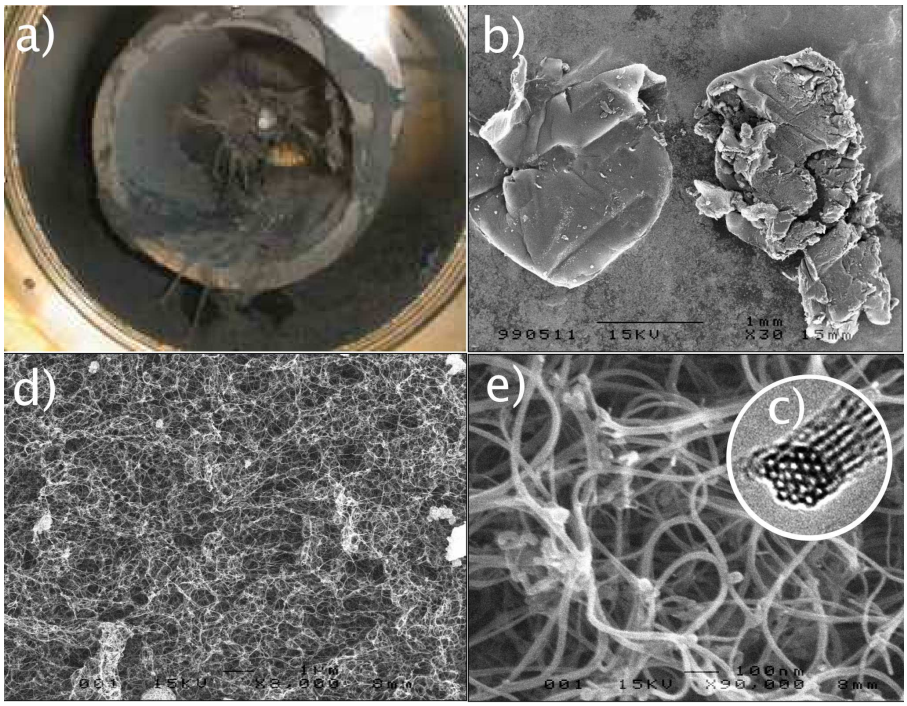

Figure 1.4: a) Open in air electric arc discharge reactor used to produce carbon nanotubes and fullerenes in Montpellier, France. Scanning electron microscographs of as-produced b) millimetric grains collected from the central part of the collaret around the deposit. Entangled network of bundles of single walled carbon nanotubes at higher magnification d) $\times$8000 and e) $\times$90000. The inset c) presents a high resolution transmission micrograph of one bundle.

Catalytic Vapor Desposition method. This process was originally developed in order to

decompose hydrocarbons e.g. methane, acetylene, methane etc over catalysts e.g. Ni, Co, Fe, Pt[19, 20]. This technique allows to grow nanotube at predefined locations on substrates where nanosized metal particles are deposited. Typical transmission electron micrograph of MWNT is shown in Figure 1.5.

To finish, one has to mention that if some methods of production are now well estab-

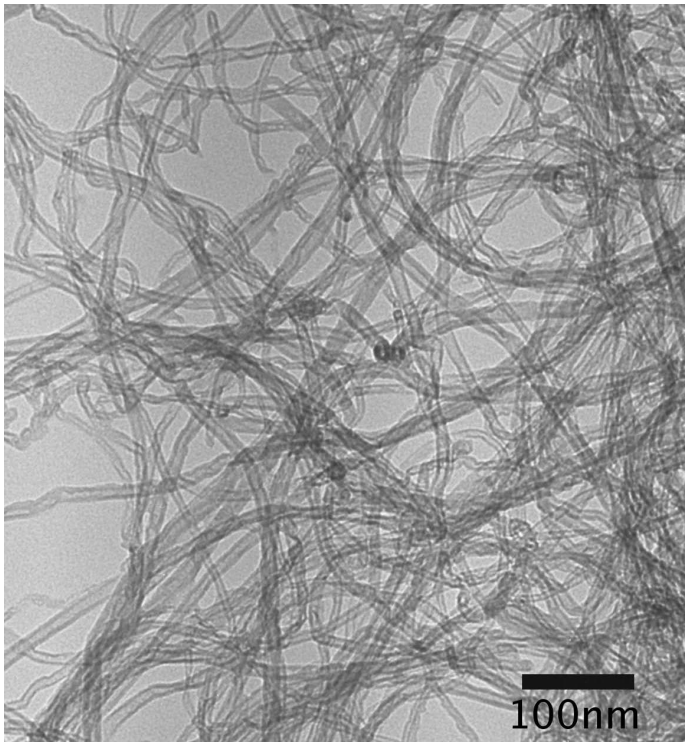

Figure 1.5: Transmission electron microscopy images of MWNT grown by catalytic chemical vapor deposition methods.

lished, nanotubes are still not prepared in pure form. For example, single walled carbon nanotubes samples are contaminated by graphitic structures, amorphous carbon and magnetic particles used as catalyst. In order to study the intrinsic properties of the nanotube, more or less sophisticated strategies of purification have been developed [21, 22]. Only with the help of magnetic fields[23] used to trap magnetic impurities, highly purified bulk samples have been obtained which offer the opportunity to use magnetic resonance spectroscopy[23, 24].

Molecular Structures of nanotubes

At a first glance, the molecular structures of carbon nanotube can be seen as single or multiple graphitic layers rolled to form a tubule. In the case of single walled nanotube, one atom thick layer is bended and welded as presented in Figure 1.6. Hence like in the

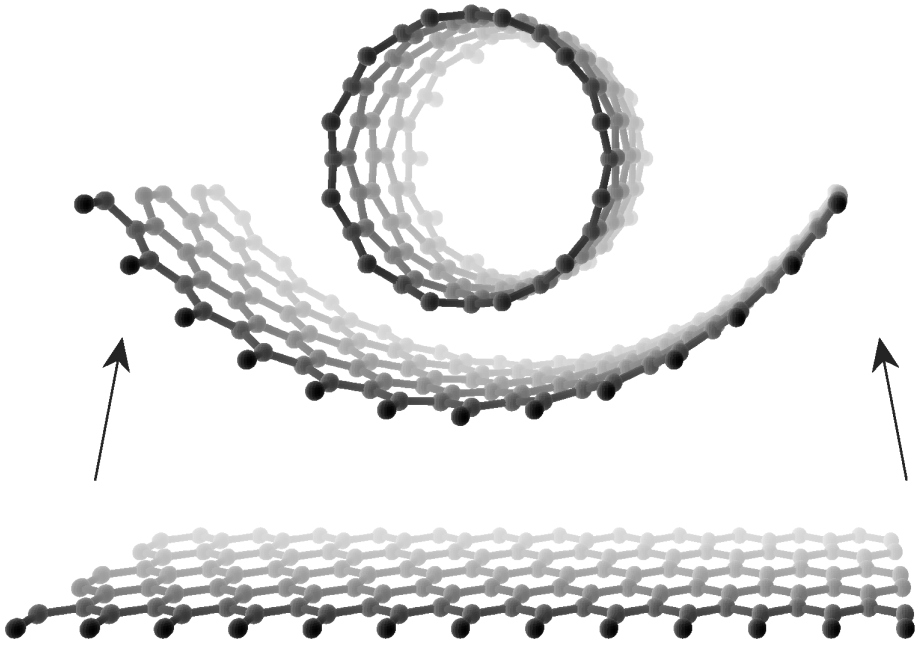

Figure 1.6: Bending a one carbon atom thick graphitic layer in order to form a (12,0) carbon nanotube.

graphite, the bonding between carbon atoms involves three neighbors and their hybridization are expected to be sp^2 like with a small s character because of the curvature. If this scenario is attractive and apparently simple, the way to form a nanotube is not unique and presents interesting features. Hence, it is challenging to classify these nanostructures and to guess their properties. The high symmetry structures of nanotubes are generally divided in three types : armchair, zigzag and chiral as illustrated in Figures 1.7,1.8 and 1.9, respectively. These labels come from the distribution of the bonds along the perimeter of the nanotube describing zigzag or an armchair. The chiral family presents forms of lower symmetries with hexagons arranged helically along the axis of the tube. Note that these three nanotubes have very similar radius $R \approx 6.6 \pm 0.4$Å. Theoretical mod-

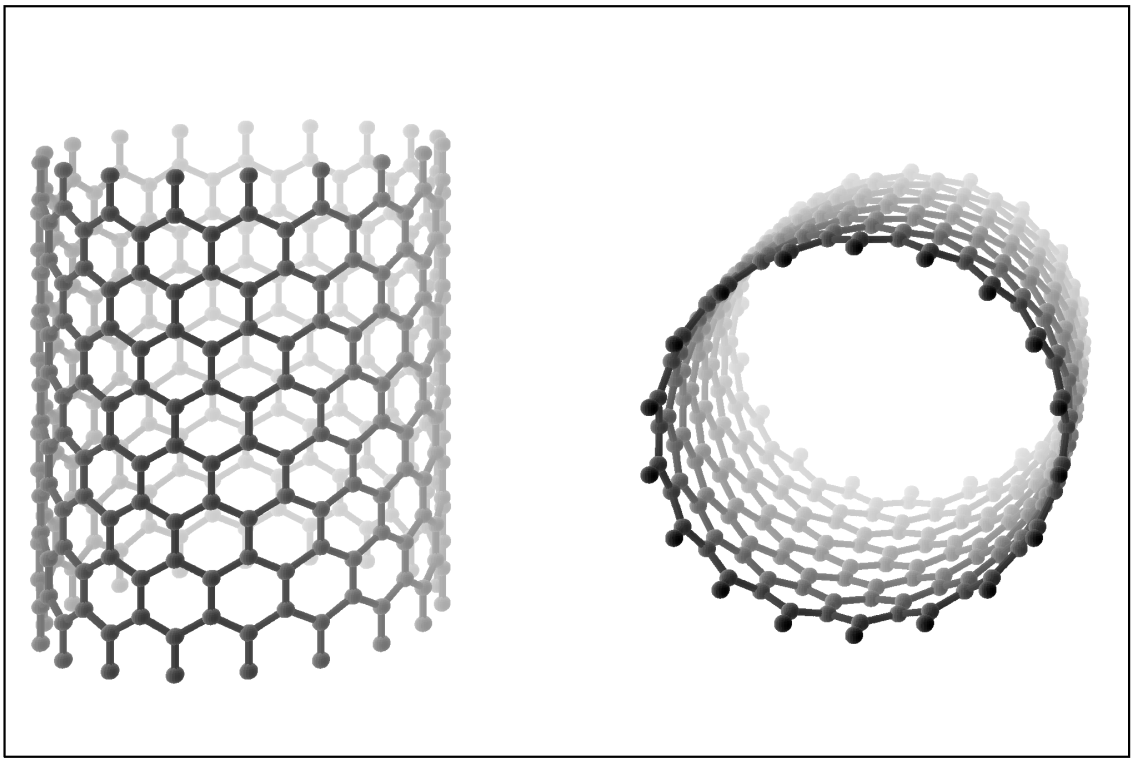

Figure 1.7: A zigzag $(18, 0)$ nanotube

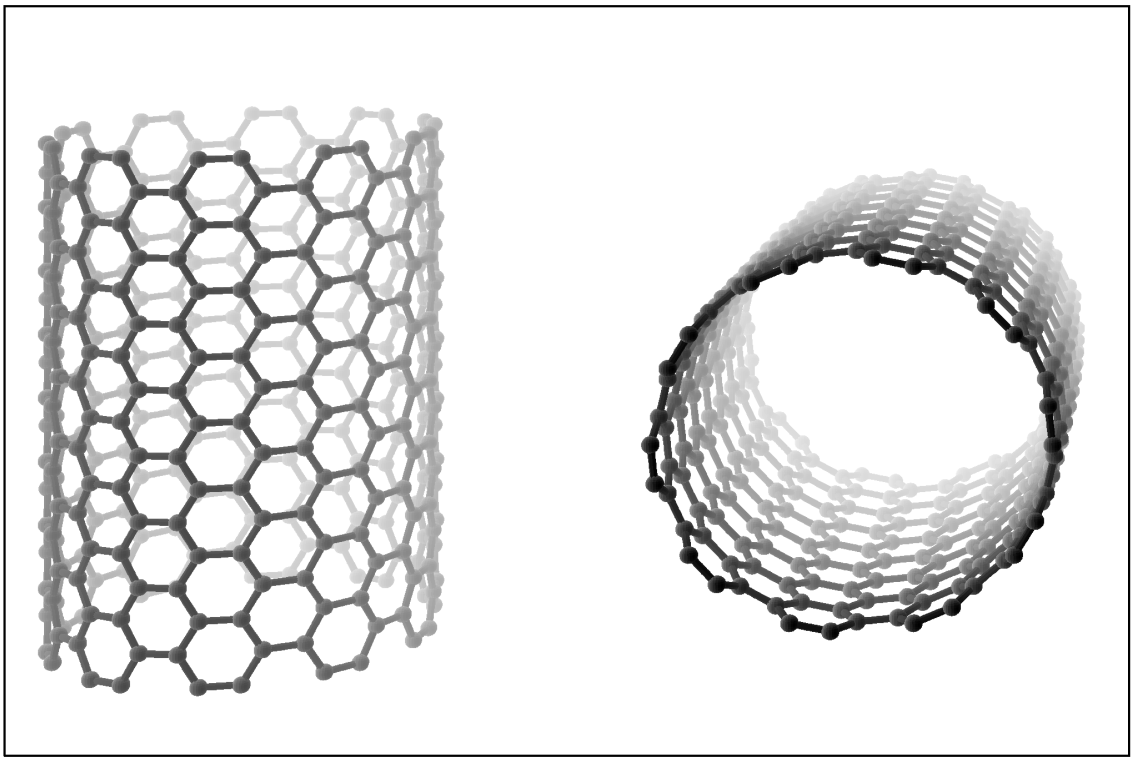

Figure 1.8: An armchair $(10, 10)$ nanotube

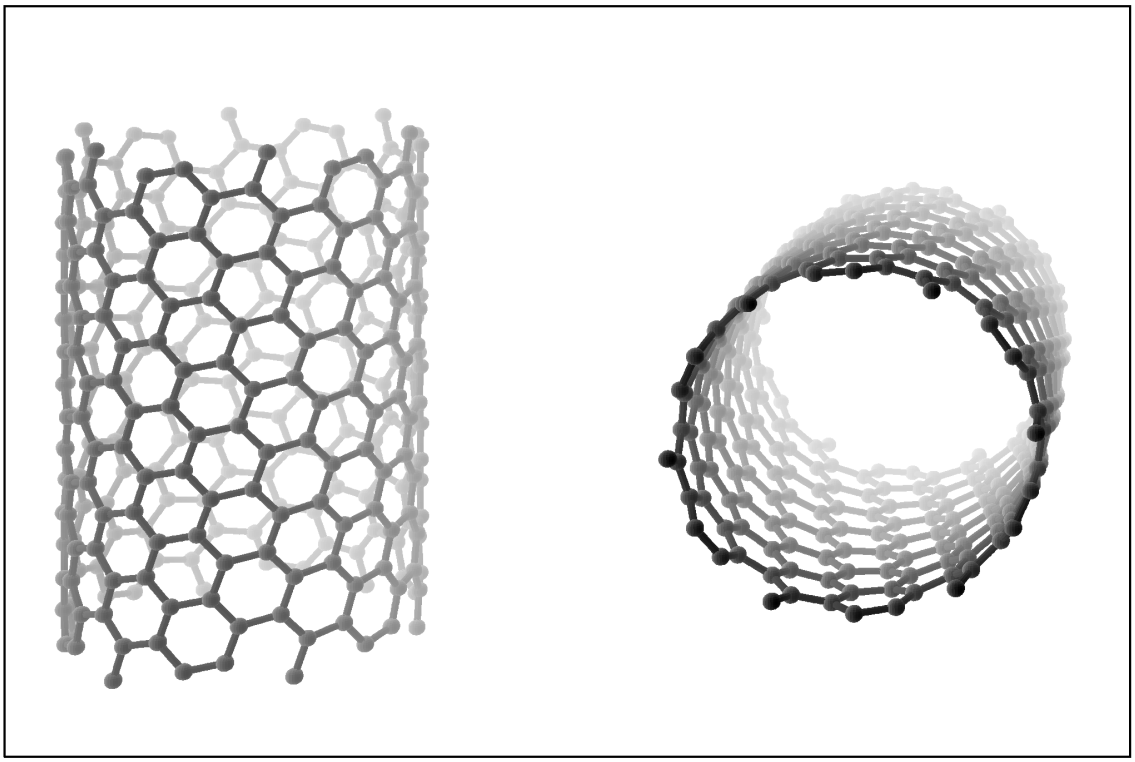

Figure 1.9: A chiral $(12, 6)$ nanotube

els of nanotubes have been proposed and a standardization is now available which helps to understand the main characteristics of both single walled nanotubes and multiwalled nanotubes[3].

Single walled nanotubes : the vector model

One way to formalize the structures of single walled nanotubes is to use the vector model presented in Figure 1.10 which completely determines the structure of a particular nanotube with a pair of integer (n, m). The vector P is defined by joining two equivalent carbon atoms of the graphene layer. The nanotube is obtained by bending up P from head to tail giving its perimeter $|P| = 2\pi R$, where R is the radius of the nanotube. Before rolling up the nanotube, P is inside the graphene plane and can be read as a linear combination of a_1 and a_2 which are the base vectors of the unit cell of the graphene. With the convention $n \geq m$, we receive

$$P = n \cdot a_1 + m \cdot a_2 \tag{1.1}$$

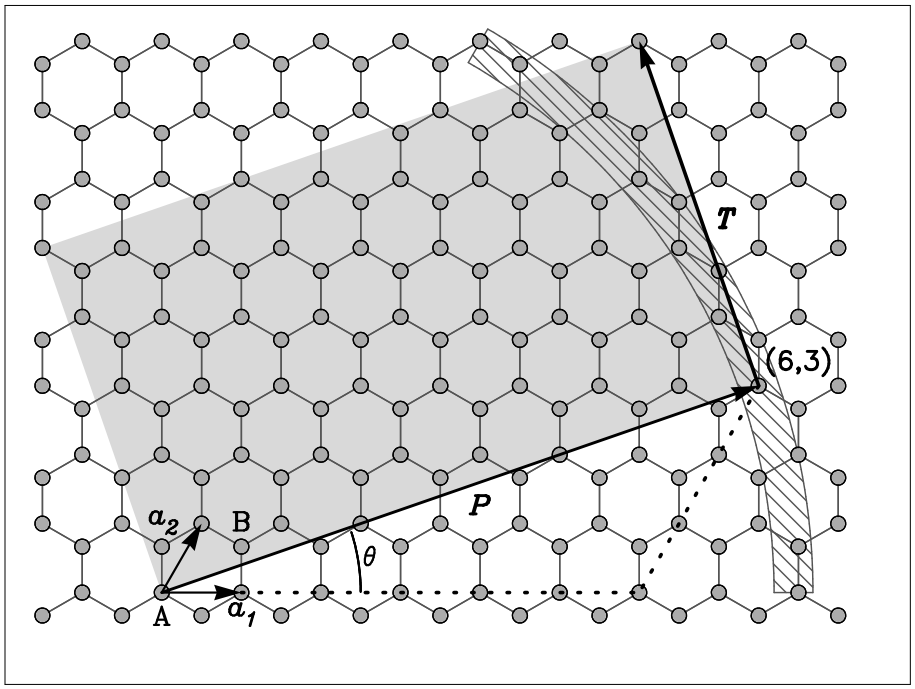

Figure 1.10: Graphene layer with the two lattice vectors a_1 and a_2. Carbons A and B are the two inequivalent atoms. The perimeter vector P, the translational vector unit T, the chiral angle θ and the unit cell (grey area) are represented for the construction of the $(6, 3)$ nanotube. Note that if the head of the vector P is inside the dashed area, the corresponding nanotubes have similar diameters and present different symetries and geometries.

It can be seen from Figure 1.10, that in cartesian coordinates

$$a_1 = \frac{a}{2} \cdot \begin{pmatrix} \sqrt{3} \\ -1 \end{pmatrix} \quad ; \quad a_2 = \frac{a}{2} \cdot \begin{pmatrix} \sqrt{3} \\ 1 \end{pmatrix} \tag{1.2}$$

where $a = 2.461$ Å. The graphene has two inequivalent carbon atoms A and B per unit cell with the following coordinates

$$A : \begin{pmatrix} 0 \\ 0 \end{pmatrix} \quad ; \quad B : \begin{pmatrix} \frac{2a}{\sqrt{3}} \\ 1 \end{pmatrix} \tag{1.3}$$

Zigzag nanotubes correspond to P colinear to a_1 i.e. $m = 0$ and for armchair nanotubes $m = n$, i.e. $P = m \cdot (a_1 + a_2)$. In all the other cases, a chiral nanotube is constructed. As a tutorial example, the vector $P = 6 \cdot a_1 + 3 \cdot a_2$ is presented in Figure 1.10. All the nanotubes constructed from carbon atoms inside the dashed area show similar radius

than the $(6,3)$. After rolling up the graphene sheet according to P, the chiral nanotube $(6,3)$ is obtained as presented in Figure 1.11.

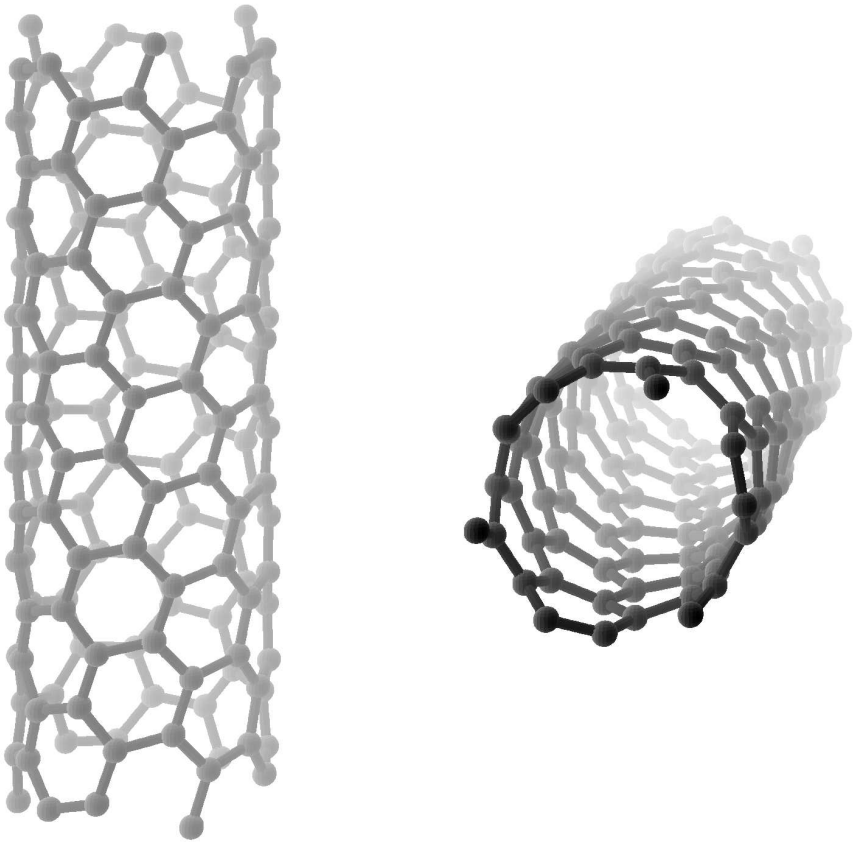

Figure 1.11: A chiral $(6,3)$ nanotube corresponding to the rolled up graphene sheet displayed in Figure 1.11.

More generally, one can write the vector

$$P = \frac{a}{2} \cdot \begin{pmatrix} \sqrt{3} \cdot (n+m) \\ m-n \end{pmatrix} \tag{1.4}$$

since $|a_1| = |a_2| = 2.461$ Å, the perimeter $|P|$ of a (n,m) nanotube is given by

$$|P| = |n \cdot a_1 + m \cdot a_2| = \frac{a}{2} \cdot \sqrt{(3(n+m)^2 + (m-n)^2} \tag{1.5}$$

then

$$|P| = 2.461 \cdot \sqrt{n^2 + m^2 + mn} \qquad (\text{Å}) \tag{1.6}$$

which gives a radius for the nanotube

$$R = \frac{2.461}{2\pi} \cdot \sqrt{n^2 + m^2 + mn} \qquad (\text{Å}) \tag{1.7}$$

Similarly, the chiral angle θ is written

$$\theta = \arctan \frac{\sqrt{3}m}{2 \cdot n + m} \tag{1.8}$$

A second vector T has to be defined which corresponds to the translational unit cell along the nanotube axis. The vector T for the $(6, 3)$ and its translational unit are displayed in Figure 1.10. It can be noticed that for zigzag and armchair nanotubes, the length of the unit cell is equal to $\sqrt{3} \cdot a$ and a, respectively. For chiral nanotubes it can be longer. This vector presents the two following properties :

- T is perpendicular to $P \Longleftrightarrow T \cdot P$=0
- T is a linear combination of a_1 and $a_2 \Longleftrightarrow T = m' \cdot a_1 + n' \cdot a_2$ where m' and n' are integers

Thus, we have to solve the following equation

$$T \cdot P = \frac{a^2}{4} \cdot \begin{pmatrix} \sqrt{3} \cdot (n+m) \\ m-n \end{pmatrix} \cdot \begin{pmatrix} \sqrt{3} \cdot (n'+m') \\ m'-n' \end{pmatrix} = 0 \tag{1.9}$$

$$3 \cdot (n+m)(n'+m') + (m-n)(m'-n') = 0 \tag{1.10}$$

which gives

$$m' = -n' \frac{2n+m}{n+2m} \tag{1.11}$$

Here, we introduce d the greatest common divisor of $2n + m$ and $n + 2m$, and we can rewrite

$$T = \frac{2m+n}{d} \cdot a_1 - \frac{2n+m}{d} a_2 \tag{1.12}$$

hence

$$T = \frac{a}{2d} \cdot \begin{pmatrix} \sqrt{3} \cdot (m-n) \\ -3(m+n) \end{pmatrix} \tag{1.13}$$

where

$$d = gcd(2n+m, n+2m) \tag{1.14}$$

A single walled nanotube has a one dimensional structure defined by the unit cell vector T. Its length is $T = \sqrt{3}|P|/d$. It can be show that one unit cell contains $4(n^2+m^2+nm)/d$ atoms, which can be large for chiral nanotube.

Bundles of single called nanotubes

As mentioned in the previous section, nanotubes are generally packed into bundles as presented in Figure1.3. A schematic illustration of the structure is shown in Figure1.12. The van der Waals interaction stabilizes the structure at a typical distance between the

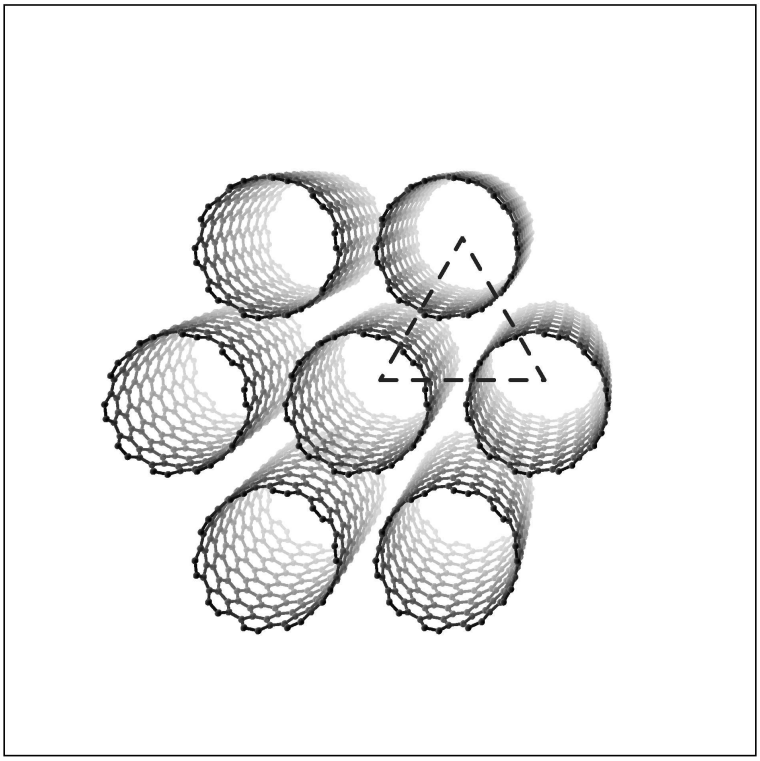

Figure 1.12: A bundle of $(10, 10)$ carbon nanotubes. A more or less triangular lattice is generally observed experimentally. Note that this situation is far from reality since randomly distributed chiralities are experimentally observed.

wall of the nanotubes about 3.14Å.

Multiwalled nanotubes

Multiwalled nanotubes consist of at least two concentric nanotubes of different diameters like Matrioschka Russian doll. Figure 1.13 presents a 3 layers MWNT made of a $(6, 5)$ inside a $(10, 10)$ inside a $(16, 11)$. The geometrical properties of each individual layer can be described by the vector model.

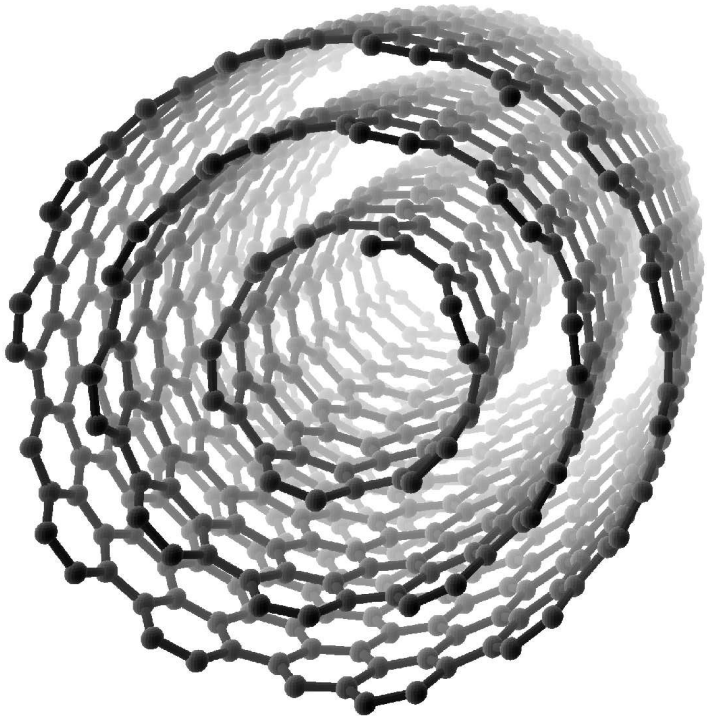

Figure 1.13: A multiwalled carbon nanotubes : $(6, 5)@(10, 10)@(16, 11)$

Electronic properties of carbon nanotubes

From the beginning, theoretical calculations have proposed that the electronic properties of the carbon nanotubes depend strongly on their geometrical structures[3, 25, 26, 27] Thus, nanotubes can be metals or semiconductors depending on their diameter or chirality. Figure 1.14 presents densities of states of different type of nanotubes. Practically, from the pair of integer (n, m), it is possible to determine the electronic properties of the

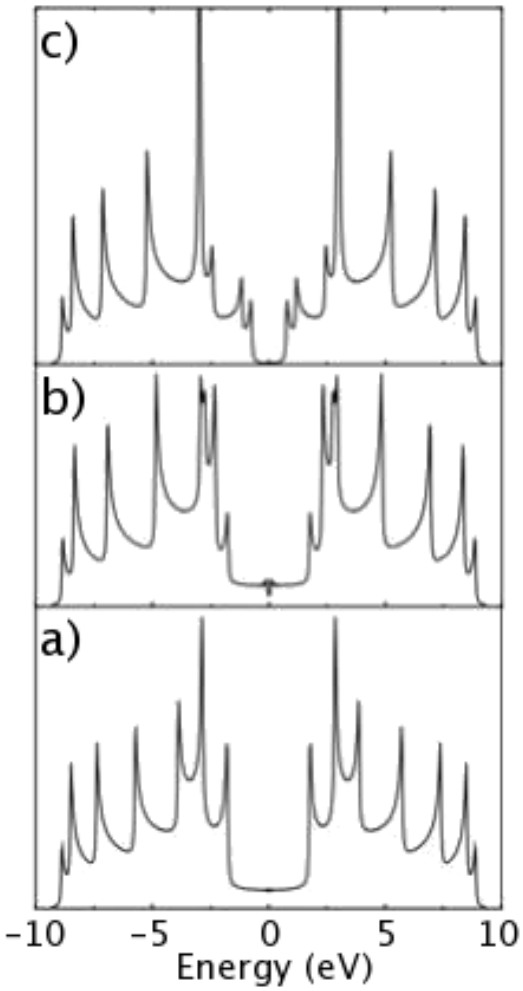

Figure 1.14: Densities of states for two metallic carbon nanotubes a) $(5, 5)$ and b) $(7, 1)$. c) is for the semiconducting $(8, 0)$. Adapted from the reference [28].

nanotubes. It was established, that if $n-m$ is a multiple of 3 the nanotube is metallic with a constant density of state over a large plateau above and below the Fermi level. In all others case, nanotubes are semiconductors with an energy gap inversely proportional to the radius R. Therefore, one third of the single walled carbon nanotubes are metallic with some exceptions for small diameters below 8Å, because of their higher curvatures. This result is easy to remain and directly related to the periodic boundary conditions along the circumference of the nanotube which discretize the electronic states in one direction perpendicular to the nanotube axis[28] Another interesting feature concerns the van Hove singularities related to the strong one dimensional character of the electronic states in

the nanotubes. Actually, in the case of armchair nanotubes $m = n$ and small radius nanotubes detailed calculations and low temperature experiments[29] have show that the curvature opens a tiny gap. However, such pseudo gap can be ignored for properties and applications around room temperature.

Recent works on individual carbon nanotubes

The last developments of the research on nanotubes concern the studies of individual objects. From theory and modelisation, an impressive number of remarkable properties have been predicted, suggesting a very broad potential of applications in energy storage, nano-electronics, mechanics, sensors, field emission... However, it is a real challenge at the nanoscale to confront theory and experiments, since it is necessary to determine at the same time the structures, the mechanical, optical and electrical properties of one individual nanotube. This feat of strength has been initiated by the use of STM spectroscopy and high resolution transmission microscopy[30, 31]. Figure 1.15 presents an atomically resolved STM measurement of a chiral carbon nanotube[33]. Later, quantum conduc-

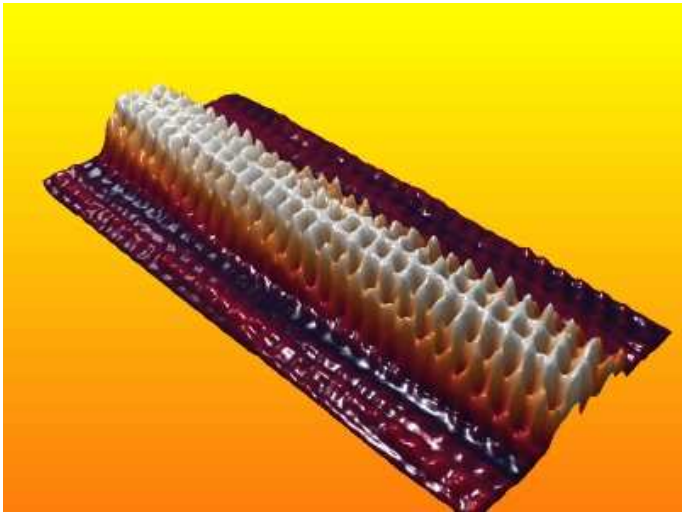

Figure 1.15: Atomically resolved STM measurement of a chiral carbon nanotube[33]

tance behavior has been observed[30] along the axis of the tube and integration of carbon nanotubes as nano-junctions in logic circuit has been demonstrated [32]. A spatially con-

trolled light emission from nanotube-field-effect transistor after the injection of electrons and holes from opposite edges was also reported [34]. The ultimate experiments have been performed on free-standing nanotubes as presented in Figure 1.16, where the two integer (n, m) have been determined by electron diffraction on several individual objects with diameter in the range of 14 to 30 Å and correlated to vibrational properties measured by micro-Raman[35].

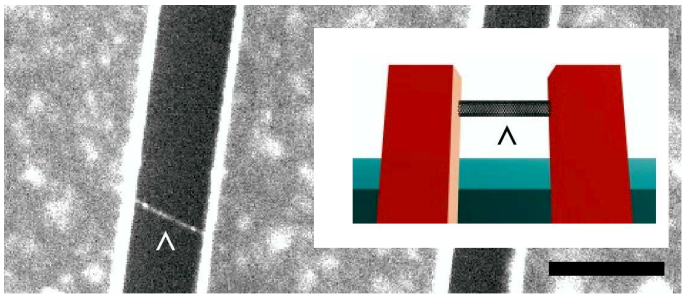

Figure 1.16: Transmission Electron Micrograph of one suspended single walled carbon nanotube which has been investigated by electron diffraction and micro-Raman in order to determine its structure and vibrational properties[35]. The arrows indicate the free standing nanotube. The scale bar is 1μm

If the knowledge on nanotubes is rapidly growing up, the field of their properties and applications is still largely unexplored. New nanostructures will be certainly discovered with their own characteristics as peapods[36] or chemically modified nanotubes by sidewall functionalization[37].

Bibliography

[1] H.W. Kroto, J.R. Heath, S.C. O'Brien, R.F. Curl and R.E. Smalley, Nature 318, 162 (1985)

[2] W. Krätschmer, L.D. Lamb, K. Fostiropoulos and D.R. Huffman, Nature 347, 354 (1990)

[3] M.S. Dresselhaus, G. Dresselhaus and P.C. Eklund, Science of fullerenes and carbon nanotubes, Academic Press, San Diego, (1996)

[4] K.M. Kadish and R.S. Ruoff, Fullerenes : chemistry, physics and technology, Wiley-Interscience (2000)

[5] S. Iijima, Nature 354 56 (1991)

[6] A. Oberlin, M. Endo, T. Koyama, J. Cryst. Growth 32, 335 (1976)

[7] G.R. Millward and D.A. Jefferson, Chem. Phys. Carbon 14 1 (1978)

[8] S. Iijima,J. Microscopy, 119 99 (1980)

[9] T.W. Ebbesen and P.M. Ajayan, Nature 358, 220 (1992)

[10] D.S. Bethune, C.H. Kiang, M.S. de Vries, G. Groman, R. Savoy, J. Vasquez and R. Beyers, Nature 363 605 (1993)

[11] S. Iijima and T. Ichihashi, Nature 363, 603 (1993)

[12] A. Thess, R. Lee, P. Nikolaev, H. Dai, P. Petit, J. Robert, C. Xu, Y.H. Lee, S.G. Kim, A.G. Rinzler, D.T. Colbert, G.E. Scuseria, D. Tomanek, J.E. Fischer and R.E. Smalley, Science 273,483 (1996)

[13] C. Journet, W. Maser, P. Bernier, A. Loiseau, M. Lamy de la Chapelle, S. Lefrant, P. Deniard, R. Lee and J.E. Fischer, Nature 388 756 (1997)

[14] J. Tersoff and R.S. Ruoff, Phys. Rev. Lett. 73, 676 (1994)

[15] J.C. Charlier, X. Gonze and J.P. Michenaud, Europhys. Lett. 29, 43 (1995)

[16] D. Golberg, Y. Bando, L. Bourgeois and K. Kurashima, Carbon 39, 1858 (1999)

[17] L. Henrard, A. Loiseau, C. Journet and P. Bernier, Eur. Phys. J. B 13, 661 (2000)

[18] T. Guillard, S. Cetout, L. Alvarez, J.L. Sauvajol, E. Anglaret, P. Bernier, G. Flamant, D. Laplaze, Eur. Phys. J. B 5, 252 (1999)

[19] M. Endo, K. Takeuchi, K. Kobori, K. Takahashi, H.W. Kroto and A. Sarkar, Carbon 33, 873 (1995)

[20] V. Ivanov, A. Fonseca, J.B. Nagy, A. Lucas, P. Lambin, D. Bernaerts and X.B. Zhang, Carbon 33 1727 (1995)

[21] A.G. Rinzler,J. Liu, H. Dai, P. Nikolaev, C.B. Huffman, F.J. Rodriguez-Macias, P.J. Boul, A.H. Lu, D. Heymann, D.T. Colbert, R.S. Lee, J.E. Fischer, A.M. Rao, P.C. Eklund, R.E. Smalley, App. Phy. A 67, 29 (1998)

[22] W. Zhou, Y.H. Ooi, R. Russo, P. Papanek, D.E. Luzzi, J.E. Fischer, M.J. Bronikowski, P.A. Willis, R.E. Smalley, Chem. Phys. Lett 350, 6 (2001)

[23] Y. Kim, O. Torrens, M. Kiikkawa, E. Abou-Hamad, C. Goze-Bac and D. Luzzi, Chem. Mater. 19 2982 (2007)

[24] C. Goze-Bac, S. Latil, P. Lauginie, V. Jourdain, L. Conard, L. Duclaux, A. Rubio, P. Bernier Carbon, 40, 1825 (2002)

[25] R. Saito, M. Fujita, G. Dresslelhaus and M.S. Dresselhaus, Phys. Rev B 46, 1804 (1992)

[26] M.S. Dresselhaus, G. Dresselhaus and R. Saito, Carbon 33, 883 (1995)

[27] N. Hamada, S. Sawada and O. Oshiyama, Phys. Rev.Lett. 68, 1579 (1992)

[28] J.C. Charlier, X. Blase and S. Roche Rev. Mod. Phys. 79 677 (2007)

[29] M. Ouyang , J.-L. Huang, C.L. Cheung, and C.M. Lieber, Science 292, 702 (2001)

[30] S.J. Tans, M.H. Devoret, H. Dai, A. Thess, R.E. Smalley, L.J. Geerligs and C. Dekker Nature 386, 474 (1997)

[31] J.W.G. Wildoer, L.C. Venema, A.G. Rinzler, R.E. Smalley and C. Dekker Nature 391, 59, 1998

[32] P.G. Collins, M.S. Arnold, P. Avouris Science 292, 706 (2001)

[33] S.G. Lemay, J.W. Janssen, M. van den Hout, M. Mooij, M.J. Bronikowski, P.A. Willis, R.E. Smalley, L.P. Kouwenhovena and Cees Dekker, Nature 412, 617 (2001)

[34] M. Freitag, J. Chen, J. Tersoff,J.C. Tsang, Q. Fu, J. Liu and P. Avouris, Phys. Rev. Lett. 93, 76803 (2004)

[35] C. Meyer, M. Paillet, T. Michel, A. Moreac, A. Neuman, G. Duesberg, S. Roth, J. Sauvajol Phys. Rev. Lett., 95, 217401 (2005)

[36] B.W. Smith, M. Monthioux and D.E. Luzzi Nature 396, 323 (1998)

[37] A. Hirsch Angew. Chem. Int. 41 1853 (2002)

Chapter 2

Structural properties of nanotubes derived from ^{13}C NMR

Structural properties of carbon nanotubes are derived from experimental and theoretical ^{13}C Nuclear Magnetic Resonance investigations. Solid state NMR experiments with Angle Spinning conditions have been performed on single and multi-walled nanotubes with diameters in the range from 0.7 to 100 nm and number of walls from 1 to 110. Depending on the size and shape, we establish the dependence of their NMR signatures and find two universal behaviors for the line shifts and line widths. Increasing the diameter D, from the smallest investigated nanotube corresponding to the inner nanotube of a double-walled to a large multi-walled nanotube, a 23.5 ppm diamagnetic shift of the isotropic line is observed which asymptotically tends to the line position expected in graphene. The experimental isotropic chemical shift follows $\delta = 18.3/D + 102.5$ ppm, in good agreement with ab initio calculations performed on semiconducting nanotubes with diameters in range from 0.7 to 1.4 nm. A characteristic broadening of the line shape is observed with increasing the number of walls. This feature can be interpreted in terms of a distribution of isotropic shifts originating from different diamagnetic shieldings on the encapsulated nanotubes and heterogeneity of the samples. NMR is definitely shown to be a major non destructive spectroscopy on bulk samples which can be used as a source of basic and complementary information to investigate carbon based nanomaterials.

Since their discovery in 1991 [1], carbon nanotubes (CNTs) have attracted the attention due to their extraordinary structural, mechanical and electronic properties [2]. They are one dimensional nanoscopic structures with natural and tunable properties which are predicted to impact many areas of our daily life[3]. However, one of the great hindrance to study their properties and to develop applications, is that specimen are usually studied as a mixture of CNTs having very different structural, physical and chemical properties [5, 6, 7]. For example, the electronic properties of CNTs depend on their chirality and diameter, two structural parameters which are hardly controlled during the synthesis or post-process. Although progress have been made to enhance purity [4] and selectivity of synthesis approaches, investigations of bulk CNTs materials suffer a lack of structural information. The length and diameter of an individual CNT may be determined by atomic force microscopy (AFM), scanning tunneling microscopy (STM), or transmission electron microscopy (TEM) techniques. Information about bulk sample may be obtained from scanning electron microscopy (SEM), X-ray diffraction, optical absorption, or Raman scattering. However, it appears that even a combination of these techniques does not fully characterize a given sample [8] and alternative methods have to be considered. Up to now, ^{13}C Nuclear Magnetic Resonance spectroscopy was not fully exploited on CNTs studies, in spite of its great potential as shown in the past for carbon materials like graphite, fullerene, conducting polymers. In particular, with the help of theoretical support, it would be of great interest to extract from NMR experiments on bulk samples, structural information like diameters and number of walls in CNTs. In the present contribution, our experimental and theoretical efforts to streamline ^{13}C NMR investigations of CNTs are reported.

Carbon nanotubes used in this study were chosen regarding to their structural characteristics, particularly diameters distribution and number of walls. The single-walled CNTs sample (SW1) was purchased from Carbon Solutions Inc and was filtered through a magnetic field of 1.1 Tesla to remove residual catalyst [4]. Double-walled CNTs sam-

ple (DW1) was fabricated by annealing peapods under dynamic vacuum for 48 hours at 1250°C. The peapods were prepared using 25% ^{13}C enriched C_{60} vapor during 10 hours at 650°C for filling CNTs, followed by 1 hour post annealing in dynamic vacuum to remove non-encapsulated fullerenes. Double-walled CNTs sample (DW2) was synthesized by CCVD technique and was purchased from Thomas Swan and Co. Company, England. Single-walled CNTs sample (SW2) is from HiPco technique at CNI, Houston, USA. The multi-walled CNTs samples named (MW1) and (MW2) were provided by the CRMD Laboratory in Orléans, France. They were prepared respectively by catalytic decomposition of acetylene diluted in nitrogen at 600 °C on $Co_xMg_{1-x}O$ as described elsewhere [9] and over Co incorporated zeolite NaY [10]. The multi-walled CNTs sample (MW3) was synthesized using the liquid aerosol pyrolysis containing both the carbon and the catalyst sources which enables to prepare clean and well-aligned carbon nanotubes. This sample was provided by Laboratoire Francis Perrin, CEA Saclay in France. The multi-walled CNTs sample (MW4) was synthesized using CCVD and was purchased from Nanocyl Company. The TEM micrographs were obtained using a philips CM20 microscope with a LaB6 filament. The operating voltage was set to 200 KV and the magnification to 200,000. Images were collected in bright field mode. ^{13}C NMR experiments were carried out using a Bruker ASX200 and a Tecmag Apollo spectrometers at a magnetic field of 4.7 T and at Larmor frequency of 50.3 MHz.

For each CNTs samples, the distributions of the diameters and the number of walls have been estimated, with the help of statistical measurements on TEM micrographs as presented in Figure 2.1. Entangled CNTs have not been counted and only parts of the images where CNTs are isolated have been considered in the statistics. CNTs were segmented into several measured sections where the diameters and number of walls are identical. The extracted structural parameters using this method are summarized in Table 2.1. The investigated diameters and the number of walls were found to range from 0.7 nm to 100 nm and from 1 to 110, respectively.

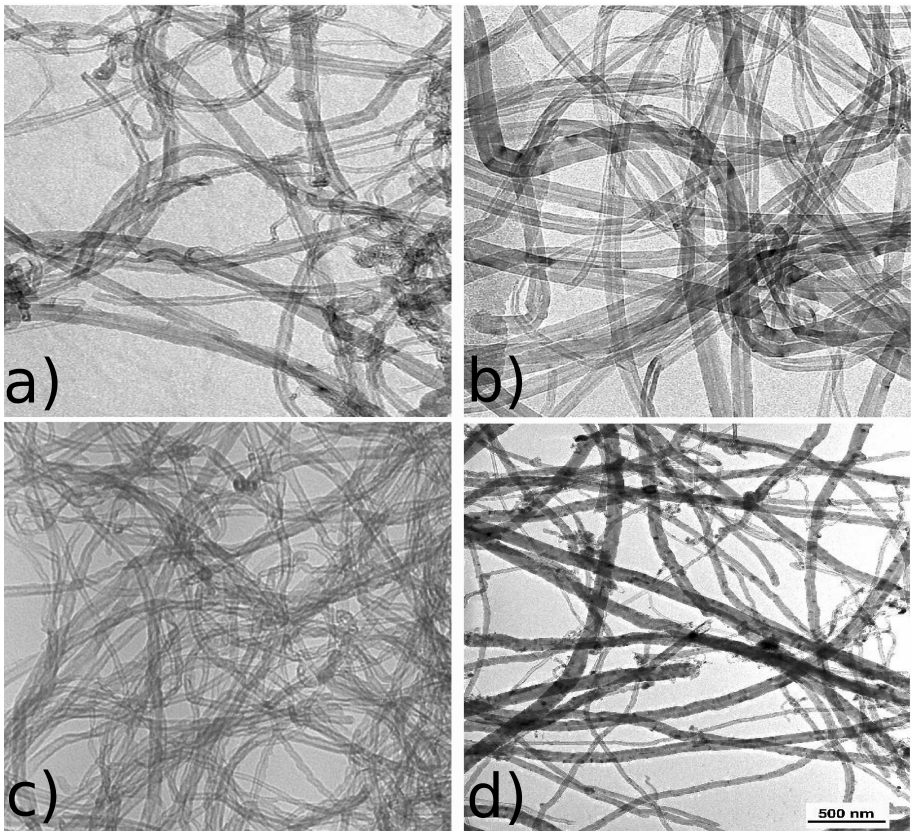

Figure 2.1: HRTEM of different multi-walled carbon nanotubes : a) MW1 b) MW2, c) MW4 and d) MW3

Figure 2.2 shows high resolution Magic Angle Spinning ^{13}C NMR measurements on these CNTs. With increasing the diameter of the CNTs, from the samples SW2 to MW3, a clear diamagnetic shift was observed. The particular case of sample DW1 in figure 2.2a) reveals two peaks which are the signature of the 0.7 nm inner CNTs. In this sample, the NMR signal is dominated by the 25% ^{13}C enriched inner CNT, the outer CNT being of natural abundance 1%. As predicted by Marques et al.[11] the peak at 99.2 ppm can be assigned to diamagnetically shifted inner CNTs due to ring current from π electrons circulating on the outer CNTs. The second peak at 125.8 ppm is also attributed to the inner CNTs but in the vicinity of defects on the outer CNTs, which are known to cancel this diamagnetic shielding[12]. Hence, the latter line position can be considered as a good estimation of the chemical shift for a free standing CNT with a diameter of 0.7 nm. For each samples, the average isotropic chemical shifts were estimated from the first moment of the isotropic lines and are listed in Table 2.1. First moments were found to range from 125.8 ppm for the CNTs with the smallest diameter, to 102.3 ppm for the largest one, in agreement with the value expected for the graphene which can be seen as a CNT with an infinite

Samples	Diameter distributions (nm)	Number of walls	δ (ppm)	Δ (ppm)
DWNTs (DW1) inner CNT 25% ^{13}C	0.7 ± 0.1	1+1 (25% ^{13}C)	125.8	19.5
SWNTs HiPCo (SW2)	1.2 ± 0.2	1	123.8	18.9
SWNTs Carbon Solution (SW1)	1.4 ± 0.2	1	118.8	16.8
DWNTs Swan (DW2)	(1.3 - 3.5) ± 0.4	2 or 3	116.3	25.8
MWNTs) Nanocyl (MW4)	(4 - 17) ± 2	15 ± 5	106.1	44.8
MWNTs Co - MgO (MW1)	(4 - 20) ± 2	15 ± 5	104.7	44.2
MWNTs Co - NaY (MW2)	(8 - 50) ± 2	90 ± 20	103.4	54.7
MWNTs Pyrolisis (MW3)	(10 - 100) ± 2	60 ± 10	102.3	51.6

Table 2.1: Structural parameters : diameters and number of walls extracted from statistics on HRTEM images and ^{13}C NMR parameters : $\delta = M_1$ and $\Delta = \sqrt{M_2}$ calculated from ^{13}C NMR isotropic lines.

diameter[13, 14]. These experimental data are presented in figure 2.3 and can be fitted by the following expression with D in nm,

$$\delta = \frac{18.3}{D} + 102.5 \quad \text{[ppm TMS]} \tag{2.1}$$

giving an empirical relation between ^{13}C NMR isotropic chemical shift δ versus the average diameter D of the CNTs sample. This relation allows to easily estimate the diameter and its distribution of an unknown CNTs sample by measuring δ, the average ^{13}C NMR isotropic line position.

We turn now to the increase of the broadening of the ^{13}C NMR isotropic lines which is observed from single to multi-walled CNTs. From the second moment M_2 of the isotropic lines, one relevant parameter $\Delta = \sqrt{M_2}$, can be estimated for each CNTs spectra displayed in figure 2.2. The results are listed in table 2.1 and figure 2.4 presents Δ versus the number of walls. Several effects contribute to the broadening of the line. It has been shown that residual catalyst used for the synthesis have a dramatic effect [15]. However in our experiments, efforts have been made to select and purify samples in order to investigate CNTs samples with minute quantity of

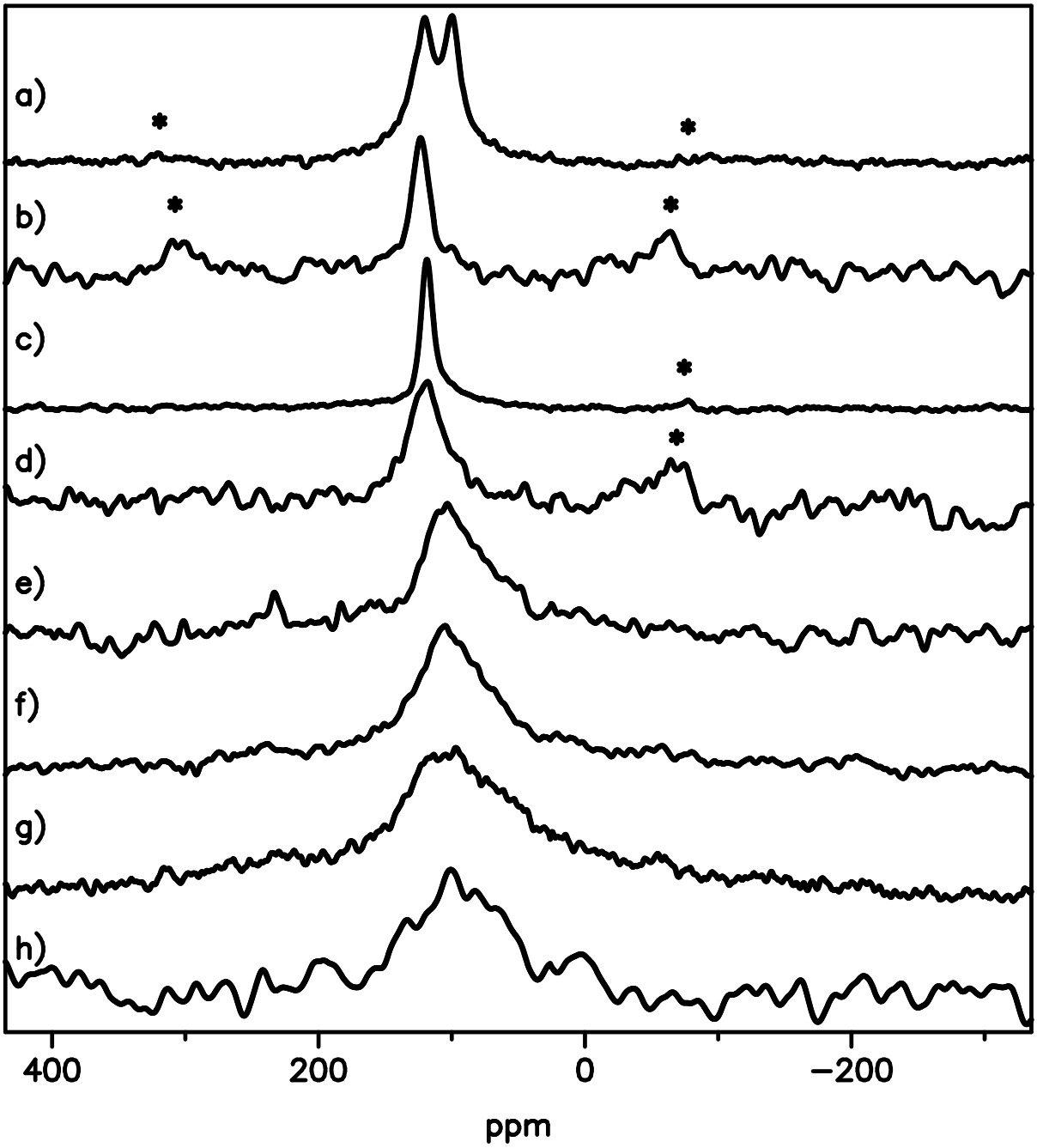

Figure 2.2: ^{13}C high resolution MAS NMR spectra on single, double, triple and multi-walled carbon nanotubes. a) DW1, b) SW2, c)SW1, d) DW1, e) MW4, f) MW1, g) MW2 and h) MW3. Their structural characteristics are listed in Table 2.1. (* are for sidebands).

impurities. Then, the main contribution to Δ is expected to be the diamagnetic shieldings [11] related to the encapsulation of CNT inside another CNT and the mixture of CNTs with different structural characteristics. Indeed, Δ is increasing with the number of walls and obviously with

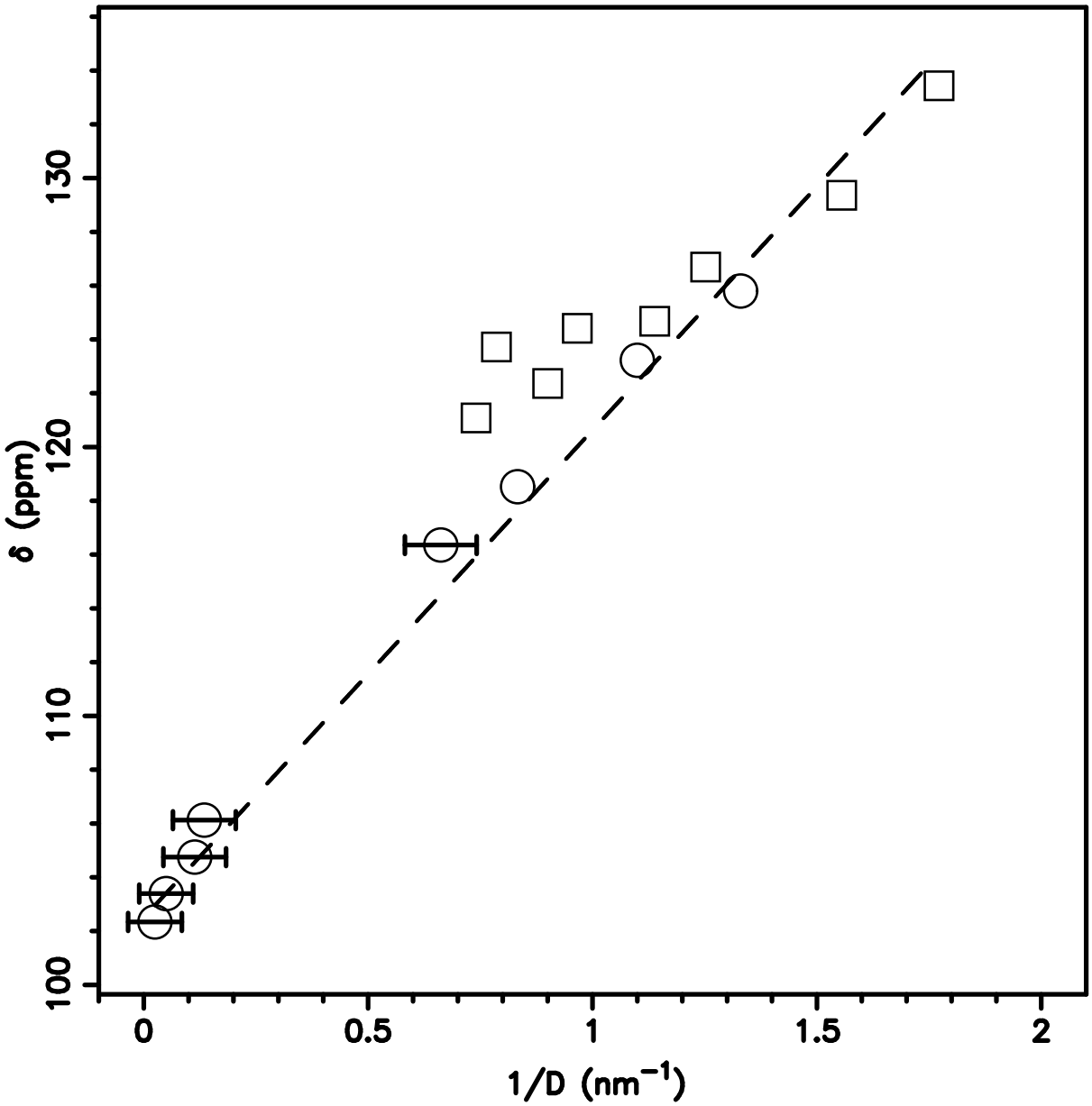

Figure 2.3: ^{13}C NMR isotropic chemical shifts for carbon nanotubes versus the inverse of their diameter (D) : experiments (open circle) and *ab initio* calculations (open square). The dashed line corresponds to δ (see Eq. 2.1), the best fit of the experimental data.

the heterogeneity of the sample, since in both cases a distribution of line shifts is predicted. Actually, for single-walled CNTs Δ was found about 18 *ppm* and for double walls about 26 *ppm*. Above, a linear dependence $\Delta \approx 45.2 + 0.14 \times N$ in *ppm*. as presented in figure 2.4, fits well the data. However, it was not possible experimentally to clearly discriminate between an increase of Δ with the number of walls or a higher heterogeneity of the samples.

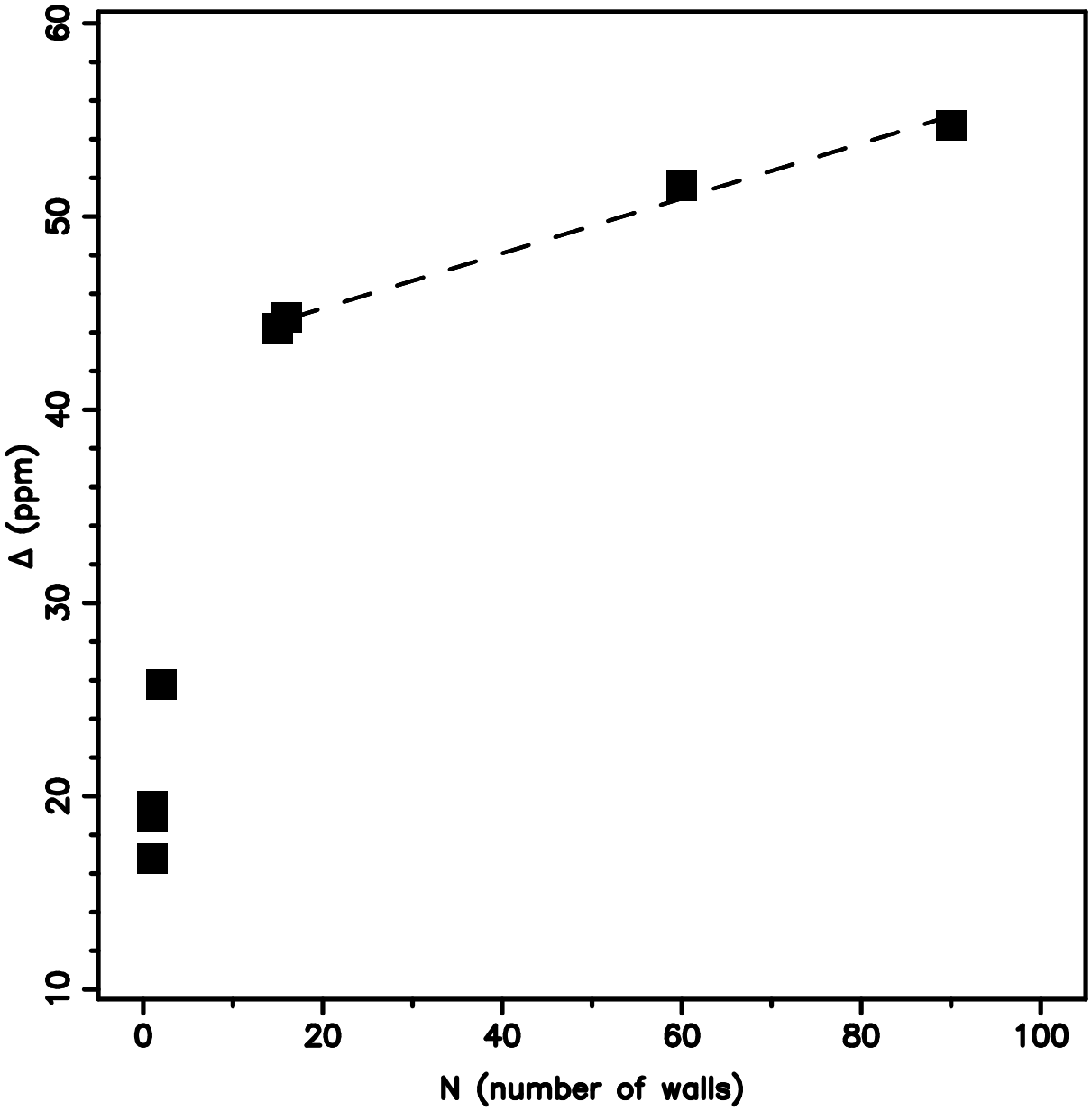

Figure 2.4: The parameter Δ versus the number of walls.

In order to support theoretically our findings, first-principles calculations were performed within the density functional theory (DFT) as implemented in the plane-wave pseudopotential PARATEC code[17]. To reduce the computational cost, we have restricted our study to zigzag (n,0) single-walled CNTs with a small diameter, $7 \leq n \leq 17$. The choice of this particular nanotube geometry allows reasonably tractable calculations due to the relatively small number of atoms in the unit cell, as well as a moderately fine grid needed to accurately sample the reciprocal Brillouin zone. However, it still provides a helpful theoretical picture to explain the peak characteristics observed in the experimental spectra, as it will be shown below. A

sufficiently large supercell size was chosen so that isolated single-walled CNT are separated by a vacuum distance of 0.9 nm at least, hereby making inter-tube interactions negligible. Exchange-correlation effects were described in the generalized gradient approximation (GGA) with the PBE functional[18], which already proved to give accurate results for a large range of systems including carbon nanotubes. A norm-conserving Troullier-Martins pseudopotential with a core radius of 1.75 a.u. was used to model the valence/core interaction. The plane-wave basis set contained components with energies up to 40 Ry. The one dimensional irreducible Brillouin zone was sampled using 13 k-points. The nanotube geometry was fully optimized with a force criterion of 0.01 eV/Å. The magnetic susceptibility and ^{13}C NMR shielding tensors of the infinite single-walled CNT were calculated using the recent gauge-including projector-augmented plane-wave (GIPAW) approach proposed by Pickard and Mauri[19]. Due to the current limitations of its implementation in PARATEC, we have focused on the two families of *non metallic* (n,0) single-walled CNTs defined by $\ell = 1$ and $\ell = 2$, where $\ell = n \bmod 3$. To be able to compare the calculated chemical shifts with the experimental data, we have use the same reference as in [11], i.e. using the experimental isotropic chemical shift of benzene $\delta^{\mathrm{TMS}}_{\mathrm{benzene}}$, which itself is usually given relatively to that of tetramethylsilane (TMS), according to:

$$\delta_{\mathrm{CNT}} = \delta^{\mathrm{unref}}_{\mathrm{CNT}} - \delta^{\mathrm{unref}}_{\mathrm{benzene}} + \delta^{\mathrm{TMS}}_{\mathrm{benzene}} \tag{2.2}$$

where $\delta^{\mathrm{unref}}_{\mathrm{CNT}}$ and $\delta^{\mathrm{unref}}_{\mathrm{benzene}}$ are the unreferenced calculation results and $\delta^{\mathrm{TMS}}_{\mathrm{benzene}} = 126.9$ ppm the experimental reference[20]. Following our convergence studies in cut-off energy, k-point sampling, supercell size, we estimate the calculated NMR chemical shifts to be converged within 1 ppm. The optimized structural parameters obtained in the present work are consistent with those published previously in the literature.[11, 21] Our *ab initio* results for the isolated CNTs are presented in figure 2.3 (open circle) together with experiments (open square). Unfortunately, *ab initio* computations on large diameter CNTs or multi-walled CNTs are not accessible. However, the comparison was feasible in the range from 0.7 to 1.4 nm where an overlap between the two approaches was possible. Interestingly, the theoretical results are in good agreement with the experiments. They reproduce the general trends and support the relations for δ and Δ obtained from the NMR experiments.

In the light of our study, it is now possible to easily determine the structural properties of single and mutli-walled carbon nanotubes bulk samples, directly from high resolution ^{13}C NMR experiments. If the line position can be exploited to measure the average diameter of the CNTs, the line width provides information on the number of walls and/or homogeneity of the samples. Our experiments are strongly supported by *ab initio* investigations and two empirical relations for the structural parameters of CNTs are proposed to work over a wide range of diameters. Our current investigations suggests to use NMR approach as an alternative and reliable source of information compare to the other existing characterization methods.

Bibliography

[1] S. Iijima, Nature, 354, 56 (1991).

[2] C. Kane, L. Balents, and M. P. A Fisher, Phys. Rev. Lett. 79, 5086 (1997).

[3] R. H. Baughman, A. A. Zakhidov, and W. A. de Heer, Science 297, 787 (2002).

[4] Y. Kim, O.N. Torrens, J.M. Kikkawa, E. Abou-Hamad, C. Goze-Bac, and D.Luzzi, Chem. Mater., 19(12), 2982 (2007).

[5] M. Yudasaka, T. Komatsu, T. Ichihashi, Y. Achiba, S. Iijima, J. Phys. Chem. B, 102, 4892-4896 (1998).

[6] M. Zhang, M. Yudasaka, S. Iijima, J. Phys. Chem. B, 108, 149-153 (2004).

[7] S. Bandow, S. Asaka, Y. Saito, A. M. Rao, L. Grigorian, E. Richter, P. C. Eklund, Phys. Rev. Lett. 80, 3779-3782 (1998).

[8] A. Minett, K. Atkinson, S. Roth, Carbon nanotubes. In Handbook of porous solids; F. Schuth, S. W. Sing, J. Weitkapmp, Eds.; Wiley-VCH: Weinheim, (2002).

[9] S. Delpeux, K. Szotack, E. Frakowiak, S. Bonnamy, F. Béguin, J. Nanosci. Nanotechnol., 2, 481 (2002).

[10] I. Willems, Z. Konya, J.F. Colomer, G. VanTendeloo, N. Nagaraju, A. Fonseca, J.B. Nagy Chem. Phys. Lett. 71, 317 (2000).

[11] M.A.L. Marques, M. d'Avezac, F. Mauri, Phys. Rev. B, 73, 125433 (2006).

[12] Submitted

[13] C. Goze-Bac, S. Latil, P. Lauginie, V. Jourdain, J. Conard, L. Duclaux, A. Rubio, P. Bernier, Carbon, 40, 1825-1842 (2002).

[14] P. Lauginie, H. Estrade-Szwarckopf, B. Rousseau, and J. Conard, C. R. Acad, Sci Paris 307II, 1693 (1998).

[15] C. Goze-Bac, S. Latil, L. Vaccarini, P. Bernier, P. Gaveau, S. Tahir, V. Micholet, and R. Aznar, Phys. Rev. B 63, 100302(R) (2001)

[16] S. Latil, L. Henrard, C. Goze-Bac, P. Bernier, A. Rubio, Phys. Rev. Lett. 86, 3160 (2001).

[17] PARAllel Total Energy code, see http://www.nersc.gov/projects/paratec/.

[18] J. P. Perdew, K. Burke and M. Ernzerhof, Phys. Rev. Lett., 77, 3865 (1996).

[19] C. J. Pickard and F. Mauri, Phys. Rev. B, 63, 245101 (2001).

[20] A. K. Jameson and C. J. Jameson, Chem. Phys. Lett., 134, 461 (1987).

[21] E. Zurek, C. J. Pickard, J. Autschbach, J. Phys. Chem. C 112, 9267 (2008); E. Zurek, C. J. Pickard, J. Autschbach, J. Phys. Chem. C 112, 11744 (2008)

Chapter 3

Intercalated nanotubes

Electronic properties and molecular dynamics of single-wall carbon nanotubes intercalated with lithium are investigated by NMR. ^{13}C *NMR experiments reveal a metallic ground state for all of the following stoichiometries* LiC_x *with* $x = 10, 7$ *and* 6*. A continuous increase of the density of states at the Fermi level according to Li concentration is observed up to* $x \approx 6$*. From* ^{7}Li *NMR, evidence of inequivalent Li sites is reported, corresponding to preferential sites of intercalation and strong interactions between Li and C. From* ^{1}H *NMR, the coupled structural and dynamical properties of the alkali and cointercalated solvent are reported.*

Since the invention of lithium-ions batteries, carbon based materials such as natural graphite, carbon fibers, pyrolitic carbon were proposed as possible candidates for the use as battery anode materials [1]. Recently, new progress has been reported in the use of single-wall carbon nanotubes (SWNT) for this purpose[2]. At the same time, it has been shown that a new class of synthetic metals based on alkali intercalated nanotubes could be synthesized [3, 4, 5]. Because of their one-dimensional electronic structure and high tensile strength[6], these one dimensional metals are promising materials. A large variety of solid state properties has been reported ranging from insulator to metal and superconductor. However, all potential applications these materials offer depend strongly on the structures, compositions and stoichiometries. In this letter, we report on chemically *Li*-intercalated SWNT at different concentrations using high resolution NMR techniques. We show how the alkali content controls the electronic properties

of the metallic ground state and clarify the structural and dynamical properties of Li and the solvent molecules.

SWNT samples used in this study were synthesized by the electric arc method under the conditions described in the references [7, 8]. In order to improve the ^{13}C NMR signal to noise ratio, 10% ^{13}C isotope enriched graphitic rods have been vaporized in the presence of a catalyst mixture in the molar proportions 96.8% C, 2.1% Rh and 1.1% Pt. The SWNT bundles are collected directly from the collerette and used as produced without any purification. We estimated a content of over 80% carbon nanotubes showing an average diameter of 1.4 nm and bundle length of several microns (see the following references [8, 15] for more details about the samples). Lithium was chemically intercalated in SWNT ropes by using solutions of aromatic hydrocarbons and tetrahydrofuran (THF). By redox reactions between the radical-anions of fluorenone, benzophenone, naphthalene and SWNT with Li^+ as counter ion, intercalated SWNT were synthesized with stoichiometries of LiC_{10}, LiC_7 and LiC_6 respectively[9]. All samples were sealed under high vacuum. The experimental sample preparation conditions as well as a detailed Raman characterization are described elsewhere [9, 10, 11]. It has been shown that an electronic charge transfer occurs from the aromatic hydrocarbons to the SWNT bundles. Similarly to the intercalation process in other carbon materials, the alkali are expected to be intercalated together with THF molecules used as a solvent, forming a ternary compound $Li(THF)_yC_x$ [12, 13, 14].

NMR experiments were carried out on a Bruker ASX200 spectrometer at a magnetic field of 4.7 T and a ^{13}C NMR Larmor frequency of 50.3 MHz. High resolution ^{13}C NMR at magic angle spinning (MAS) was performed at room temperature with spinning frequencies from 4 kHz up to 9 kHz. ^{13}C NMR static spectra were obtained in the temperature range of $50 - 300$ K. ^7Li and ^1H NMR measurements were performed on a home built pulsed NMR spectrometer equipped with a sweep magnet working at 4.2 T and 6 T. In this study, the corresponding Larmor frequencies have been used : 70.2 MHz and 100 MHz for ^7Li and 180.5 MHz for ^1H. ^{1}H and ^{13}C NMR line shifts were referred to TMS, ^7Li NMR line shifts to 1M $LiCl$ as an external standard. All spectra were recorded using a Hahn echo pulse sequence and Fourier transformation. Spin-lattice relaxation rates T_1^{-1} were obtained using a saturation recovery pulse technique and a Hahn echo as a detection sequence.

Static and high-resolution MAS ^{13}C NMR spectra of the pristine and Li-intercalated SWNT are presented in figure 3.1. The static spectra on the left side show the evolution of the sp^2

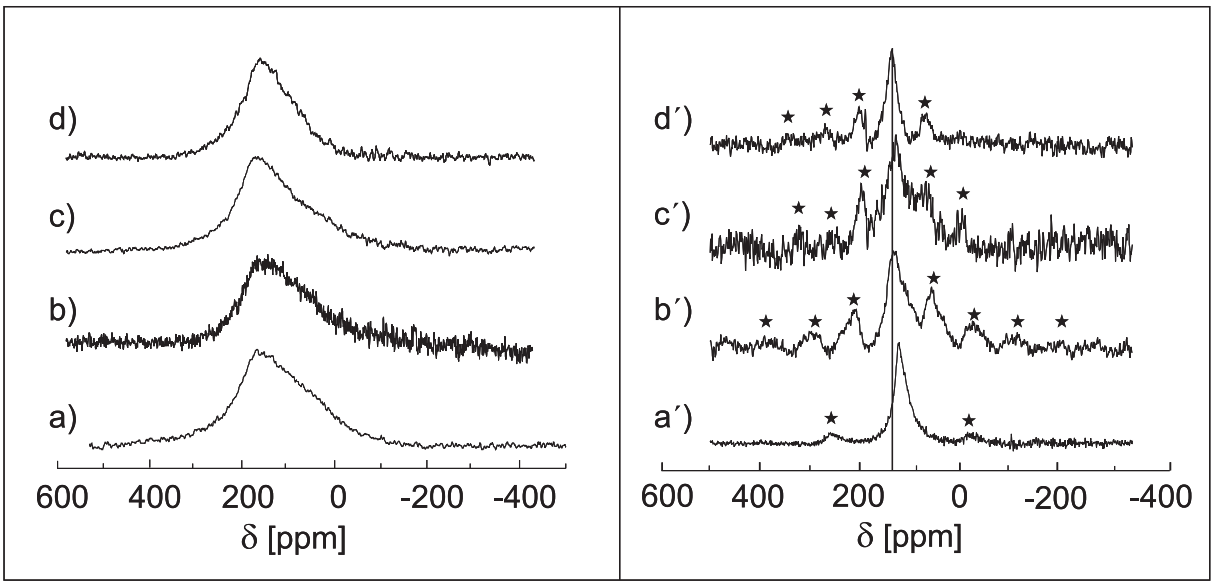

Figure 3.1: ^{13}C NMR spectra ($\omega_0 = 50.3\ MHz$) at room temperature of pristine SWNT [15] a) and LiC_x intercalated compounds with $x = 10, 7, 6$, b), c) and d), respectively. On the left side, the static ^{13}C NMR spectra are presented and on the right side the high resolution ^{13}C MAS NMR spectra. The symbols $\star$ are for the spinning sidebands. Spinning rates are about 9 kHz in a') and 4 kHz in b'), c') and d')

powder pattern lineshape of SWNT under Li intercalation. A clear reducing of the anisotropy is observed with increasing the amount of intercalated Li. The sideband distributions on the corresponding MAS spectra on the right side of figure 3.1 confirms this fact. We estimated a reduction of the anisotropy of about 200 ppm from LiC_{10} to LiC_6. In addition, the isotropic lines positions δ_{iso} are paramagnetically shifted from 126 ppm for the pristine SWNT [8, 15] up to 136 ppm in LiC_6. According to literature on carbon intercalation compounds[16, 17], these observations indicate important modifications of the electronic properties and suggest that all samples exhibit a metallic state tunable by the amount of intercalated Li. In order to interpret our data, we developed the following analysis. The observed shift δ can be separated into two parts, the chemical shift σ and the Knight shift $\mathbf{K}$ according to

$$\delta = \sigma + \mathbf{K}. \tag{3.1}$$

σ and $\mathbf{K}$ are second rank tensors consisting of an isotropic and an anisotropic part. The chemical

shift σ arises from local orbital magnetic fields caused by local currents in the sample. The Knight shift **K** arises from the hyperfine coupling of conduction electron spins to nuclear spins [18] and tends to narrow the ^{13}C NMR lineshape in carbon intercalation compounds [16]. The isotropic part of the Knight shift is paramagnetic and proportional to the conduction electron probability at the nucleus $|\Psi(0)|^2$ and the density of states at the Fermi level $n(E_F)$:

$$K_{iso} = \frac{8\pi}{3}|\Psi(0)|^2\mu_B^2 n(E_F) \tag{3.2}$$

K_{iso} has been estimated in pristine metallic SWNT to be less than 10 ppm[15, 20]. Since the isotropic Knight shift is proportional to $n(E_F)$, our measurements suggest an increasing of $n(E_F)$ with Li concentration. However, it is not trivial to estimate $n(E_F)$ directly from the isotropic line position because of the unknown isotropic chemical shift in charged SWNT.

In order to obtain a better estimate of $n(E_F)$, we performed ^{13}C NMR spin-lattice relaxation measurements as a function of temperature. The inset of figure 3.2 presents the magnetization recovery at room temperature for pristine and LiC_6 SWNT. For all Li intercalated samples, 96% of the ^{13}C NMR signal exhibits a single T_1 component which can be fitted by an exponential recovery curve after saturation[21, 22]. The corresponding T_1^{-1} relaxation rates are plotted in figure 3.2. Above a temperature of 50 K, we observed a linear regime with a slope depending on the lithium intercalation level. Below 50 K, the relaxation rate increases again, which is attributed to relaxation by magnetic catalyst impurities present in the sample[8]. The linear increase of the relaxation rate above 50 K is typical for a metallic Fermi liquid system. In metals the major relaxation mechanism is caused by the hyperfine coupling of conduction electron spins with the observed nuclei. This leads to the Korringa relation given by

$$\frac{1}{T_1 T} = \frac{2\pi k_B}{\hbar} A_{iso}^2 n(E_F)^2, \tag{3.3}$$

where A_{iso} is the isotropic hyperfine coupling constant[18]. As previously reported in pristine SWNT[8, 15, 23], we assume a hyperfine coupling of $A_{iso} = 8.2 \times 10^{-7}\ eV$ and fit the linear regime part of the ^{13}C NMR spin lattice relaxation. Hence, we were able to estimate the evolution of the $n(E_F)$ with the Li concentration, as reported in table 3.1. In agreement with lineshape modifications, the highest $n(E_F)$ corresponds to a large amount of Li-intercalation.

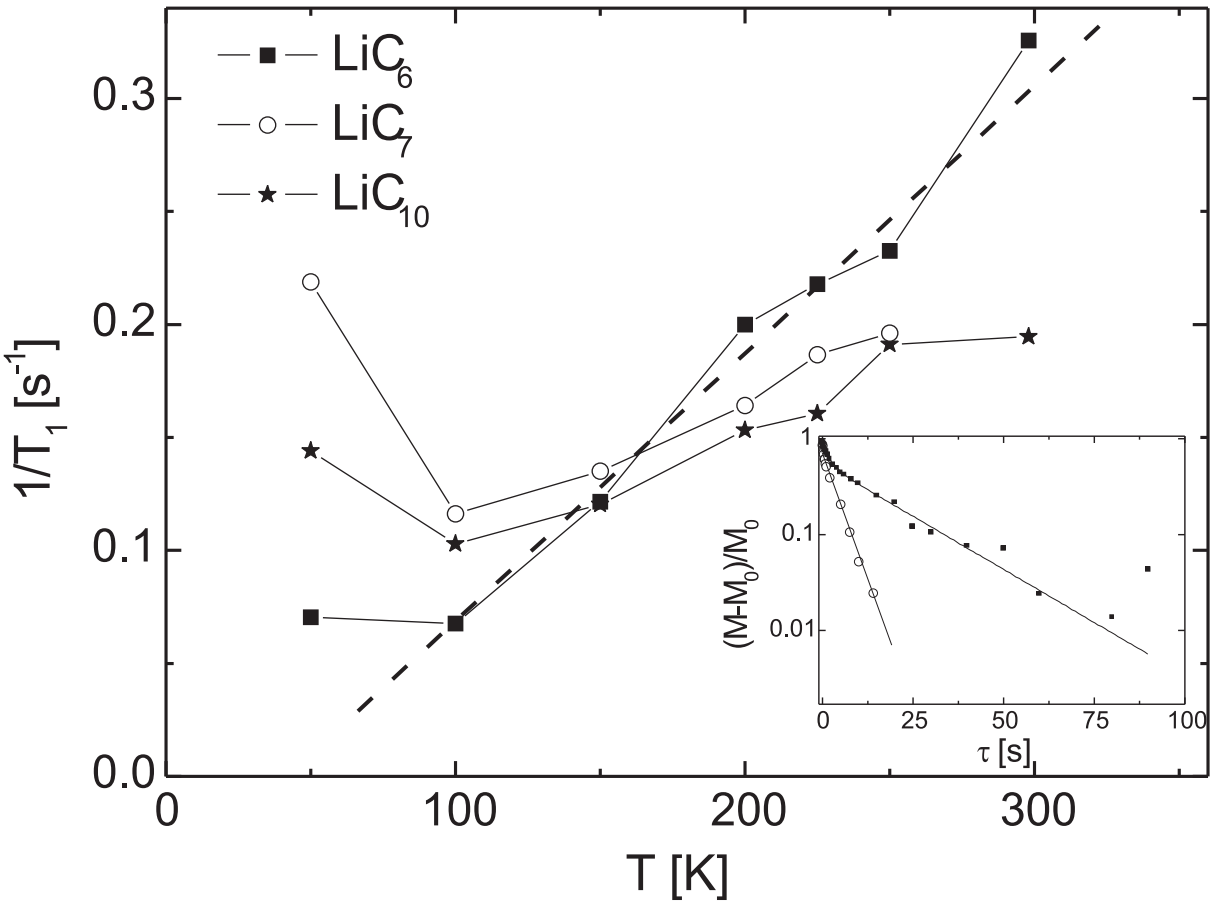

Figure 3.2: Temperature dependent ^{13}C NMR spin lattice relaxation rates ($\omega_0 = 50.3\ MHz$) for LiC_{10} : ★, LiC_7 : ∘ and LiC_6 : ■ . Inset : ^{13}C NMR magnetization recovery at room temperature for LiC_6 : ∘ and pristine SWNT : ■[15].

We turn now to the ^7Li NMR spectrum and spin-lattice relaxation measurements in the temperature range from 50 K to 465 K. In all the samples for all temperatures, the recovery of the magnetization follows a biexponential curve corresponding to two relaxation rates suggesting two inequivalent Li sites that we label α and β with $T_1^\alpha > T_1^\beta$. From the fits of the magnetization recovery, the following ratios between α and β sites can be estimated : for LiC_{10} [$\alpha : 70\%$ $\beta : 30\%$], for LiC_7 [$\alpha : 55\%$ $\beta : 45\%$] and for LiC_6 [$\alpha : 50\%$ $\beta : 50\%$]. We found that the first intercalated Li are of type $Li^{+\alpha}$ and increasing the Li concentration a second type $Li^{+\beta}$ is adsorbed by the SWNT host. In order to estimate the corresponding ^7Li NMR resonances, we investigate the lineshift and linewidth during the relaxation measurements. The inset of figure 3.3 shows the spectra for LiC_{10} at 50 K during the magnetization recovery experiment at two different delays. The best fits of the partially recovered spectrum (figure 3.3a) and fully

SWNT Sample	$n(E_F)$ states/eV spin atom
LiC_6	0.032
LiC_7	0.020
LiC_{10}	0.021
Pristine metallic SWNT	0.015[15, 23]

Table 3.1: Density of states at the Fermi level $n(E_F)$ for LiC_x with $x = 6, 7, 10$ and pristine metallic SWNT.

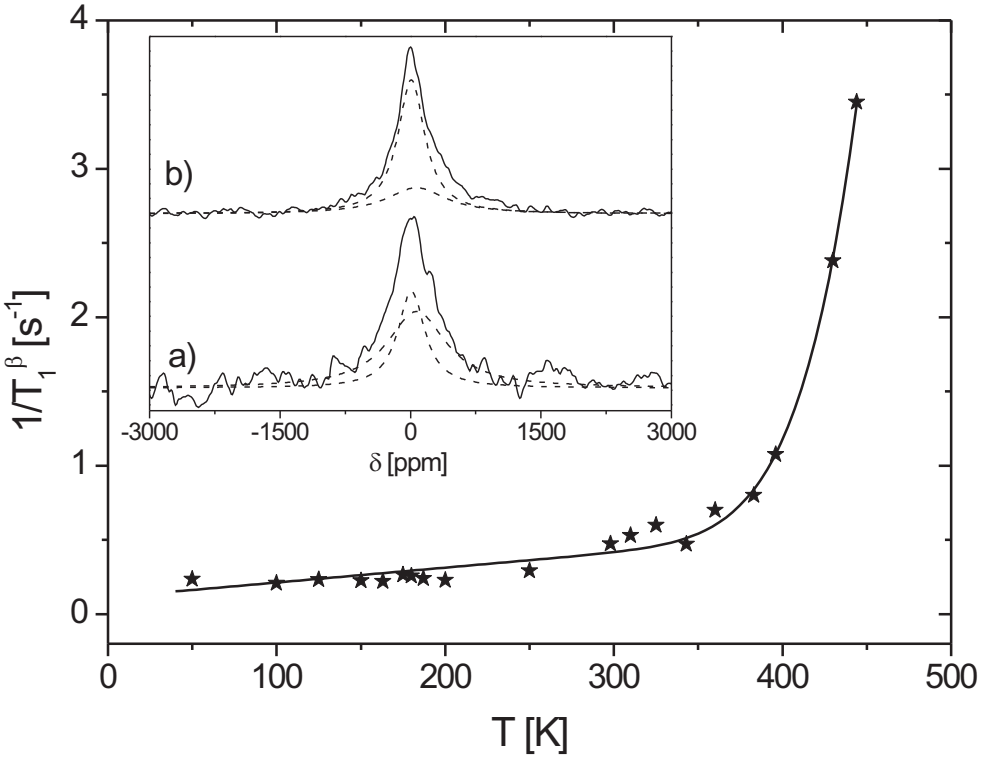

Figure 3.3: Temperature dependent ^7Li NMR spin lattice relaxation rate $1/T_1^{\beta}$ ($\omega_0 = 100\ MHz$) for LiC_{10} : ★. The solid line is a fit according to equations 3.4. Inset: ^7Li NMR spectra in LiC_{10} at 50 K extracted from magnetization recovery experiments : a) partially recovered spectrum at a short delay : 0.8 s and b) fully relaxed spectrum at a long delay 22 s. The ratios in a) [$\alpha : 37\%\quad \beta : 63\%$] and in b) [$\alpha : 70\%\quad \beta : 30\%$] are obtained from a deconvolution (dashed lines) with one sharp-α and one broad-β Lorentzian line as described in the text.

relaxed one (figure 3.3b) were performed assuming one sharp-α and one broad-β Lorentzian line at $\delta_\alpha \approx 10$ *ppm* and $\delta_\beta \approx 70$ *ppm*, respectively. Their intensities were determined according to their relaxation behaviors : $T_1^\alpha \approx 3.8$ *s* and $T_1^\beta \approx 0.54$ *s* and their ratios extracted from the magnetization recovery curve. These results confirm the presence of two different cations ; one $Li^{+\alpha}$ with an ionicity close to +1 and a $Li^{+\beta}$, *i.e.* $+1 \approx \alpha > \beta$. The paramagnetic shift of the β-line can be interpreted as a Knight shift which is typical for a limited charged transfer of the $2s$ electron of the Li stored in a dense form in nanoporosity [24]. The quadrupolar broadened ^7Li NMR β-line as observed in our spectrum, suggests the presence of strong interactions between C and $Li^{+\beta}$ like in GIC (graphitic intercalation compounds). The origin for the two inequivalent sites is unknown, but it is certainly related to the complex structure of bundles of carbon nanotubes which presents different adsorption sites [25, 26] giving inequivalent environments and hybridized electronic states for the Li. According to recent calculations[26], the outside-Li adsorption is energetically more favorable than the Li inside the SWNT. In particular, the curvature of the graphene layer in SWNT and the presence of high reactive dangling bonds localized on defects tend to enhance the adsorption capabilities[2, 16]. Solid state electrochemistry revealed that electrochemical Li intercalation in SWNT is only partially reversible. The authors claim that upon de-doping some Li remains trapped in the SWNT host [27]. This would confirm the strong interactions between Li and C in our samples. Figure 3.3 presents the $1/T_1^\beta$ relaxation rate of the ^7Li NMR β-line for LiC_{10}. We observe a linear regime below 400 K and a rapid increase above. According to the Korringa relation[18], the linear relaxation regime is typical for the hyperfine coupled Li nuclei to the conduction electrons. Fitting our data we obtain $1/T_{1K}^\beta T \approx 0.00081\ s^{-1}K^{-1}$. This value is close to $1/T_{1K}T \approx 0.0016\ s^{-1}K^{-1}$ for a first stage Li-graphite intercalation compound LiC_6[29] and well below $1/T_{1K}T \approx 0.023\ s^{-1}K^{-1}$ for pure Li^0 metal [28]. These results again suggest a strong interaction between the Li with the nearly free electron π system of the SWNT. Let us now turn to the rapid increase of $1/T_1^\beta$ above 400 K. We attributed this deviation from the Korringa's law to a diffusion or motion modulated quadrupolar interaction. A thermally activated diffusion path of Li is expected along the channels of the carbon nanotube bundles. Therefore the relaxation of the ^7Li nuclei promoted by conduction electrons and fluctuation of local electric field gradients can be readily expressed

according to Ref [19] as

$$\frac{1}{T_1^\beta} = \frac{1}{T_{1B}^\beta} + \frac{1}{T_{1K}^\beta} + \frac{1}{T_{1Q}^\beta}, \qquad \frac{1}{T_{1Q}^\beta} = \frac{2}{25}\Delta\omega_Q^2 \left[J^{(1)}(\omega_0) + J^{(2)}(\omega_0) \right]. \tag{3.4}$$

where $\Delta\omega_Q$ is quadrupolar coupling constant and $J^{(i)}(\omega_0)$ are the spectral densities corresponding to a thermally activated process,

$$J^{(1)}(\omega_0) = \frac{\tau_c}{1+\omega_0^2\tau_c^2}, \qquad J^{(2)}(\omega_0) = \frac{4\tau_c}{1+4\omega_0^2\tau_c^2}, \qquad \tau_c = \tau_0 \exp\left(\frac{\Delta E}{k_B T}\right) \tag{3.5}$$

where ω_0 is the Larmor frequency, $\tau_0 \approx 10^{-12} s$ is the infinite temperature correlation time and ΔE is the activation energy. We estimated a constant background $1/T_{1B}^\beta \approx 0.12\ s^{-1}$ and $\Delta E \approx 400\ meV$ from a fit shown in figure 3.3. This value is about 2 times higher than reported for a first stage Li-GIC compound LiC_6 with $\Delta E = 221\ meV$ [30]. Our activation energy is expected to be higher since strong interactions between Li and C and diffusion along nearly one dimensional channels should be overcome.

In order to understand the role of the cointercalated solvent molecules THF, we performed also ^1H NMR measurements versus temperature. The ^1H NMR spectra for LiC_7 are shown in the inset of figure 3.4. At low temperatures the spectrum consists of a broad Lorentzian line diamagnetically shifted to $\delta = -29\ ppm$. This negative diamagnetic chemical shift is unusual and remarkably high for organic materials. ^1H NMR chemical shifts usually range from 0 to +12 ppm. We explain this observation by an extremely large diamagnetic shielding of the carbon nanotubes. Therefore the diamagnetic susceptibility caused by π-electron orbital magnetism of the sp^2 carbon bonds should also be very large for SWNT. Besides the broad line at low temperatures a second sharp Lorentzian line around $\delta = -3.2$ ppm shows up around room temperature. This clearly indicates the existence of two inequivalent proton sites. With increasing temperature a line narrowing is observed giving evidence for molecular motion. As spin-lattice relaxation is sensitive to local field fluctuations induced by the motion of the nuclei we have performed temperature dependent ^1H spin-lattice relaxation experiments. Figure 3.4 presents the ^1H NMR T_1^{-1} data of the sharp line. It is interesting to note that we found a similar temperature dependance for the ^7Li NMR T_1^{-1} data suggesting that THF molecules and Li^+ show thermally activated dynamics above 300 K. It has been shown in GIC that THF

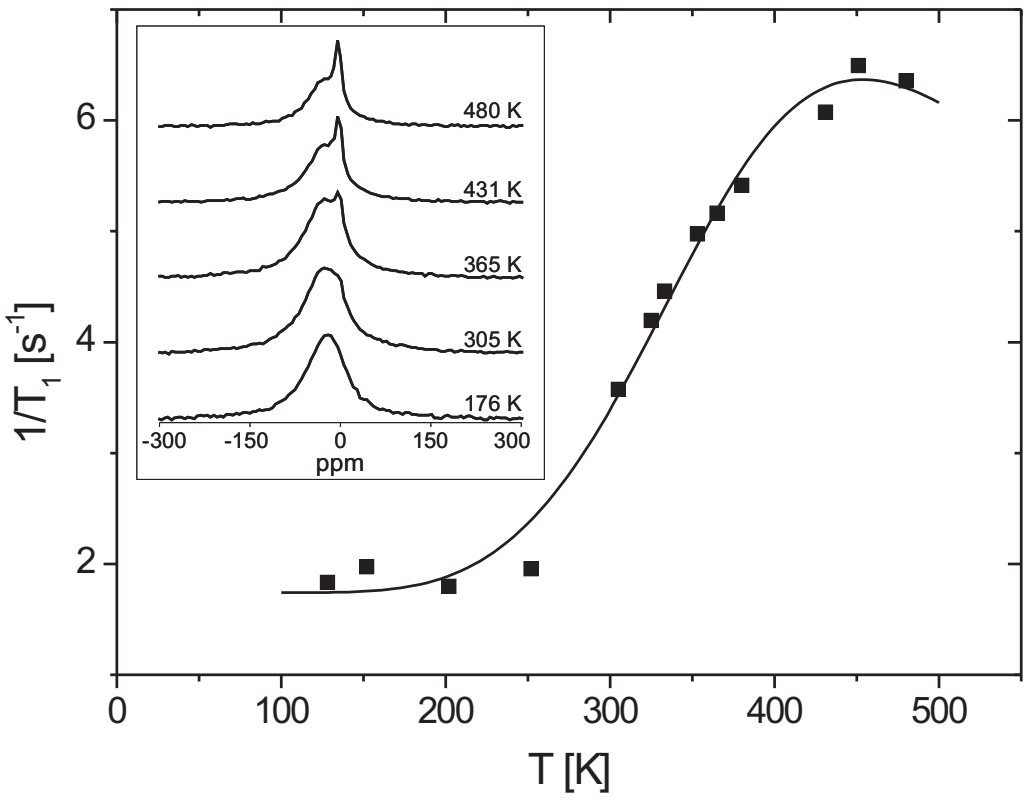

Figure 3.4: ^1H NMR ($\omega_0 = 180.5\ MHz$) spin-lattice relaxation rates for LiC_7 and its fit according to thermally activated dynamics : $\Delta E \approx 100\ meV$. Inset : ^1H static NMR spectra in temperature which show one broad line and one thermally activated sharp line.

molecules are rotating between the graphene planes [12] hence similar dynamics could take place inside SWNT bundles above room temperature.

In summary, we have performed ^{13}C, ^7Li and ^1H solid state NMR measurements on Li intercalated SWNT. We have shown that Li is intercalated as a ternary compound $Li(THF)_yC_x$ ($x = 10$, 7, 6 and $y \approx 2$). Using ^{13}C NMR, we measured a variable charge transfer which depends on the Li content and calculated the density of states at the Fermi level. We found the existence of two inequivalent α and β sites for Li and suggest the existence of strong interactions between Li and C which limits the electronic charge transfer. We also point out that THF molecules and Li show thermally activated dynamics. We attribute this to both a Li-diffusion along the channels of the carbon nanotube bundles as well as a THF molecules rotation above 300 K. From ^1H NMR the observed large diamagnetic chemical shift gives evidence for a very high

diamagnetic susceptibility of SWNT. However this has to be confirmed by other methods which requires highly purified and catalyst free SWNT.

Bibliography

[1] M. Endo, C. Kim, K. Nishimura, T. Fujio and K. Miyashita, Carbon, 38, 183 (2000)

[2] B. Gao, A. Kleinhammes, X.P. Tang, C. Bower, L. Fleming, Y.Wu and O. Zhou, Chem. Phys. Lett. 307, 153 (1999)

[3] R.S. Lee, H.J. Kim, J.E. Fischer, A.Thess and R.E. Smalley, Nature (London) 388 255 (1997)

[4] A.M. Rao, P.C. Eklund, S. Bandow, A. Thess and R.E. Smalley, Nature (London) 388 257 (1997)

[5] A. Claye, PhD Thesis, University of Pennsylvania, (2000)

[6] E. Hernandez, C. Goze, P. Bernier and A. Rubio, Phys. Rev. Lett. 80, 4502 (1998)

[7] C. Journet, W.K. Maser, P. Bernier, A. Loiseau, M.L. de la Chapelle, S. Lefrant, P. Deniard, R. Lee and J.E. Fischer, Nature (London) 388, 756 (1997)

[8] C. Goze-Bac, S. Latil, L. Vaccarini, P. Bernier, P. Gaveau, S. Tahir, V. Micholet, R. Aznar, A. Rubio, K. Metenier and F. Beguin, Phys. Rev. B 63, 100302 (2001)

[9] P. Petit, E. Jouguelet and C. Mathis, Chem. Phys. Lett. 318, 516 (2000)

[10] N. Bendiab, E. Anglaret, J.L. Bantignies, A. Zahab, J.L. Sauvajol, P. Petit, C. Mathis and S. Lefrant, Phys. Rev. B 64, 245424 (2001)

[11] J.L. Sauvajol, N. Bendiab, E. Anglaret and P. Petit, C.R. Physique 4 (2003)

[12] L. Facchini, M. Quinton and A. Legrand, Physica B 99, 525 (1980)

[13] O. Tanaike and M. Inagaki, Carbon 35, 831 (1997)

[14] M. Inagaki and O. Tanaike, Carbon 39, 1083 (2001)

[15] C. Goze-Bac, S. Latil, P. Lauginie, V. Jourdain, J. Conard, L. Duclaux, A. Rubio and P. Bernier, Carbon 40, 1825 (2002)

[16] P. Lauginie, Ph.D. thesis, University of Paris-Sud, centre d'Orsay, (1988)

[17] P. Petit, C. Mathis, C. Journet and P. Bernier, Chem. Phys. Lett. 305, 370 (1999)

[18] A. Abragam, *Les Principes du Magnétisme Nucléaire*, Presses Universitaires de France, Paris (1961)

[19] M. Mehring and A. Weberruss, *Object-Oriented Magnetic Resonance*, Academic Press, San Diego, San Francisco, New York, Boston, London, Sydney, Tokyo, (2001)

[20] S. Latil, L. Henrard, C. Goze-Bac, P. Bernier and A. Rubio, Phys. Rev. Lett. 86, p 3160 (2001)

[21] M. Schmid, C. Goze-Bac, M. Mehring, S. Roth and P. Bernier, Electronic Properties of Novel Materials, XVII International Winterschool, Ed. H. Kuzmany, K. Fink, M. Mehring and S. Roth, World Scientific 723, 238 (2004),

[22] H. Shimoda, B. Gao, X.P. Tang, A. Kleinhammes, L. Fleming, Y. Wu and O. Zhou, Phys. Rev. Lett. 88, 15502 (2002)

[23] X.P. Tang, A. Kleinhammes, H. Shimoda, L. Fleming, K.Y. Bennoune, S. Sinha, C. Bower, O. Zhou and Y. Wu, Science 288, 492 (2000)

[24] K. Tatsumi, J. Conard, M. Nakahara, S. Menu, P. Lauginie, Y. Sawada and Z. Ogumi, J. Power Sources 81, 397 (1999)

[25] J. Lu, S. Nagase, S. Zhang and L. Peng, Phys. Rev. B 69, 205304 (2004)

[26] Y. Liu, H. Yukawa and M. Morinaga, Computational Materials Science 30, 50 (2004)

[27] A. Claye, J.E. Fischer, C.B. Huffman, A.G. Rinzler and R.E. Smalley, J. Electrochem. Soc. 147 2845 (2000)

[28] A.G. Anderson and A.G. Redfield, Phys. Rev. 116, 583 (1959)

[29] H. Estrade, J. Conard, P. Lauginie, P. Heitjans, F. Fujara, W. Buttler, G. Kiese, H. Ackermann and D. Guerard, Physica B 99, 531 (1980)

[30] P. Yu, B.N. Popov, J.A. Ritter and R.E. White, J. Eclectrochem. Soc. 146, 8 (1999)

Chapter 4

Nanomagnetic shieldings

The understanding and control of the magnetic properties of carbon-based materials is of fundamental relevance in applications in nano and bio-sciences. Ring-currents do play a basic role in those systems. In particular the inner cavities of nanotubes offer an ideal environment to test and manipulate the magnetic properties of hybrid materials systems at the nanoscale. Here, by means of ^{13}C high resolution NMR of the encapsulated molecules in peapod hybrid materials, we report the largest diamagnetic shifts (down to -68.3 ppm) ever observed in carbon allotropes, which is connected to the enhancement of the aromaticity of the nanotube envelope upon doping. This diamagnetic shift can be externally controlled by in-situ modifications like doping or electrostatic charging. Moreover, defects like C-vacancies, pentagons and chemical functionalization of the outer nanotube quench this diamagnetic effect and restore NMR signatures to slightly paramagnetic shifts compared to non-encapsulated molecules. The magnetic interactions reported here are robust phenomena independent of temperature and proportional to the applied magnetic field. The magnitude, tunability, and stability of the magnetic effects make the peapod nanomaterials potentially valuable for nanomagnetic shielding in nanoelectronics and nanobiomedical engineering. All hybrid carbon nanotube materials are expected to exhibit similar behaviors.

Carbon nanotubes are intriguing new forms of carbon, offering molecular-scale cylinders expected to provide important solutions for challenges of 21^{st} century materials engineering. Since 1991[1], they have been extensively studied due to their unique properties presaging potential applications in electronic devices, composites, chemical and biochemical sensors. They have diameters in the range of nanometers and lengths of several centimeters. Filling the interior

of molecular cylinders like multiwall nanotubes with Pb metal[2] or single wall nanotubes with fullerene C_{60} [3] have been demonstrated. The discovery of these new hybrid materials , which have been given the vernacular name "peapods" has generated a considerable amount of fundamental and experimental studies on their structural and electronic properties. However, little is known regarding their magnetic properties, since experiments are quite difficult to elucidate due to the difficult-to-avoid presence of residual ferromagnetic catalyst in the samples. In this letter, highly magnetically purified samples[4] and specific isotopic enrichment have been used to circumvent this crucial problem. Hence, ^{13}C Nuclear Magnetic Resonance turns out to be suited to measure accurately the intrinsic local magnetic properties of hybrid materials such as peapods.

Studies of nanotubes, as with fullerenes ten years ago[6, 7], are expected to further our understanding of the magnetism of individual molecules and its relationship with their aromatic character. In the case of peapod materials, the control and manipulation of the magnetism at the nanoscale inside the nanotubule can be considered through the possibility to tune the flow of currents around the ring system of the outer nanotube.

In the experiments discussed here, the magnetic properties of five different types of hybrid materials characteristic of the peapods with different preparation routes have been investigated. Separate batches of electric arc nanotubes were produced at the University of Montpellier and purchased from Carbon Solutions Inc. They were purified using a novel magnetic filtration method [4] at the University of Pennsylvania. The encapsulation of 25% ^{13}C enriched fullerenes (purchased from MER Corporation) within the nanotubes was conducted at the University of Pennsylvania and at the University of California Berkeley by using vapor phase filling [8]. The experimental procedures for the hydrogenation of C_{60} (University of Umeå) and the Rb intercalation (University of Pennsylvania) can be found in the following references, respectively [9] and [10, 11]. X-ray diffraction and Transmission Electron Microscopy were used to ensure the high quality of the peapod samples[4] . High-resolution ^{13}C NMR experiments were carried out at the University of Montpellier on spectrometers Bruker ASX200 and Tecmag Apollo at magnetic fields of 9.4 T, 4.7 T and 3.3 T corresponding to Larmor Frequencies of 100.6 MHz, 50.3 MHz and 35.8 Mhz, respectively. In all the experiments, the spin-lattice relaxation times were considered in order to measure NMR spectra under qualitative and quantitative conditions.

Figure 4.1 presents the high resolution ^{13}C NMR spectra recorded for magnetically purified empty nanotubes compared to the five peapod samples. A summary of line-positions and

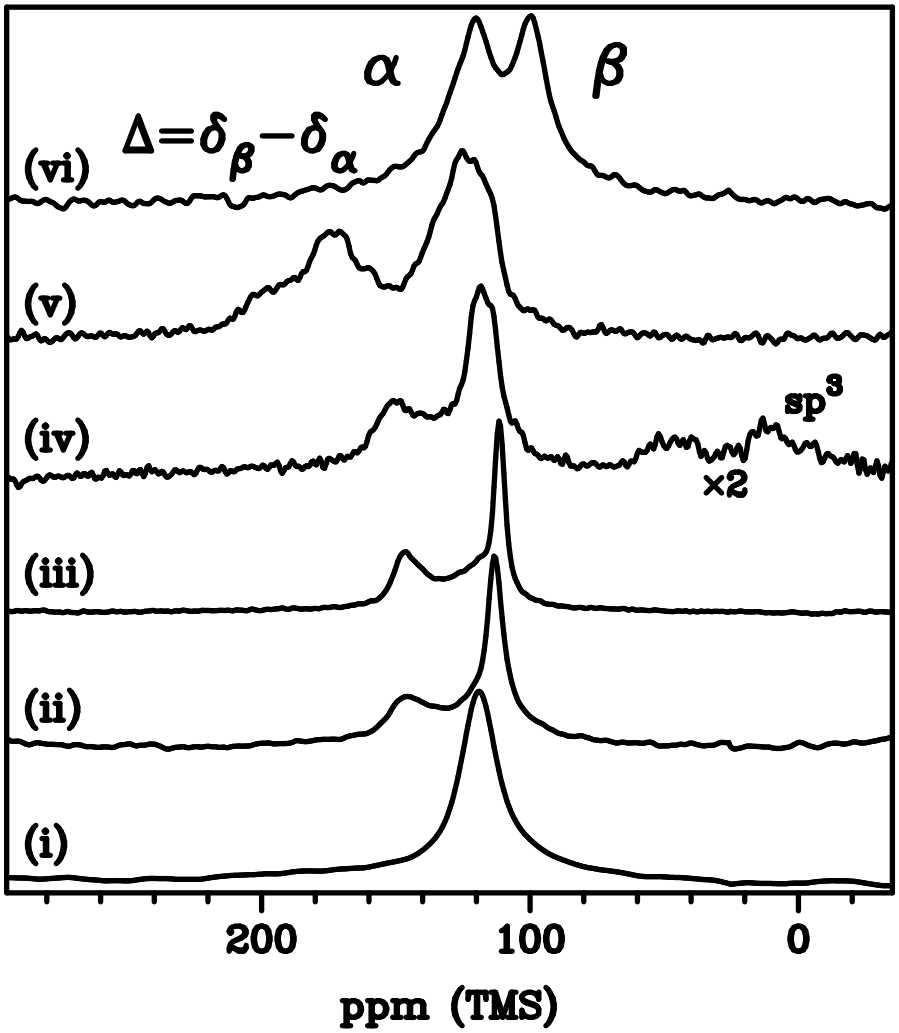

Figure 4.1: ^{13}C NMR isotropic lines from high resolution MAS experiments (50.3MHz) at a spinning rate of 10 kHz of (i) magnetically purified single wall carbon nanotubes of 1.4 nm diameter and hybrid peapod materials with encapsulated molecules like (ii) and (iii) fullerene C_{60}, (iv) hydrogenated $C_{60}H_x$ with x<18 , (v) Rb-intercalated C_{60} and (vi) carbon nanotubes of 0.7nm diameter (double-walled carbon nanotubes with the inner tube produced through the heating-induced coalescence of encapsulated C_{60} molecules). All the spectra from (ii) to (vi) present two contributions labelled α and β (line shifts and splittings are reported in Table 4.1). Note that on spectrum (iv), the same Δ splitting is observed on C-C sp^2 and C-H sp^3 lines located at 45 ppm, clearly confirming the magnetic shieldings.

line-splittings can be found in Table 4.1. According to the natural abundance of 1.1% of ^{13}C in the outer nanotube, the 25% abundance of ^{13}C in the enriched and encapsulated C_{60} fullerene

Encapsulated Molecules	δ_α (ppm)	δ_β (ppm)	I_β (%)	$\Delta = \delta_\beta - \delta_\alpha$ (ppm)	$\delta_{\text{outer-NT}}$ (ppm)
C_{60} (ii)	148.2	111.3	68.2	-36.9	118.8
C_{60} (iii)	147.2	112.2	75.0	-35.0	118.8
Hydrogenated C_{60} (iv)	152.1	117.8	68.6	-34.3	118.8
Rb Intercalated C_{60} (v)	186.0	117.4	55.2	-68.3	128.0
Inner NT $\approx$ 0.7 nm (vi)	125.8	99.2	59.6	-26.6	118.8

Table 4.1: ^{13}C NMR isotropic lines parameters for different encapsulated molecules inside carbon nanotubes. Paramagnetic α and diamagnetic β lines are observed in all the hybrid peapod materials in agreement with localized ring currents at the surface of the outer nanotube. We used I_α+I_β=100%, which gives directly the percentage between α and β encapsulated molecules. The 16% contribution of the outer nanotube is calculated from the integral of the spectra.

and a filling factor of ≈70% of the inner cylindrical space of the nanotubes, the contribution to the total NMR signal intensity from the outer nanotube in the spectra of all the peapods from (ii) to (vi) is estimated to be ≈16%. Consequently, these NMR spectra are dominated by the signal from the encapsulated molecules. A tutorial fit of the ^{13}C spectrum of a C_{60} peapod sample (ii) is given in Figure 4.2. The lineshape of the outer nanotube is fixed according to the spectrum presented in Figure 4.1(i) and its intensity following the previous remark . Two more contributions are needed to accurately fit the experimental data. The first line α at the position δ_α shows a paramagnetic shift of about +5 ppm from the line positions in *fcc*-C_{60} crystal[6] or in polymeric-C_{60} phases[12]. The second line β at the position δ_β presents a larger diamagnetic shift in the range of $\Delta = \delta_\beta - \delta_\alpha \approx -36$ ppm. Approximately 75% of the signal is of β type and diamagnetically shifted with respect to normal *fcc*-C_{60}. As presented in Figure 4.3, no dependence on temperature down to 20 K was observed in the spectra and Δ was clearly found to be proportional to the applied magnetic field. For all the investigated hybrid peapod materials, these two contributions α and β were observed with similar features as presented in Figure 4.1 and Table 4.1. This phenomenon is universal and even enhanced ($\Delta \approx -68.3$ ppm) in the case of the sample (v) corresponding to Rb intercalated C_{60} peapods for which the outer nanotubes are charged with electrons transferred from the alkali[13].

We show that peapods with several encapsulated molecules in the presence of an external magnetic field present robust diamagnetic and paramagnetic effects (Fig.4.1) which are independent of temperature and proportional to the magnetic field strength (Fig.4.3). Our results can be interpreted in terms of the magnetism of the carbon honeycomb structure with the retention

Figure 2

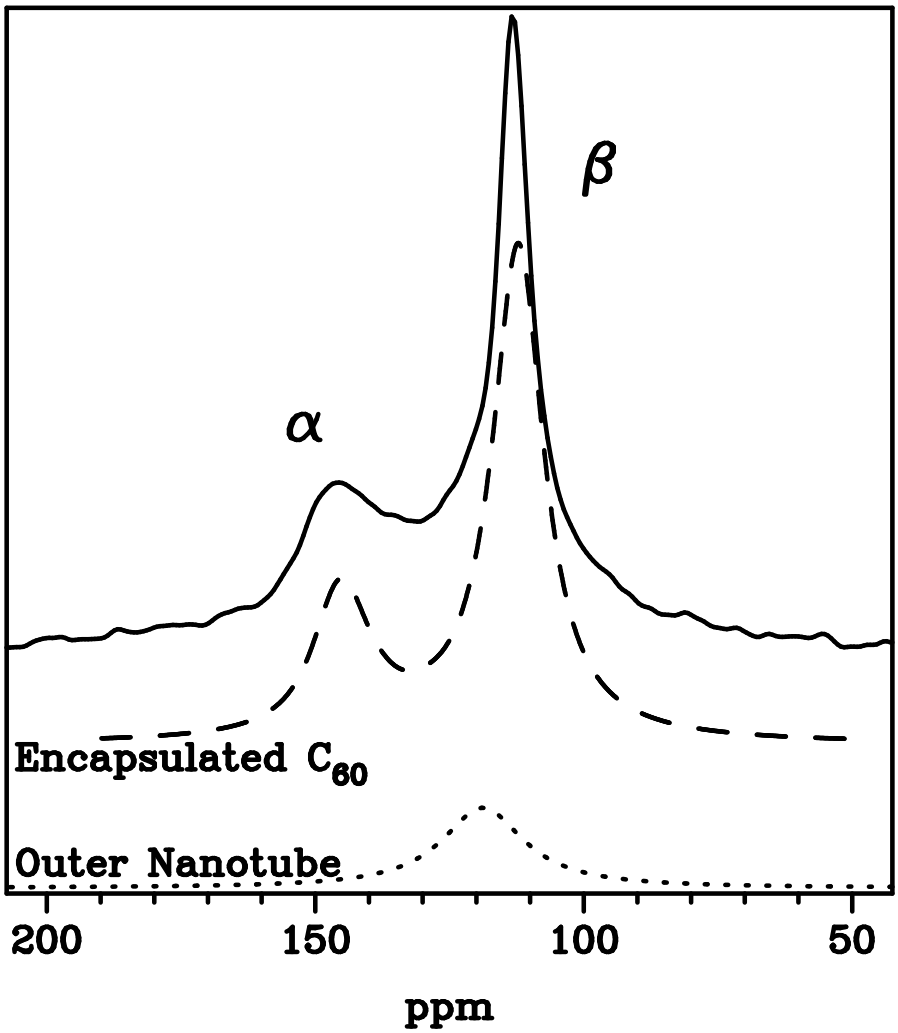

Figure 4.2: ^{13}C NMR isotropic lines from high resolution MAS experiments (50.3 MHz) at a spinning rate of 10 kHz of 25% ^{13}C enriched C_{60} "peas" encapsulated inside natural abundance carbon nanotube "pods" (solid line), 16% outer nanotubes contribution (dotted line), paramagnetic shifted α line and diamagnetic shifted β line from encapsulated C_{60} molecules.

and the destruction of delocalized π ring currents circulating around the outer nanotube. Our experimental findings definitively support important theoretical works on the diamagnetism of carbon materials which have been published in the past[5, 6, 7] and more recently[14, 15]. Such magnetic properties are of great interest and in particular the case of charged C_{60} peapods which presents the largest diamagnetic shielding ever encountered in carbon allotropes. These experimental results provide new insight into the magnetic properties of carbon allotropes and ring current computations[5, 6] as they clearly show that the largest obtainable diamagnetic

Figure 3

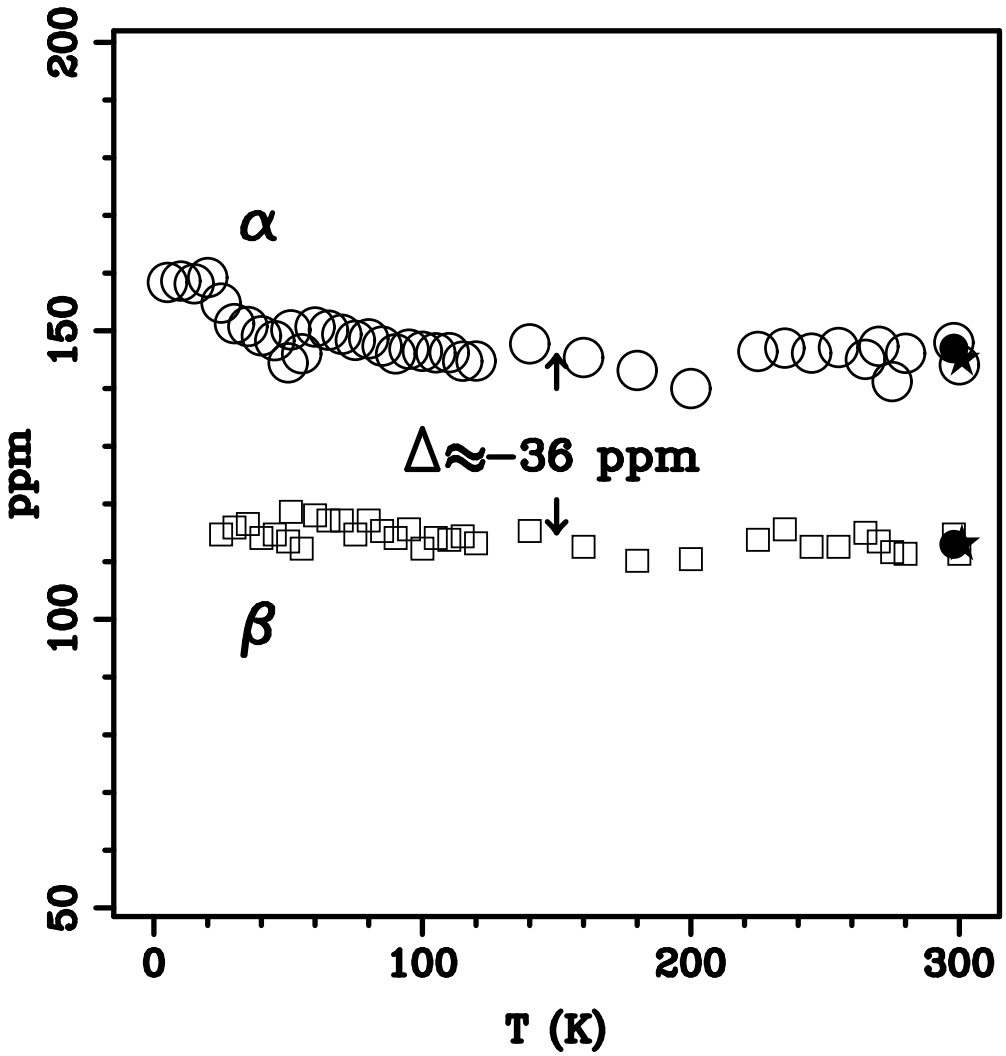

Figure 4.3: Temperature dependence of the ^{13}C NMR lines positions at 4.7 T (50.3 MHz) of the 25% ^{13}C enriched C_{60} peapods, comprised of 1-D chains of C60 molecules encapsulated inside natural abundance carbon nanotubes. Open circles are for δ_α and open squares for δ_β. Solid circles and stars correspond to experiments performed at 9.4 T (100.6 MHz) and 3.3 T (35.0 MHz), respectively. Δ is proportional to the applied magnetic field and shows no dependence on temperature down to 20 K. At lower temperature, the broadening of the β line prevents an accurate determination of its shift.

shielding is not inside a doped C_{60} ball[7] but inside a doped carbon nanotube.

Concerning the slightly paramagnetic shifted line α, we suggest, consistent with theoretical studies, that topological defects such as vacancies, bond rotations and holes in the outer shell will enhance the local paramagnetic ring currents[16, 17, 18]. π electrons are not free to precess in the magnetic field but are constrained to move along the bonds and the defects of the outer nanotube. This phenomenon is well known[6] to quench diamagnetism in carbon allotropes via Van

Vleck paramagnetism. The data presented here provides strong evidence that this mechanism exists also in carbon nanotubes and peapods ; this phenomenological observation suggests several unprecedented possibilities. If incorporating defects produces paramagnetic ring currents, electrostatic charging or electron charge transfer by intercalation or substitution are expected to enhance the diamagnetism by increasing the aromaticity of the outer shell.

Peapod hybrid materials present π electrons moving in the outer nanotube which govern the magnetic fields inside the one-dimensional cavity of the nanotube. In the light of our study, it is now possible to tune and control the magnetic properties of peapods at the nanoscale by tailoring the molecular and electronic structures of the encapsulating nanotube. One potential and important application of this phenomenon in Magnetic Resonance Imaging or Spectroscopy would be to interface nanotubes with living cells[19] and to track them at the nanoscale through hyperlocalyzed diamagnetic or paramagnetic magnetic fields which affect nuclear magnetic resonance conditions[20]. Our current investigations presage that peapod hybrid materials and nanotubes in general, are suitable for nanomagnetic shielding in nanoelectronics and nanobiomedical engineering and will presumably enhance in the near future experimental resolution to unprecedented levels.

Bibliography

[1] S. Iijima, Nature 354, 56 (1991)

[2] P. Ajayan, S. Iijima, Nature 361 333 (1993)

[3] B. Smith, M. Monthioux and D. Luzzi, Nature 396, 323 (1998)

[4] Y. Kim, O. Torrens, J. Kikkawa, E. Abou-Hamad, C. Goze-Bac and D. Luzzi, Chem. Mater. 192982 (2007)

[5] A. Pasquarello, M. Schlueter, and R. C. Haddon, Science 257, 1660 (1992)

[6] R. Haddon, Nature 378 249 (1995)

[7] G. Wang, B. Weedon, M. Meier, M. Saunders and R. Cross, Org. Lett. 2, 2241 (2000)

[8] B. Smith and D. Luzzi, Chem. Phys. Lett. 321 169 (1999)

[9] T. Wågberg, D. Johnels, A. Peera, M. Hedenström, Y. Schulga, Y. Tsybin, J. Purcell, A. Marschall, D. Noreus, T. Sato and A. Talyzin, Org. Lett. 7 5557 (2005)

[10] R. Meyer, J. Sloan, R. Dunin-Borkowski, A. Kirkland, M. Novotny, S. Bailey, J. Hutchisonx and M. Green, Science 289, 1324 (2000)

[11] T. Pichler, H. Kuzmany, H. Kataura and Y. Achiba, Phys. Rev. Lett. 87 267401 (2001)

[12] C. Goze, F. Rachdi, L. Hajji, M. Núñez-Regueiro, L. Marques, J. L. Hodeau and M. Mehring, Phys. Rev. B 54 R3676 (1996)

[13] M. Schmid, C. Goze-Bac, S. Kramer, M. Mehring, P. Petit and C. Mathis, Phys. Rev. B 74 073416 (2006)

[14] M. Marques, M. d'Avezac and F. Mauri, Phys. Rev. B 73 125433 (2006)

[15] N. Besley and A. Noble, J. Chem. Phys. 128 101102 (2008)

[16] H. Imai, P. Babu, E. Oldfield, A. Wieckowski, D. Kasuya, T. Azami, Y. Shimakawa, M. Yudasaka, Y. Kubo and S. Iijima, Phys. Rev. B 73 125405 (2006)

[17] M. Ling, T. Finlayson and C. Raston, Aust. J. Phys. 52 913 (1999)

[18] F. Lopez-Urias, J. Rodriguez-Manzo, E. Muñoz-Sandoval, M. Terrones and H. Terrones, Optical Materials 29 110 (2006)

[19] X. Chen, A. Kis, A. Zettl and C. Bertozzi, PNAS 104 8218 (2007)

[20] J. Pope, D. Jonas and R. Walker, Magn. Reson. Imaging, 13 763 (1995)

Chapter 5

Molecular dynamics and phase transition in one dimensional crystal of C_{60} encapsulated inside single wall carbon nanotubes

One dimensional crystal of 25% ^{13}C enriched C_{60} encapsulated inside highly magnetically purified SWNT was investigated by following the temperature dependence of the ^{13}C NMR line-shapes and relaxation rates from 300 K down to 5 K. High Resolution MAS techniques reveal that 32% of the encapsulated molecules so called the C_{60}^{α} are blocked at room temperature and 68% labelled C_{60}^{β} are shown to reversly undergo molecular reorientational dynamics. Contrary to previous NMR studies, spin-lattice relaxation time reveals a phase transition at 100 K associated with the changes in the nature of the dynamics of the C_{60}^{β}. Above the transition, the C_{60}^{β} exhibit continous rotational diffusion ; below the transition, C_{60}^{β} execute uniaxial hindered rotations certainly along the nanotubes axis and freeze out below 25 K. The associated activation energies of these two dynamical regimes are measured to be 6 times lower than in fcc-C_{60} suggesting a quiet smooth orientational dependence of the interaction between C_{60}^{β} molecules and the inner surface of the nanotubes.

Among the various properties of Single Wall carbon NanoTube [1, 2, 3, 4, 5] the quasi one

dimensional inner space they provide is unique. They are molecular cylinders of few nanometers in diameter and length of the order of centimeters. Peapod being one dimensional array of molecules inside SWNT is the archetype of molecular engineering at the nano-scale [6, 7]. Many interesting applications have been predicted in nanoelectronics, nanochemistry and nanobiomedical based on the physical properties of encapsulated molecules which are expected to be different from those in bulk, because of the one dimensional confinement and the reduction in the number of neighbors [8]. Unfortunately, from an experimental point of view, little is known about the real packing and dynamics of encapsulated species at this level. The discovery of confined fullerenes inside SWNTs by D. Luzzi and coworkers [6, 7] initiates the launch of intensive efforts to study such properties in SWNTs. Peapod made of C_{60} inside SWNT has turned to be a case study for such hybrid materials.

The discovery of fullerenes in 1985 by Kroto et al. was followed by extensive studies of their electronic, optical and biological properties[9, 10, 11, 12, 13, 14, 15, 16]. Looking backward, NMR investigations have played a major role in the understanding of the properties of fullerenes. In particular, the dynamical properties of the plastic crystalline phase of C_{60} was elucidated by NMR [12, 13, 14, 15]. C_{60} molecules undergo molecular reorientational dynamics with temperature with a phase transition at 260 K. From 300 K to 260 K, they show free rotations with the face centered cubic fcc-structure. From 260 K to 100 K, they perform hindered rotations while changing their structure to simple cubic by orientational ordering [12]. In this temperature range, single or double bonds face the centers of pentagons or hexagons to maximize Coulomb attraction [15]. The hindered rotations stop below 85 K where C_{60} molecules finally freeze out. With the recent success of the magnetic methods of purification of the SWNTs [17, 18], NMR spectrocopy is expected also to reveal its high potentialities in nanotube materials. In the present temperature dependence study, with the help of highly purified materials and high resolution Nuclear Magnetic Resonance, we investigate C_{60} encapsulated inside SWNTs which has been partly studied by NMR [19] and inelastic neutron scattering [20] and the source of recent confusion. To clarify the debate, our experimental NMR work definetly reveals the strong modifications by one dimensional confinement inside SWNTs, of the molecular reorientational dynamics of C_{60} and the existence of a phase transition at 100 K.

The 25% isoptopically enriched in ^{13}C fullerenes C_{60} were purchased from MER Corporation. As received PII-SWNTs purchased from Carbon Solutions Inc. were purified with the novel magnetic filtration method as described in references[17] and [18]. The magnetically purified SWNT materials (30 mg) and ^{13}C enriched fullerenes (20 mg) were out gassed in a dynamic vacuum 10^{-9} Bar for one hour at 650°C and 300°C, respectively. The quartz tube containing the SWNTs and fullerene materials was sealed and annealed at 650°C for 10 hours in order for the fullerenes to fill the interiors of the SWNTs. After the filling step, the resulting peapods materials were post-annealed in a dynamic vacuum at 650°C for an hour to remove the non-encapsulated fullerenes. X-ray diffraction (XRD copper Kα with a wavelength of 1.54 Å) was used to assess the filling efficiency of the fullerenes into the SWNTs. The micro structures of peapods were examined using a JOEL 2010 transmission electron microscope at 80 keV to avoid electron beam damage. Based on TEM and XRD measurements, a minimum of 70% C_{60} filling ratio was found in our samples. Hence, taking into account the 25% ^{13}C isotope enrichment, a contribution of 16% from the SWNTs to the total NMR signal was estimated. Therefore in our study, the observed ^{13}C NMR signal is safely dominated by the contribution of encapsulated C_{60} molecules. High resolution ^{13}C Magic Angle Spinning NMR experiments were carried out using Bruker and Tecmag spectrometers at a static magnetic field of 4.7 T operating at Larmor frequencies of 50.3 MHz. Spectra were recorded by spin echo pulse sequence with four phase alternation an synchronized with the spinning rate for the MAS experiments. The spin-lattice relaxation time T_1 was measured by a conventional saturation-recovery pulse sequence with echo detection. The spin-spin relaxation time T_2 was measured by Carr Purcell Meilboom Gill multiple echoes pulse sequence. Temperature studies were performed in a sealed glass tube after being evacuated overnight at a secondary dynamic vacuum.

Figure 5.1 presents the HR-MAS ^{13}C NMR spectrum of the magnetically purified peapods sample at a spinning rate about 10 kHz. Two sharp resonances labelled α at 148.2 ppm and β at 113.3 ppm are observed with the following ratios 32% and 68%, repectively. According to the line-positions and line-widths, these resonances can not be attributed to SWNTs or non-encapsulated C_{60} or polymerized phase of C_{60}. They can been interpreted in terms of C_{60}^{α} and C_{60}^{β}, the latter is diamagnetically shifted by -36.9 ppm from its normal position at 146.3 ppm by

π electrons circulating on the SWNTs [21]. Therefore, the ^{13}C NMR spectra of peapods should be decomposed in three contributions : 16% SWNTs, 27% C_{60}^{α} and 57% C_{60}^{β}. Figure 5.2 displays the static ^{13}C NMR spectrum at room temperature

with its fit based on the sum of three powder patterns corresponding to SWNT, C_{60}^{α} and C_{60}^{β}. In agreement with previous studies [22], the following Chemical Shift Anisotropy tensor principal values δ_{11}^{NT}=-42.2 ppm, δ_{22}^{NT}=164.8 ppm and δ_{33}^{NT}=233.8 ppm have been used for the SWNTs. The C_{60}^{α} components develops a lineshape characteristic of a CSA powder pattern with CSA tensor principal values δ_{11}^{α}=38.5 ppm, δ_{22}^{α}=187.5 ppm and δ_{33}^{α}=218.5 ppm. Figure 5.5 reveals that the second moment of C_{60}^{α} (solid square) is constant from 300 K down to 5K. This feature suggests that C_{60}^{α} are blocked already at room temperature. It has been point out that the cancellation of the diamagnetic shielding from SWNT occurs in the vicinity of defects or holes in its sidewall [23, 24] In addition, we suggest that these defects or holes freeze out also the rotational diffusion of C_{60}^{α} molecules through strong Coulombic interaction ; the energy barrier becoming to high. We turn to the case of the C_{60}^{β} resonance line which is sharp meaning that the C_{60}^{β} molecules are reorienting rapidly. The residual broadening of the line is attributed to the anistropic diamagnetic shielding from the SWNTs [21]. The following axially symmetric Chemical Shift Anisotropy tensor principal values $\delta_{11}^{\beta} = \delta_{22}^{\beta}$=106.9 ppm and δ_{33}^{β}=119.9 ppm was obtained. According to our findings, the investigation of the molecular reorientional dynamics of C_{60} molecules encapsulated inside perfect SWNTs should concentrate on the C_{60}^{β} contribution. Hence, our temperature dependence ^{13}C NMR study presented below, is focussed on the molecular reorientational dyncamics of the C_{60}^{β} molecules.

Figure 5.1 shows static ^{13}C NMR spectra as a function of the temperature from 300 K down to 5 K. The sharp C_{60}^{β} at 111.3 ppm is observed from 300 K down to 30 K with no shift of the resonant frequency. Below 25 K, the line gradually broadens and develops a lineshape characteristic of a chemical shift anisotropy powder pattern. At low temperature, the C_{60}^{β} presents a lineshape characteristic of a CSA powder pattern with tensor principal values δ_{11}^{α}=1.4 ppm, δ_{22}^{α}=150.4 ppm and δ_{33}^{α}=181.4 ppm. This feature indicates that for most molecules, the rate of large amplitude molecular reorientation has become slow compared to the CSA width (3 kHz at 4.7 T). Above 25 K, large rotational motion of the C_{60}^{β} molecules averages the CSA and results

in the motional narrowing of the powder spectrum [25].

The complete temperature dependence of the spin-lattice relaxation time T_1 is shown in Figure 5.3 and should be compared with experiments reported in reference [19].

There is an obvious discrepancy between the two data sets around 100 K that should be clarify. These differences could originate from different type of SWNTs samples . In particular, we report a discontinuity in the temperature dependence of T_1 which is expected if a phase transition occurs. In our experiments, the molecular reorientional motions that dominate the spin-lattice relaxation in C_{60} change abruptly at 100 K. In order to go further in our interpretation and to fit T_1 relaxation over the complete range of temperature, we use two different sets of parameters corresponding to above and below the phase transition temperature T_c=100 K. The following contributions to the T_1 relaxation have been introduced [25] :

$$\frac{1}{T_1} = \frac{1}{T_{10}} + \frac{1}{T_{1M}} + \frac{1}{T_{1D}} \tag{5.1}$$

where T_{10}^{-1} is a temperature independent constant background, T_{1D}^{-1} represents the contribution due to fluctuating ^{13}C dipole-dipole interaction and T_{1M}^{-1} is caused by fluctuating CSA, the two latter are due to molecular reorientation and depend on temperature. T_{10}^{-1} amounts in our case to 0.1 s^{-1} which is quite small compared with other relaxation rates. It is most likely caused by paramagnetic impurities.

We discuss first the relaxation time T_{1M} caused by fluctuating local magnetic fields due to the reorientational motion of the C_{60}^{β} molecules. The CSA at the local ^{13}C site, leads to a variation of the local field when the molecule reorients. The fluctuation $\Delta\omega_M$ will depend on the details of the isotropic and anisotropic molecular reorientations, but will never exceed the total shift anisotropy. Since the details of the reorientations are not known, it will serve as an adjustable parameter. The corresponding spin-lattice relaxation rate can be readily expressed as [25, 26, 27]

$$\frac{1}{T_{1M}} = \frac{6}{40}\Delta\omega_M^2 \frac{2\tau}{1+\omega_0^2\tau^2} \tag{5.2}$$

where ω_0 is the Larmor frequency. The relaxation rate is proportional to B_0^2 for $\omega_0\tau \ll 1$ and

field independent for $\omega_0\tau \gg 1$, which explains the different behaviors at higher field reported in the reference [19]. A minimum in the relaxation time T_1 is expected according to Bloembergen, Purcell and Pound [27] when $\omega_0\tau = 1$. The temperature dependence of the autocorrelation time τ follows an Arrhenius law :

$$\tau = \tau_0 \exp^{\frac{\Delta E_M}{k\ T}} \tag{5.3}$$

with an activation energy ΔE_M, reflecting the rotational barrier between different molecular orientations and τ_0 the autocorrelation time at infinite temperature.

Due to the isotope enrichment of our samples, we have to take into account the homonuclear dipolar couplings. This contribution is modeled by the additional term [25] :

$$\frac{1}{T_{1D}} = \frac{2}{3}\Delta\omega_D^2 \left(\frac{\tau}{1+\omega_0^2\tau^2} + \frac{4\tau}{1+4\omega_0^2\tau^2} \right) \tag{5.4}$$

where $\Delta\omega_D$ represents the averaged fluctuations of the dipole-dipole interaction.

The Equations from 5.1 to 5.4 have been applied successfully to the fit of the spin-lattice relaxation times T_1 above and below T_c. Table 5.1 summarizes these two sets of fitting parameters corresponding to two different molecular reorientation regimes.

Experiments Model	T_1 peapods T_c=100 K	T_1 peapods T_c=100 K	T_2 peapods T_c=100 K	$\delta\nu$ peapods T_c=100 K	T_1 fcc-C_{60}[13] T_c=260 K	T_1 fcc-C_{60}[13] T_c=260 K
T (K)	5 to 100	100 to 300	5 to 100	5 to 100	193 to 246	263 to 323
$\Delta\omega_M$ (s^{-1})	2π 2541	2π 3465	-	-	-	-
$\Delta\omega_D$ (s^{-1})	2π 475	-	-	-	-	-
$\Delta\omega_S$ (s^{-1})	-	-	2π 747	-	-	-
ΔE_M (meV)	27	8	28	35	250	42
τ_0(s)	5 10^{-11}	5 10^{-11}	5 10^{-11}	5 10^{-11}	3 10^{-14}	5 10^{-12}

Table 5.1: Reorientational motion parameters : activation energy ΔE, autocorrelation time τ_0 and local field fluctuations $\Delta\omega$ corresponding to T_1, T_2, and $\delta\nu$ in peapods and fcc-C_{60} fullerenes.

The obtained values $\Delta\omega_M^{HT} = 2\ \pi\ 3465\ s^{-1}$ above T_c, $\Delta\omega_M^{LT} = 2\ \pi\ 2541\ s^{-1}$ and $\Delta\omega_D^{LT} = 2\ \pi\ 475\ s^{-1}$ below T_c are in reasonable agreement with the CSA linewidth at low temperatures (below 25 K). The activation energies $\Delta E_M^{HT} = 8$ meV and $\Delta E_M^{LT} = 27$ meV are estimated

using an attempt autocorrelation time $\tau_0 = 5\ 10^{-11} s$.

We turn now to the discussion on spin-spin relaxation T_2 which is sensitive to fluctuating local fields on a time scale of about the line-width (3 kHz in our case at 4.7 T). Figure 5.4 presents the T_2^{-1} relaxation rate from 300 K down to 5 K. A peak appears in T_2^{-1} around 25 K. In order to model the T_2^{-1} relaxation rate, we apply the following relation [25, 28]:

$$\frac{1}{T_2} = \frac{1}{40}\Delta\omega_S^2 \left(3\frac{2\tau}{1+\omega_0^2\tau^2} + 4\frac{2\tau}{1+\Delta\omega_S^2\tau^2} \right) \tag{5.5}$$

where $\Delta\omega_S$ corresponds to CSA fluctuations caused by reorientational process. The slow motion regime is observed when $\Delta\omega_S\ \tau \gg 1$ and the fast motional narrowing case for $\Delta\omega_S\ \tau \ll 1$. A peak in the T_2^{-1} relaxation rate is expected when $\Delta\omega_S\ \tau = 1$. Equation 5.5 has been applied to fit the experimental data below T_c as presented in Figure 5.4. The results are reported in Table 5.1. In agreement with T_1 relaxation, an activation energy of 28 meV was found. As expected above T_c, the T_2^{-1} relaxation rate is independent of temperature with a $T_2 \approx 11$ ms.

Figure 5.5 presents the second moment of the C_{60}^{β} line from 300 K down to 5 K. The motional narrowing around 25 K, clearly indicates that the C_{60}^{β} rotational motion drastically changes at this temperature on a time scale of about 100 μs. The influence of rotational motion on the temperature-dependent line-width can be described by the following implicit equation [25] :

$$(\delta_\nu)^2 = (\delta_\nu^{HT})^2 + (\Delta_\nu)^2 \frac{2}{\pi} \arctan(\delta_\nu \tau) \tag{5.6}$$

where δ_ν^{HT} is the line-width at high temperatures, Δ_ν the change in the line-width from high to low temperatures. Using an autocorrelation time $\tau_0 = 5\ 10^{-11}$ s, a self consistent calculation gives an activation energy of 35 meV, in good agreement with previous estimations from T_1 and T_2 relaxation rates. Results are reported in Table 5.1.

Table 5.1 summarizes the reorientational motion parameters of one dimensional encapsulated C_{60} fullerenes inside SWNTs. The parameters extracted from the fits of T_1, T_2, and $\delta\nu$ are listed

for comparison with the one from fcc C_{60}[13]. Above T_c=100 K, the measured temperature dependance T_1, T_2, and $\delta\nu$ clearly indicate fast reorientational dynamics of the C_{60} molecules. The relatively small value of the activation energy barrier (8 meV) suggests that the motion in the high temperature phase approximates continuous rotational diffusion. Rotational diffusion would appear as orientational disorder in diffraction measurements. The dramatic change in kinetic parameters below 100 K, reflects a drastic change in the nature of the molecular dynamics which could be explain by an anisotropic uniaxial molecular rotations, along the axis of the SWNTs. The activation energies below $T_c = 100$ K obtained from the fits of T_1, T_2 and $\delta\nu$ are 27 meV, 28 meV, and 35 meV, respectively. The differences are within the experimental error. The high rotational mobility of the C_{60} molecules is kept down to 25 K where it freezes out. These features suggest a smooth interaction between C_{60} and SWNTs.

Below T_c, an average value of 30 meV is almost one eighth of the one admitted in fcc-C_{60} (250 meV). Above T_c, 8 meV is one fifth of that in fcc-C_{60} (42 meV). Yildirim et al. has predicted that in fcc C_{60} [15], a single or double bond in a fullerene prefers to face a center of a pentagon or a hexagon in neighboring fullerene to maximize Coulomb attraction.[29, 30] Therefore, the activation energy for a rotation, which is a function of Van der Waals interaction as well as the Coulomb attraction, would be as a first approximation, proportional to the number of nearest neighbors. The ratio of the number of nearest neighbors in peapods to that in fcc C_{60} is one sixth. which is consistent with the ratios of the activation energies mentioned above.

Reorientational motion of one dimensional C_{60} array inside SWNTs has been investigated by ^{13}C NMR spectroscopy. The encapsulated fullerenes undergo a phase transition at T_c=100 K (fcc-C_{60} at 260 K) from continuous rotational diffusion to uniaxial rotations and freeze out at 25 K (85 K in fcc-C_{60}). The significant changes in the dynamical properties of C_{60} encapsulated inside SWNTs results from the reduction of the number of nearest neighbours and its smooth interaction with the SWNTs sidewalls.

Figure 5.1: Static ^{13}C NMR spectra of C_{60} molecules encapsulated inside SWNTs at indicated temperatures. Bottom spectrum, HR-MAS ^{13}C NMR showing the isotropic lines of the C_{60}^{α} and C_{60}^{β}.

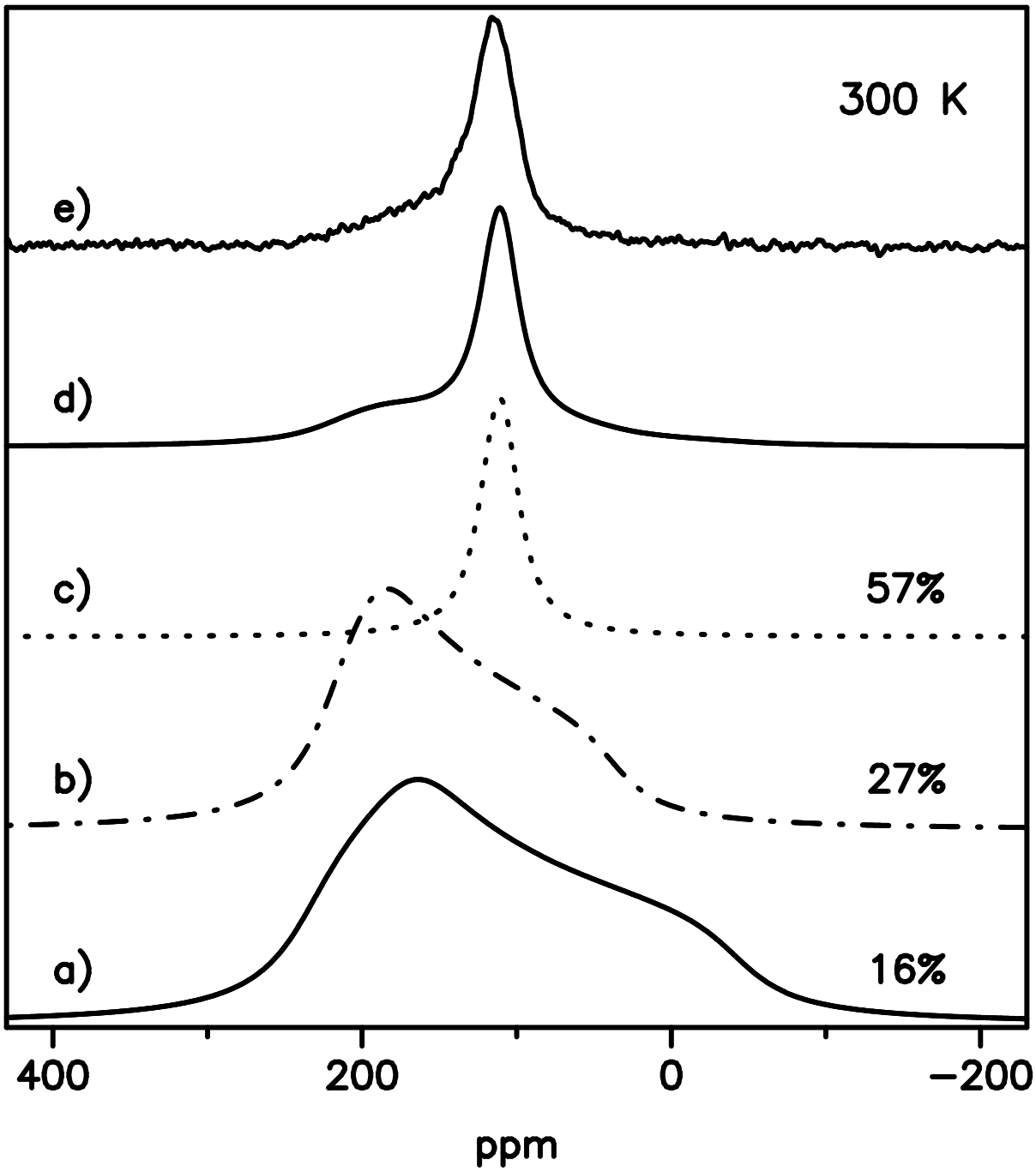

Figure 5.2: Simulated powder pattern line-shape according to CSA tensor values described in the text, for a) SWNTs, b) blocked C_{60}^{α}, c) rotating C_{60}^{β}, d) the fit of the experimental spectrum e) according to the indicated ratios.

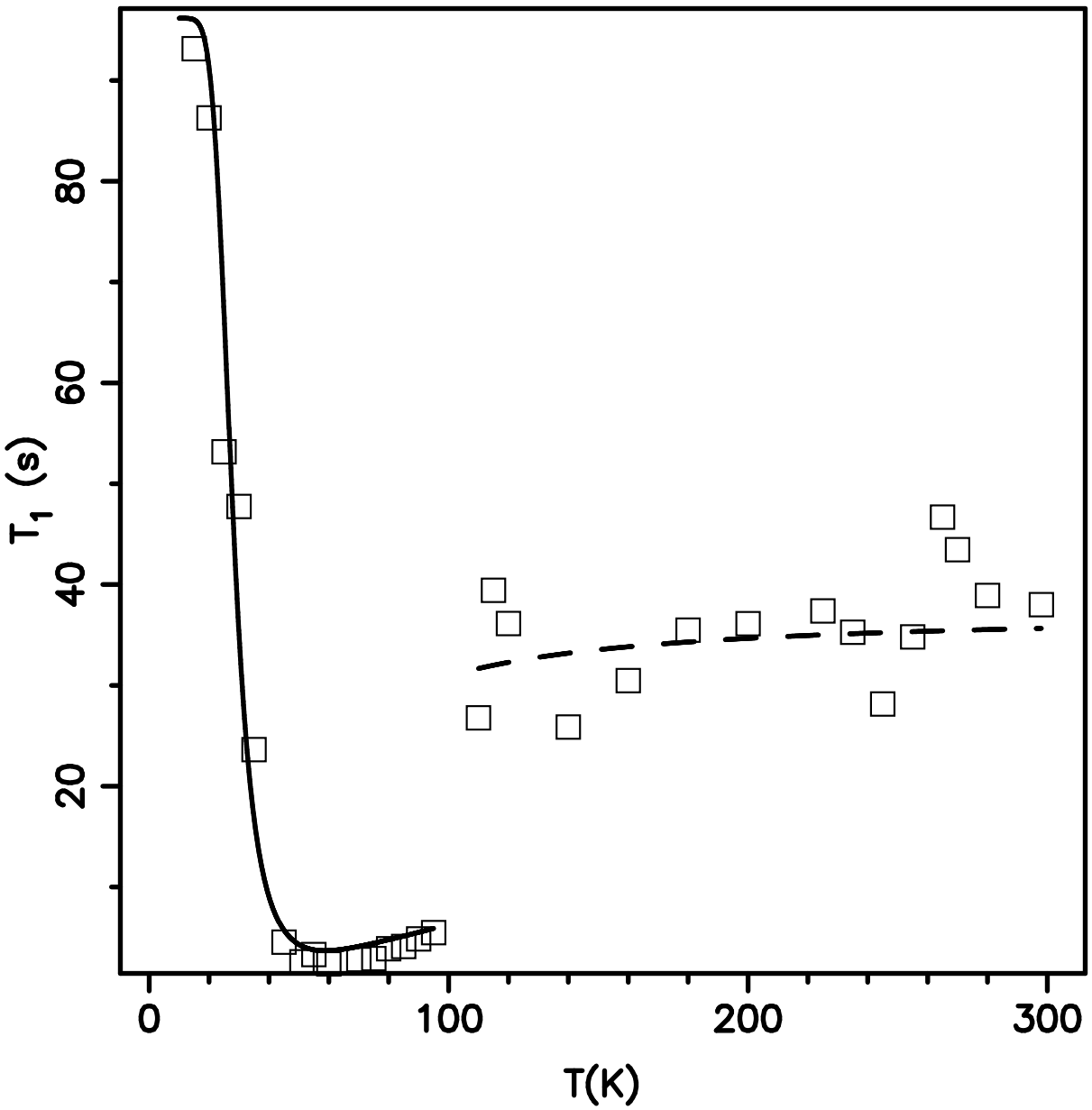

Figure 5.3: Spin-lattice relaxation time T_1 of C_{60}^{β} in peapods as a function of temperature. The phase transition occurs at T_c=100 K. Note the abrupt change at T_c which occurs when C_{60}^{β} change from continous rotational diffusion (dashed line) to uniaxial rotation along SWNTs axis (solid line).

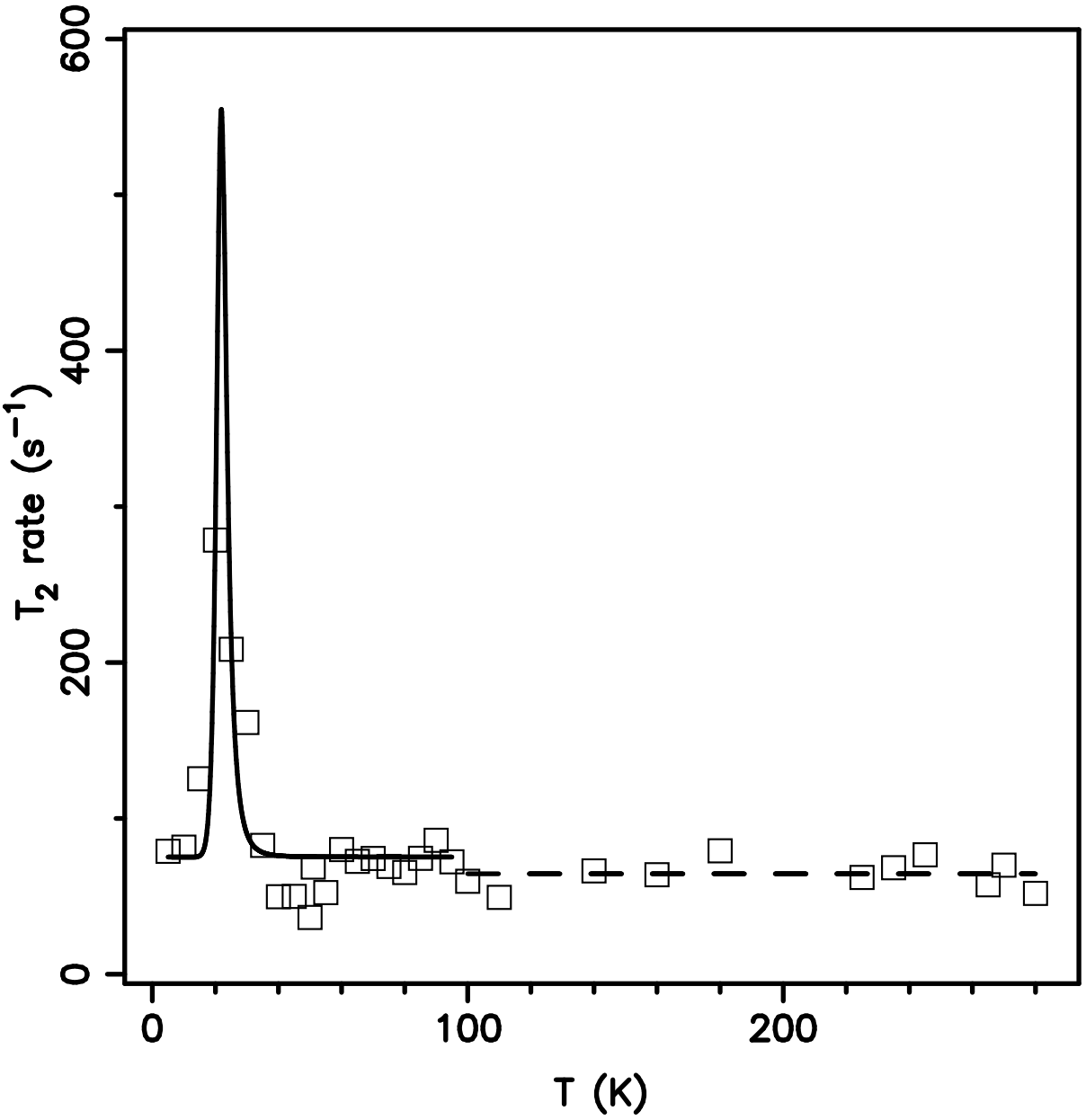

Figure 5.4: Spin-spin relaxation time T_2 of C_{60}^{β} in peapods as a function of temperature. The peak occurs when autocorrelation rate τ^{-1} is in the order of the line-width (3 kHz at 4.7 T). Below 25 K, all the C_{60} molecules the α and β are blocked.

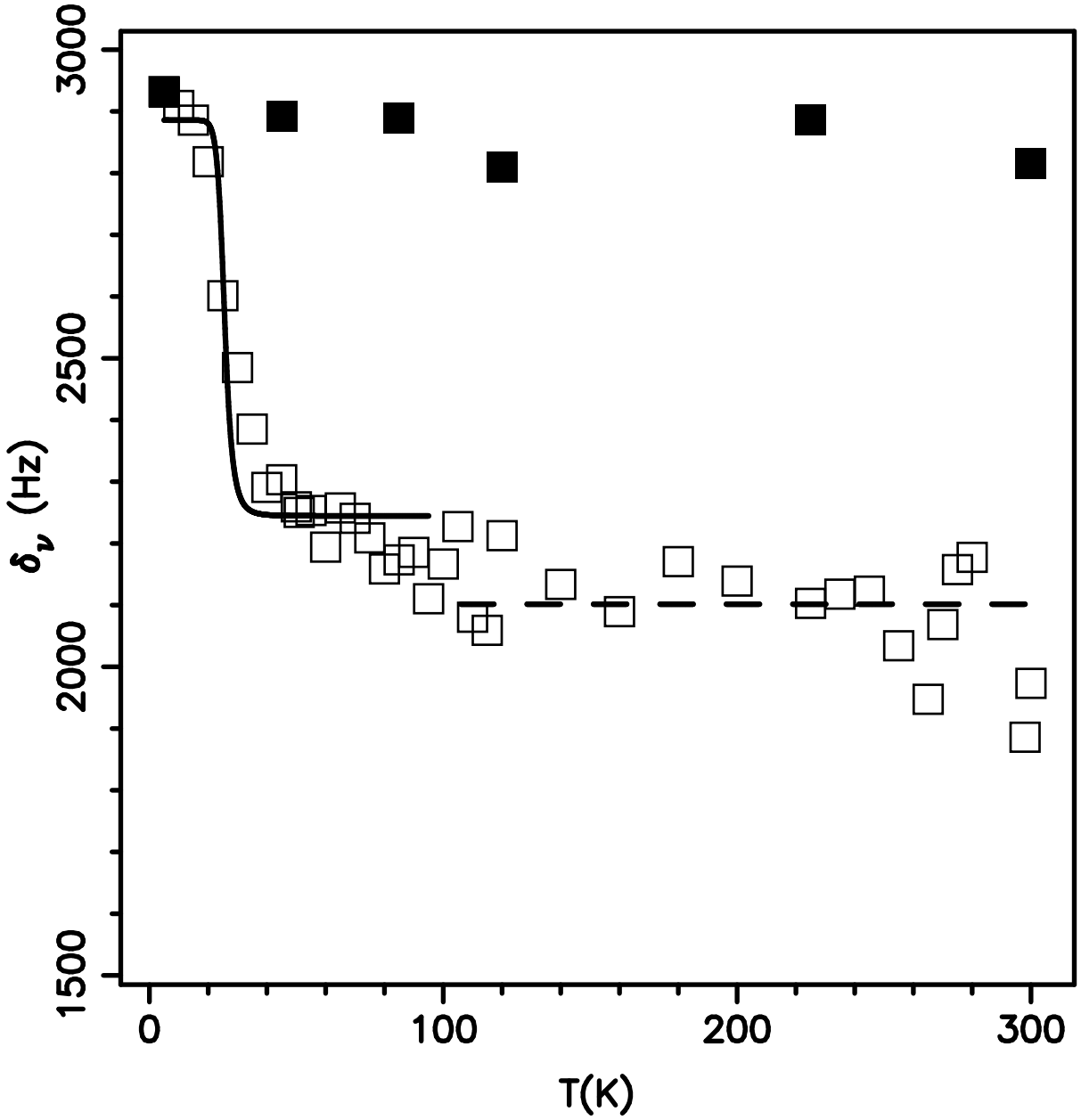

Figure 5.5: Second moment of the lines of the C_{60}^{α} (solid square) and C_{60}^{β} (open square). Note the small increase (200 Hz) at T_c from the continuous rotational diffusion (dashed line) to uniaxial rotational motion along the axis of the SWNTs (solid line). Below 25 K, the C_{60}^{β} molecules are blocked which is evidenced by an increase of $\approx$ 800 Hz in $\delta\nu$.

Bibliography

[1] E. D. Minot, Y.Yaish, V. Sazonova, and P. L. McEuen, Nature 428, 536 (2004).

[2] M. E. Itkis, S. Niyogi, M. E. Meng, M. A. Hamon, H. Hu, and R. C. Haddon, Nano Lett. 2, 155 (2002).

[3] R. Saito, M. Fujita, G. Dresselhaus, and M. S. Dresselhaus, Appl. Phys. Lett. 60, 2204 (1992).

[4] H. Ishii, H. Kataura, H. Shiozawa, H. Yoshioka, H. Otsubo, Y. Takayama, T. Miyahara, S. Suzuki, Y. Achiba, M. Nakatake, T. Narimura, M. Higashiguchi, K. Shimada, H. Namatame, and M. Taniguchi, Nature 426, 540 (2003).

[5] A. Javey, J. Guo, Q. Wang. M. Lundstrom, and H. Dai, Nature 424, 654 (2003).

[6] D. J. Hornbaker, S. -J. Khang, S. Misra, B. W. Smith, A. T. Johnson, E. J. Mele, D. E. Luzzi, A. Yazdani, Science 2002, 295, 828.

[7] B. W. Smith, M. Monthioux, D. E. Luzzi, Nature 1998, 396, 323.

[8] A. I. Kolesnikov, J. M. Zanotti, C. K. Loong and P. Thiyagarajan Phys. Rev. Lett. 93 3 35503 (2004).

[9] H. W. Kroto, J. R. Heath, S. C O'Brien, R. F. Curl, and R. E. Smalley, Nature, 318, 162 (1985).

[10] L. J. Dunne, A. K. Sarkar, H. W. Kroto, J. Munn, P. Kathirgamanathan, U. Heinen, J. Fernandez, J. Hare, D. G. Reid, and A. D. Clark, J. Phys.: Condens. Matter 8, 2127 (1996).

[11] S. R. Wilson, in: K. Kadish, R. Ruoff (Eds.), The Fullerene Handbook, Wiley, New York (2000).

[12] P. A. Heiney, J. E. Fischer, A. R. McGhie, W. J. Romanow, A. M. Denenstein, J. P. McCauley Jr., and A. B. Smith, Phys. Rev. Lett. 66, 2911 (1991).

[13] R. Tycko, G. Dabbagh, R. M. Fleming, R. C. Haddon, A. V. Makhija, and S. M. Zahurak, Physt. Rev. Lett. 67, 1886 (1991).

[14] R. Blinc, J. Seliger, J. Dolinsek, and D. Arcon, Phys. Rev. B 49, 4993 (1994).

[15] T. Yildirim, A. B. Harris, and S. C. Erwin, Phys. Rev. B 48, 1888 (1993).

[16] R. Tycko, R. C. Haddon, G. Dabbagh, S. H. Glarum, D. C. Douglass, and A. M. Mujsce, J. Phys. Chem. 95, 518 (1991).

[17] Y. Kim, D. E. Luzzi, J. Phys. Chem. B. 2005, 109, 16636.

[18] Y. Kim, O. N. Torrens, J. M. Kikkawa, E. Abou-Hamad, C. Goze-Bac, D. E. Luzzi, Chem. Mater. 2007, 19(12), 2982.

[19] K. Matsuda, Y. Maniwa and H. Kautara Phy. Rev. B 77, 075421 (2008).

[20] S. Rol, J. Cambedouzou, M. Chorro, H. Schober, V. Agafonov, P. Launois, V. Davydov, A. V. Rakhmanina, H. Kataura and J.-L. Sauvajol Phys. Rev. Lett., 101 065507 (2008)

[21] M. Marques, M. d'Avezac and F. Mauri, Phys. Rev. B 73 125433 (2006)

[22] C. Goze-Bac, S. Latil, P. Lauginie, V. Jourdain, J. Conard, L. Duclaux, A. Rubio, P. Bernier, Carbon, 40, 1825-1842 (2002).

[23] F. Lopez-Urias, J. Rodriguez-Manzo, E. Muñoz-Sandoval, M. Terrones and H. Terrones, Optical Materials 29 110 (2006)

[24] Y. Kim, E. Abou-Hamad and al. (submitted).

[25] M. Mehring, Principles of high resolution NMR in solids, Springer-Verlag, Berlin, Heidelber, New York (1983).

[26] A. Abragam, principles of Nuclear Magnetism (Oxford Science, New York, 1989).

[27] N. Bloembergen, E. M. Purcell, and R. V. Pound, Phys. Rev 73, 679 (1948).

[28] J. Rautter, A. Grupp, M. Mehring, J. Alexander, K. Mullen, and W. Huber, Mol Phys, 76, 37 (1992).

[29] L. A. Girifalco, M. Hodak, and R. S. Lee, Phys. Rev. B 62, 13104 (2000).

[30] M. Hodak, and L. A. Girifalco, Phys. Rev. B 68, 085405 (2003).

Chapter 6

Hydrogenated nanotubes

Ever since the discovery of peapods[1], single walled nanotubes (SWNTs) has been proposed as potential ultra clean nano reactors[2, 3] or gas transport system[4]. We report experimental evidences showing that controlled chemical reactions at the interior space of SWNT is, indeed, feasible. Hydrogenation of C_{60} molecules inside SWNT was achieved by direct reaction with hydrogen gas at elevated pressure and temperature. Evidence for the C_{60} hydrogenation in peapods is provided by isotopic engineering with specific enrichment of encapsulated species and high resolution ^{13}C and ^{1}H NMR spectroscopy with the observation of typical diamagnetic and paramagnetic shifts of the NMR lines and the appearance of sp^3 carbon resonances. It is estimated that approximately 78 % of the C_{60} molecules inside SWNTs are hydrogenated to an average degree of 14 hydrogen atoms per C_{60} molecule. As a consequence, the rotational dynamics of the encapsulated $C_{60}Hx$ molecules are clearly hindered. In contrast, hydrogenation is not observed on the wall of the SWNTs in peapods and for the non-filled SWNTs after exactly the same hydrogenation treatment. Our successful hydrogenation experiments open completely new roads to understand and control confined chemical reactions at the nano scale.

Carbon nanotubes provide unique possibilities for the studies of nano scale physics and chemistry in the confined interior space of SWNTs. They can be filled not only by C_{60} but also with many other molecules like e.g. pentacene[5], metalloscenes[6] and hexamethylelamine[7]. However, only very few attempts have been made to modify encapsulated species. At present date, these are intercalation of C_{60} with alkali metals[8], high pressure polymerization of C_{60}[9, 10] and catalyst growth of nanotube inside SWNTs[11]. It is well known that C_{60} reacts with

hydrogen gas at given temperature and pressure[12] and that with correctly chosen conditions hydrofullerenes of high isomeric purity can be synthesized[13, 14]. Therefore, it is of great interest, as a case study, to verify if the same reaction is possible and to follow the eventual modifications in the chemical composition, the molecular dynamics and the magnetic properties in the confined space of SWNT. Three samples : peapods, bulk fullerene powder, and reference non-filled SWNTs same as used for filling experiments were exposed to hydrogen gas at 13 Bar and 670-680 K. Analysis of XRD patterns recorded from the reference C_{60} sample proved successful hydrogenation with an approximate composition of the final product as $C_{60}H_x$ with x≈18[14]. However, it is not given that fullerene molecules encapsulated in SWNT are also hydrogenated at the same conditions. Most likely, molecules close to the open ends or to hole defects of the nanotube will be hydrogenated, but will hydrogen be able to access the whole space of the peapod ? Another open question concerns the possible reaction of hydrogen with nanotube walls. This possibility should be considered and could complicate the analysis further. In order to clarify this important points, we performed solid state Nuclear Magnetic Resonance (NMR) which is widely used for the studies of structural and dynamical properties of fullerene compounds[15, 16] but surprisingly limited in the case of SWNTs compounds[17, 18, 19]. This progress was largely hindered by two main reasons. First, the presence of magnetic catalyst impurities commonly present in SWNT samples. This problem can be circumvented by using magnetically purified SWNT samples[30]. Second, isotopic engineering with specific enrichment of C_{60} molecules should be implemented in order to discriminate between the signal of carbons originating from the nanotube walls and from the encapsulated molecules. In this study, nanotubes with 1% ^{13}C natural abundance and C_{60} with 25 % enriched ^{13}C have been used, leading to an enhancement of the signal of the encapsulated molecules under interest. The filling factor of C_{60} inside SWNTs prior to hydrogenation was estimated from high resolution transmission electron microscope measurements to be ≈ 70%, see 6.1. The NMR study was performed first, on an empty SWNT sample, then on a peapod sample synthesized from these SWNTs and finally on that very same peapod sample subjected to hydrogenation treatment. Comparing the NMR data obtained for pristine and hydrogenated peapods it is possible to assign the observed effects confidently only to molecules of C_{60} situated in the interior space of SWNT.

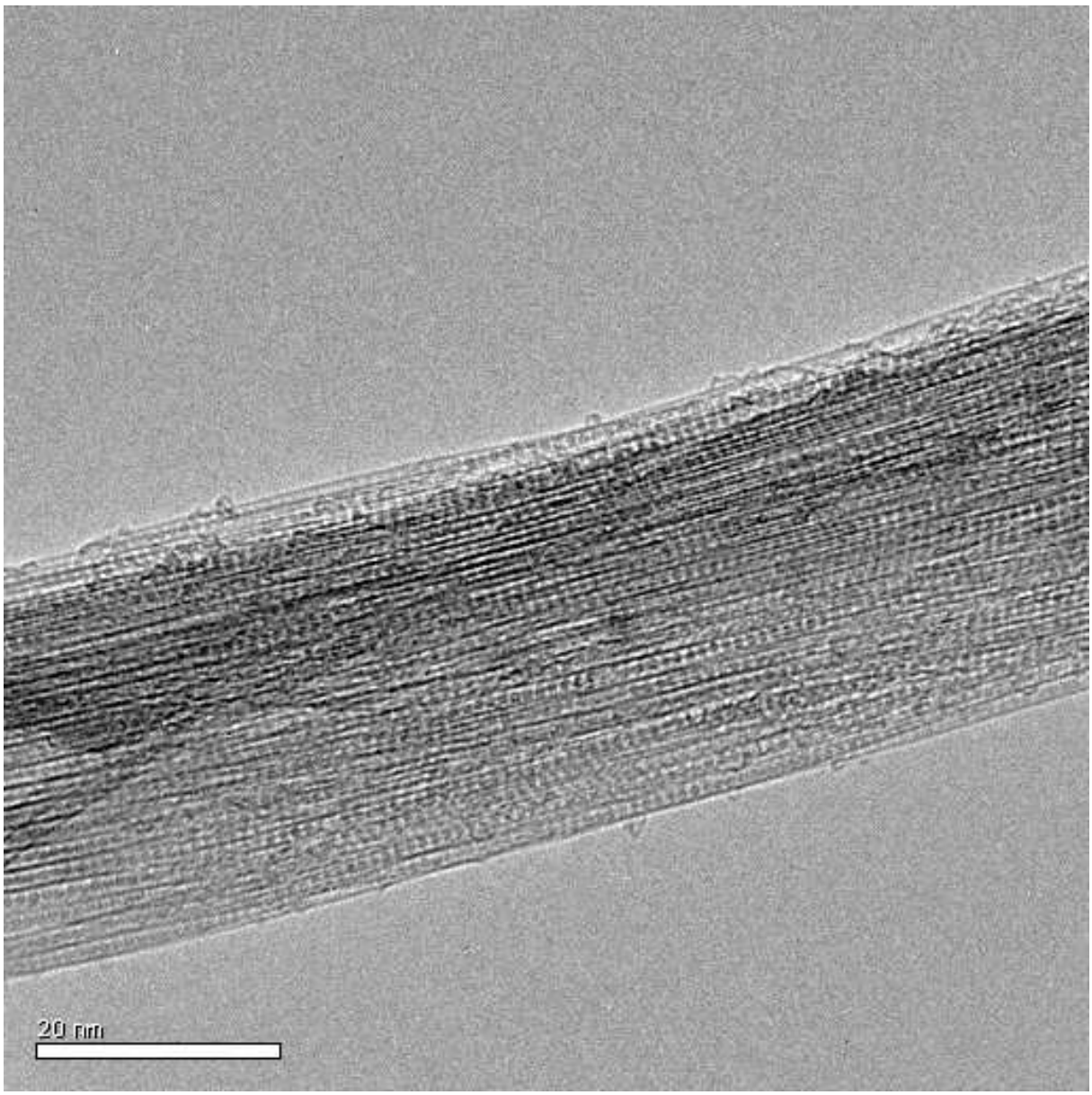

Figure 6.1: HR-TEM picture of untreated peapod sample before hydrogenation process.

Figure 6.2 shows the magic angle spinning NMR spectra of untreated peapods (III) and hydrogen treated peapods (IV) together with pristine C_{60} (I) and empty SWNTs (II). The signal from the untreated peapods (III) can be fitted with three lines, the first at 111.3 ppm (α-position), a second at 118.8 ppm, and a third at 148.2 ppm (β-position). The line at 111.3 ppm is assigned to C_{60} molecules in the interior of the SWNT. This signal is diamagnetically shifted from the normal position of FCC C_{60}, located at 143.6 ppm (trace I). The diamagnetic shift occurs due to a local magnetic field on the C_{60} molecules produced by ring currents circulating on the honeycomb surface of the nanotube[21]. The same effect has been observed for ^{3}He encapsulated

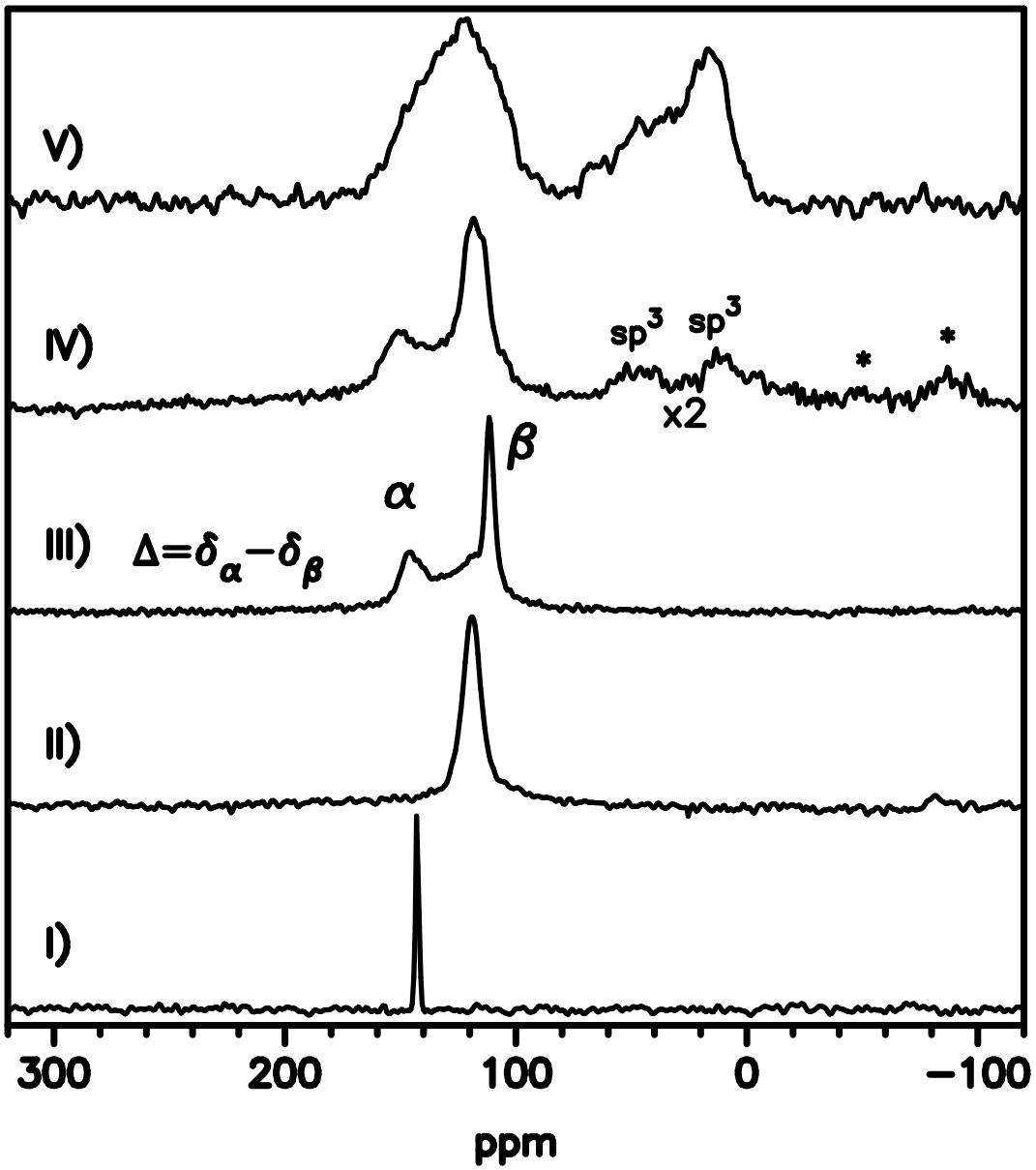

Figure 6.2: ^{13}C MAS of pristine C_{60} (I), Single walled nanotubes (empty) (II), normal peapods (III), hydrogen treated peapods (IV), and CPMAS of hydrogen treated peapods (V).

inside fullerene molecules[20]. The very sharp character of this line, together with the static spectra (Figure 6.3) discussed below, indicates that the C_{60} molecules are still rotating inside the carbon nanotubes (β-position). This result is in agreement with semi-empirical calculations [22] and recent experiments[23], which show that C_{60} molecules inside nanotubes rotate at the NMR time scale at room temperature. More details about dynamics of C_{60} inside SWNTs are reported in the next chapter. The signal at 118.8 ppm represents the NMR response of the carbons in the SWNTs as in trace II for empty nanotubes[17, 18]. Finally the line at 148.2

ppm represents C_{60} molecules at the interior of SWNT but located at tube defects, giving rise to a slight paramagnetic shift of the NMR line position compared to pristine C_{60} (I). Its significant broadening compared to freely rotating C_{60} suggests that the C_{60} molecules are no longer rotating when located in the vicinity of nanotube defects (α-position). The broadening indicates also that C_{60} molecules are not located outside the SWNT, which would show up as a narrow line at 143.6 ppm[24]. A more distinct sign that the C_{60} molecules are static in α-position is the presence of rotational side bands when spinning the sample at 4 kHz instead of 10 kHz (not shown). The hindered rotation is also supported by static NMR measurements as discussed below. Hydrogenation of peapods results in drastic modifications of the NMR spectra. The ^{13}C NMR MAS spectrum (Figure 6.2 IV) shows that the signals of α- and *beta*- molecules keep their individual ratio but the line positions and their FWHM is changed (see also table 6.1). Both the line representing C_{60} located at defects (α-position) and the line representing C_{60} in β-position are paramagnetically shifted from the values in untreated peapods. The paramagnetic shift, caused by the charge transfer between hydrogen and fullerenes provides clear evidence for hydrogenation of the C_{60} molecules and the sp^2 line position. This experimental observation is in good agreement with ^{13}C NMR shifts between C_{60} and $C_{60}H_{18}$[14]. In addition we can extract, information about the dynamics of hydrogenated C_{60} inside of SWNT from the spectrum shown in Figure 6.2 IV). This is important since it helps to clarify the interactions between the C_{60} molecules and the nanotube walls. The presence of spinning side bands from both resonances, the line at 152.1 ppm (α-positionk) and the line at 117.8 ppm (β-position) suggests that after hydrogenation the α- and β- C_{60} molecules are static, indicating an increase of the fullerene-nanotube interaction probably due to steric effects. Further evidence for hydrogenation of C_{60} in peapods is provided by the appearance of two sp^3 lines located at 48.7 ppm and 14.4 ppm, attributed to C-H bonds from the α- and β-hydrogenated C_{60} molecules, respectively. The sp^3 line at 48.7 ppm is interpreted to originate from the sp^3 carbon located at defects and thus expected to be not diamagnetically shifted because of the absence of nanotube ring currents at these positions. Additional support for the succesfull hydrogenation of C_{60} is found in the Cross Polarized Magic Angle Spinning (CPMAS) experiments on the hydrogen treated sample (trace V in figure 6.2. The CPMAS enhances the signal of carbon spins either directly bonded to a hydrogen (sp^3 carbons) or in its vicinity (sp^2 carbons adjacent to sp^3 carbons), making it

	α-sp^2 (ppm)	β-sp^2 (ppm)	α-sp^3 (ppm)	β-sp^3 (ppm)
Peapods	148.2 (31.7%)	111.3 (68.3%)	-	-
Hydrogenated Peapods	152.1 (25.7%)	117.8 (56.3%)	48.7 (5.6%)	14.4 (12.4%)

Table 6.1: Line positions and ratios corresponding to ^{13}C NMR MAS experiments.

possible to observe the quite large distribution of the sp^3 carbon signal indicating a high degree of C_{60} hydrogenation.

To ensure that the signal from hydrogenated carbons does not come from the hydrogenation of the nanotube walls in the peapod sample or from hydrogenated graphitic nanoparticles we performed the same hydrogenation treatment on a purified nanotube sample (containing no C_{60} molecules) of the same starting nanotube material that was used to prepare peapods. NMR measurements performed on this sample did not reveal any signals from hydrogenated carbons which mean that nanotube walls and carbon particles are not hydrogenated at the treatment conditions used in our experiments. This result clearly proves that all hydrogenation observed in peapods occurs on the C_{60} molecules. Fitting the NMR data for hydrogenated peapods (see Figure 6.3) and taking into account the distribution of the magnetic field inside the nanotube, allows us to estimate that the SWNT provides 16% contribution to the measured signal whereas the remaining 84% comes from encapsulated C_{60}. This result agrees with 70% filling factor of peapods and 25% enrichment of encapsulated C_{60} by ^{13}C[30]. The results of MAS-NMR experiments are summarized in table 6.1 and show the line position for each signal and its intensity in relation to the total carbon signal from C_{60}. The ratio between the sp^2 and sp^3 carbons contributions allows us to estimate the number of hydrogenated carbon atoms as ≈ 17 % of all carbons in C_{60} molecules. This means that if all C_{60} molecules were homogeneously hydrogenated to the same degree (which is probably not the case, as discussed below) they would have a hydrogen content of about 10 hydrogen atoms per C_{60} molecule. Summarising, our MAS ^{13}C NMR spectra provides clear evidence for hydrogenation of C_{60} encapsulated in peapods and shows that hydrogenation hinders the rotational freedom of the C_{60} molecules.

Additional support to the conclusions extracted from the MAS NMR data is obtained from static ^{13}C NMR spectra (see Figures 6.4 and 6.5). As before, the ^{13}C spectra from untreated peapods sample is presented first (Fig. 6.4), followed by a discussion of the differences due to hydrogenation (Fig. 6.5).

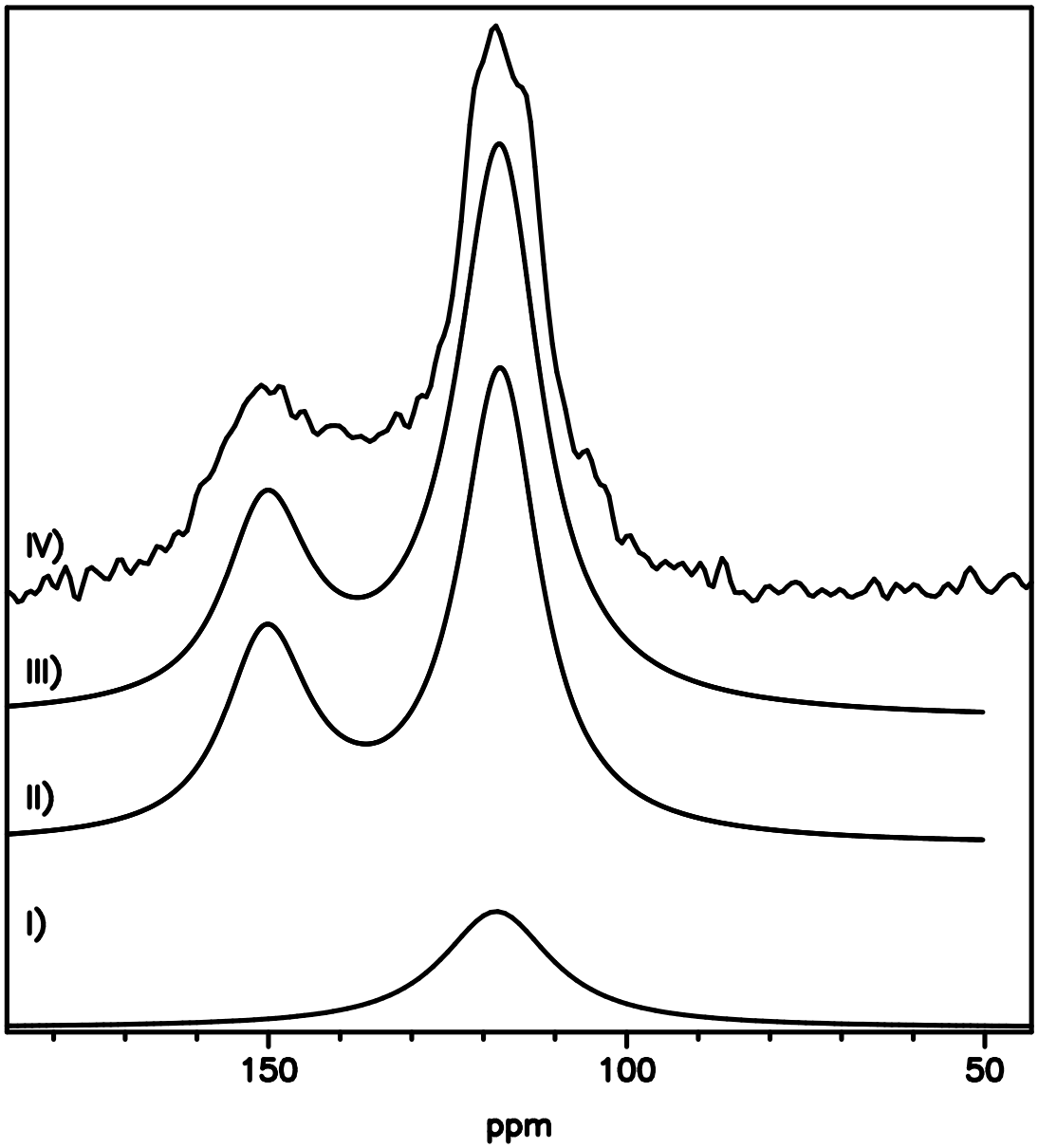

Figure 6.3: Fit of high resolution MAS NMR spectrum of hydrogen treated peapods. SWNT content (I), paramagnetically and diamagnetically shifted C60 (II), fitted curve (III), and experimental NMR spectrum (IV). Figure 3 a) ^{13}C Static NMR spectra of peapods fitted with the tensors of SWNT (I), static C60 (II) and freely rotating C60 (III). The total fit is shown in (IV) and the experimental data in (V).

The static spectrum of the untreated peapods has three main contributions: a) the typical powder line shape from SWNTs with a contribution fixed to 16% from the results of the MAS spectrum (figure 6.4, I), b) the Chemical Shift Anisotropy tensor (CSA) of static paramagnetically shifted C_{60} (figure 6.4, II) and c) the rotating diamagnetically shifted C_{60} (Figure 6.4, III). Note that the broad line shape for rotating C_{60} as compared to FCC C_{60} is related to the anisotropic currents on the outer nanotubes[25, 26]. Fitting the tensors allows to estimate the

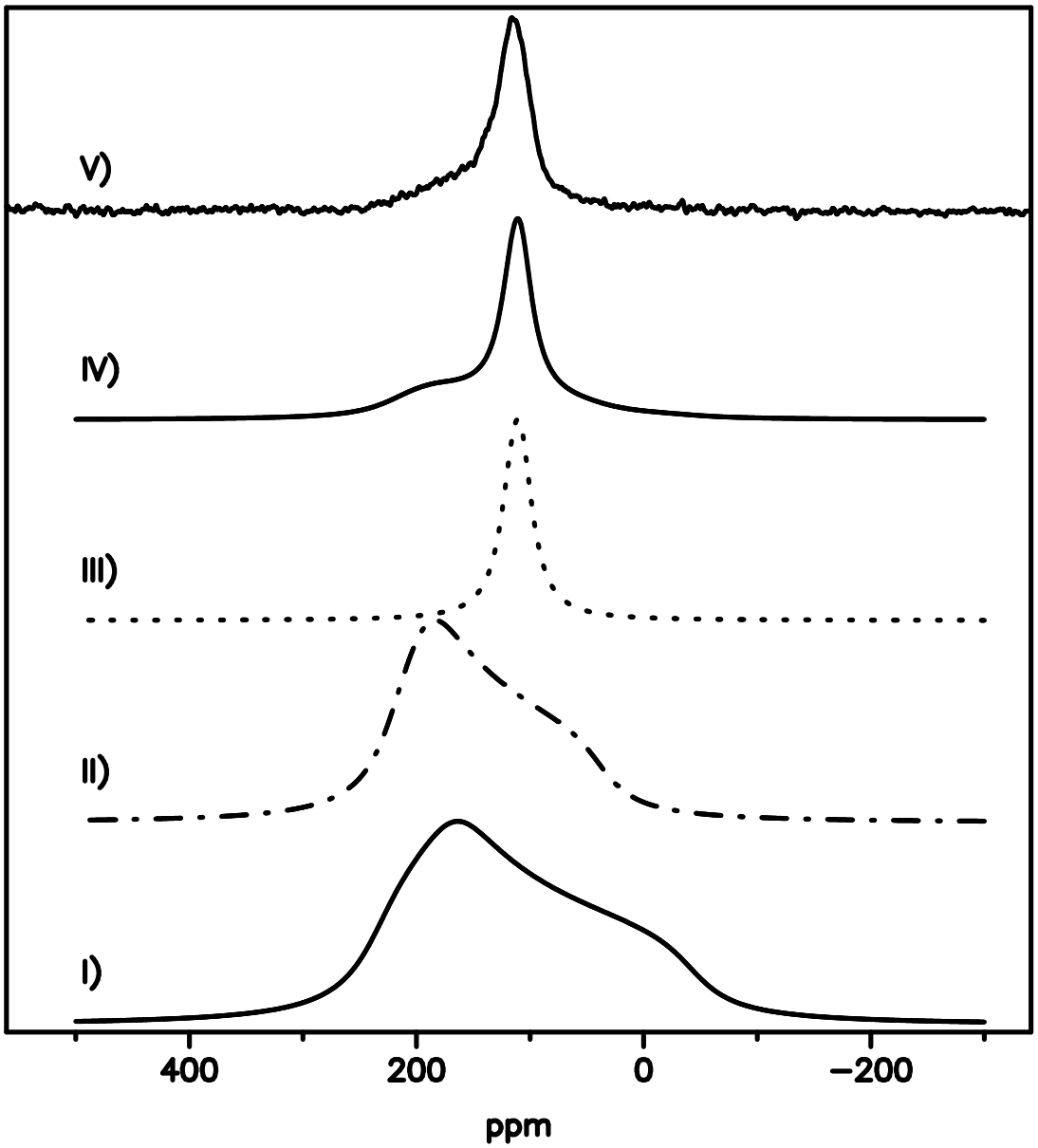

Figure 6.4: ^{13}C Static NMR spectra of peapods fitted with the tensors of SWNT (I), static C60 (II) and freely rotating C60 (III). The best fit is shown in (IV) and the experimental data in (V).

proportion of blocked C_{60} at defects versus rotating C_{60} (shifted diamagnetically) as 31.7:68.3. The C_{60} signal here is normalized to 100 % since we find no hydrogenation of the SWNT walls. This new estimation is consistent with the MAS spectra. By comparing now the spectra of the reference peapods with the hydrogenated peapods, (Fig. 6.5, VI) the broadening of the sharp line of the C_{60} clearly indicates that most of the originally freely rotating C_{60} molecules have been blocked by the hydrogenation. The fit of the experimental data includes contributions from the tensors corresponding to blocked hydrogenated C_{60} at defects, blocked hydrogenated C_{60}

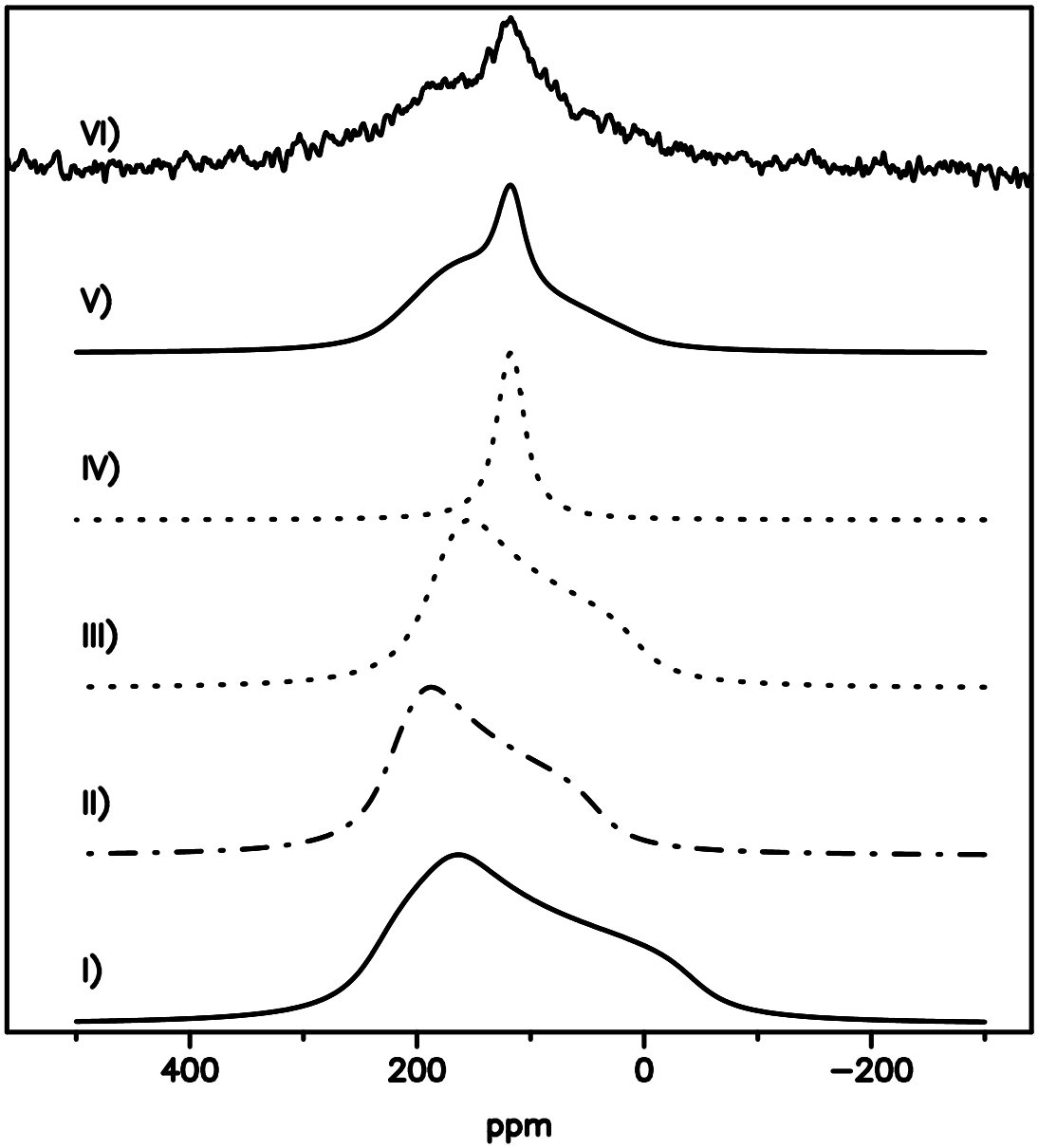

Figure 6.5: ^{13}C Static NMR spectrum of hydrogenated peapods has been fitted with the tensors1 of SWNT(I), static hydrogenated C60 (II), static hydrogenated C60 that is shifted diamagnetically (III), and freely rotating C60 that is shifted diamagnetically (IV). The total fit is shown in (V) and the experimental data in (VI).

(shifted diamagnetically): rotating C_{60} (shifted diamagnetically), in the ratio of 31.7: 45.8: 22.5. This indicates that 22.5% of the C_{60} molecules are still freely rotating after the hydrogenation treatment, probably because they are either not hydrogenated at all or hydrogenated to a lower degree. Recalculating the previous ratio 0.17 for sp^3/sp^2 carbons using the fact that the sp^3 signal only comes from 77.5% of the molecules, we obtain a hydrogenation degree of 22% which would correspond to a hydrogen content of 14 hydrogen atoms per C_{60} molecule. This refinement

of our previous estimation using all available experimental data, should be considered as a more precise determination since it takes into account the fraction of non-hydrogenated molecules present in peapods even after treatment. Another direct proof of C_{60} hydrogenation inside of peapods is found by ^{1}H NMR. (see Fig. 6.6). Consistent with the ^{13}C NMR data, the same

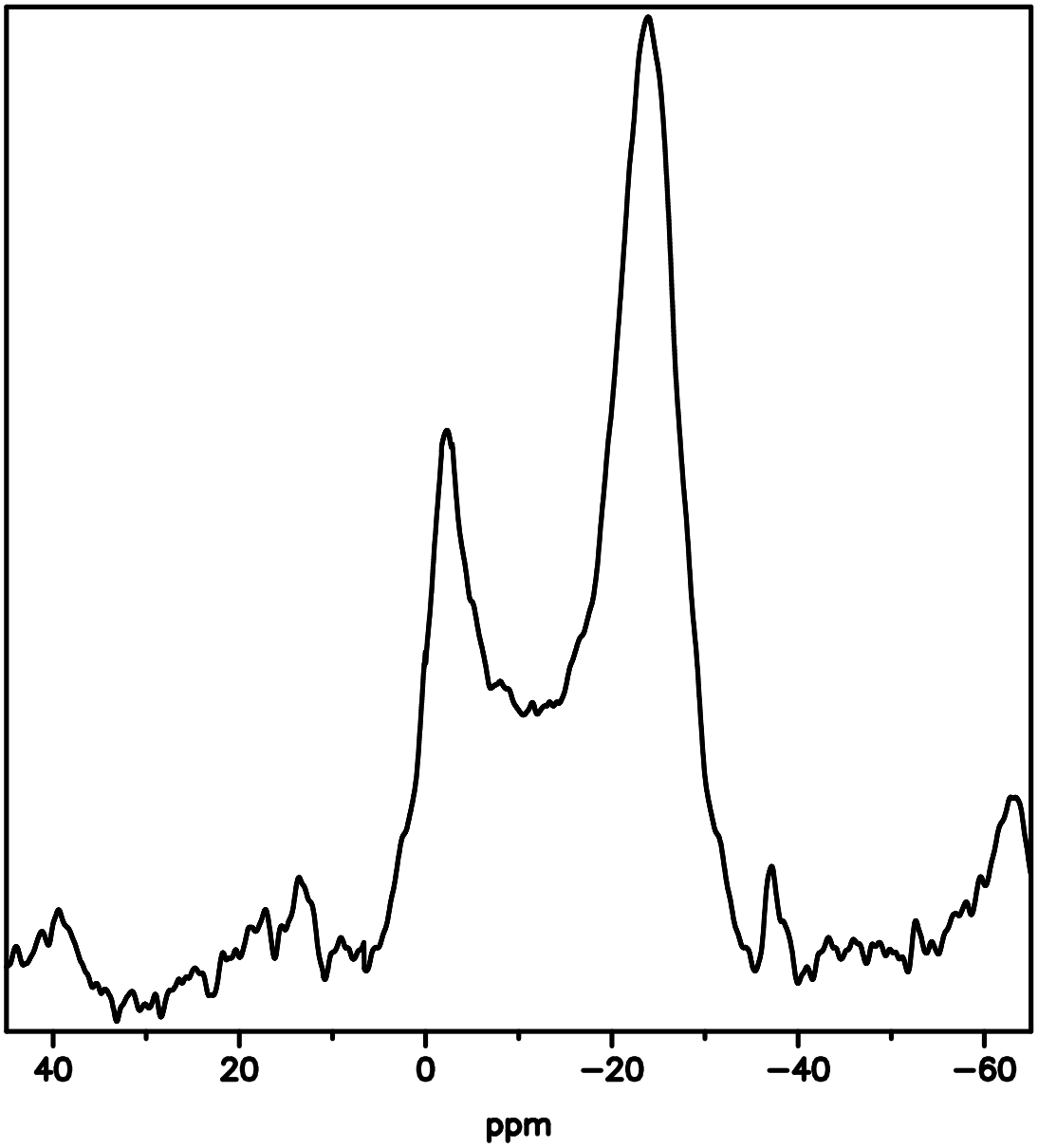

Figure 6.6: ^{1}H-MAS-NMR of hydrogen treated peapods.

general trend is observed, with one line assigned to the protons on the C_{60} molecules located at β-position inside the SWNTs (-25 ppm) and one line attributed to the protons on the C_{60} molecules located at α-position (2 ppm). The latter shift is in very good agreement with the normal ^{1}H chemical shift that usually lies between 0-10 ppm, while the first diamagnetically shifted

line clearly supports the magnetic shielding inside the nanotubes and consequently the presence of hydrogen inside the SWNTs. The average diameter of SWNT in our sample was estimated using Raman spectroscopy (by the position of the radial breathing mode[27]) to be 1.57 nm and 1.46 nm. The outer diameter of C_{60} molecules is about 1 nm while hydrogen molecule in gas phase has a kinetic diameter of $\approx$ 4 Å[28]. Taking into account a van der Waals distance from carbon walls of SWNT ($\approx$ 3.2 Åfrom each side), it seems to be difficult for molecular hydrogen to penetrate into the whole lengths of peapods. Our experiments however indicate a rather high amount of structural defects at the nanotube shell (giving rise to hindered C_{60} rotation) which could open up channels in the nanotubes where hydrogen could penetrate. Nevertheless, this still probably can not fully explain the quite high hydrogenation degree of encapsulated C_{60} that we observe in our experiments. Therefore, some mechanism which involves atomic hydrogen should be suggested. Taking into account the high reaction temperature a high mobility of hydrogen atoms on the surface of C_{60} seem to be likely. Migration of atomic hydrogen on the surface of carbon materials is currently actively discussed in connection to hydrogen storage in carbon materials doped with metal nanoparticles ("spill over" mechanism, see e.g. ref [29]). In this model molecular hydrogen split on atoms by some metallic nanoparticles and migrates in atomic form along the surface on carbon substrate. A somewhat similar mechanism could be proposed for peapods as well. Hydrogen molecules split on the C_{60} molecule closest to the nanotube entrance, migrate to the inner walls of the nanotube and diffuse along the walls to fullerene molecules situated deeper inside of nanotube. More theoretical and experimental work is required to verify the proposed mechanisms of C_{60} hydrogenation in peapods.

In conclusion, high temperature treatment of peapods with hydrogen gas results in selective hydrogenation of the C_{60} molecules inside of SWNT, but not the walls of the nanotube. ^{13}C NMR MAS/static and ^{1}H NMR provide compiling evidence that encapsulated C_{60} molecules in hydrogen treated peapods are indeed hydrogenated and consequently that the rotation of these molecules is blocked. The effect of C_{60} hydrogenation is revealed by the freezing of the C_{60} molecules, the observations of diamagnetic/paramagnetic line shifts, the appearance of sp^3 carbon lines. It is very likely that also chemical reactions with some other gases (e.g.

fluorine, chlorine and possibly even formation of fullerenols) could be possible inside SWNTs thus expanding the research into a new field of physics and chemistry in confined one dimensional nano vessels.

Bibliography

[1] Smith, B. W., Monthioux, M. and Luzzi, D. E. Encapsulated C60 in carbon nanotubes. Nature 398, 323-324 (1998).

[2] Dujardin, E., Ebbesen, T. W., Hiura, H. and Tanigaki, K. Capillarity and wetting of carbon nanotubes. Science 265, 1850-1852 (1994).

[3] Pfeiffer, R., et al. Unusual high degree of unperturbed environment in the interior of single-wall carbon nanotubes. Phys. Rev. Lett. 90, 225501 (2003).

[4] Skoulidas, A. I., Ackerman, D. M., Johnson, J. K. and Sholl, D. S. Rapid transport of gases in carbon nanotubes. Phys. Rev. Lett. 89, 185901 (2003).

[5] Takenobu, T., et al. Y. Stable and controlled amphoteric doping by encapsulation of organic molecules inside carbon nanotubes. Nature Materials 2, 683-688 (2003).

[6] Li, L. J., Khlobystov, A. N., Wiltshire, J. G., Briggs, G. A. D. and Nicholas, R. J. Diameter-selective encapsulation of metallocenes in single-walled carbon nanotube. Nature Materials 4, 481-485 (2005).

[7] Ren, Y. and Pastorin, G. Incorporation of Hexamethylmelamine inside capped carbon nanotubes. Advanced Materials 20, 2031-2036 (2008).

[8] Pichler, T., Kukovecz, A., Kuzmany, H., Kataura, H. and Achiba, Y. Quasicontinuous electron and hole doping of C60 peapods. Phys. Rev. B 67, 125416 (2003).

[9] Kawasaki, S., et al. Pressure-polymerization of C60 molecules in carbon nanotubes. Chem. Phys. Lett. 418, 260-263 (2006).

[10] Zou, Y. G., et al. Raman spectroscopy study of carbon nanotube peapods excited by near-IR laser under high pressure. Phys. Rev. B 76 195417 (2007).

[11] Shiozawa, H., et al. A catalytic reaction inside a single-walled carbon nanotube. Adv. Materials 20, 1443-1449 (2008).

[12] Talyzin, A. V., Shulga, Y. M. and Jacob, A. Comparative study of hydrofullerides C60Hx synthesized by direct and catalytic hydrogenation. Applied Physics A: Materials Science and Processing 78, 1005-1010 (2004).

[13] Talyzin, A.V., et al. Time-Resolved Reaction of Hydrogen Gas with C60 at Elevated Pressure and Temperature: Hydrogenation and Cage Fragmentation. J. Phys. Chem. A 110, 8528-8534 (2006).

[14] Wågberg, T., et al. Selective synthesis of the C-3v isomer of C60H18. Org. Lett. 7, 5557-5560 (2005).

[15] de Swiet, T. M., et al., Electron Spin Density Distribution in the Polymer phase of CsC60: Assignment of the NMR Spectrum. Phys. Rev. Lett., 84, 717-720 (2000).

[16] Persson P.-A., et al. NMR and Raman characterization of pressure polymerized C60. Chem. Phys. Lett. 258, 540-546 (1996).

[17] Tang, X. P., et al. Electronic structures of single-walled carbon nanotubes determined by NMR. Science 288, 492-494 (2000).

[18] Goze-Bac, C., et al., Magnetic interactions in carbon nanostructures. Carbon, 40, 1825-1842 (2002).

[19] Singer, P. M., Wzietek, P., Alloul, H., Simon, F. and Kuzmany, H. NMR evidence for gapped spin excitations in metallic carbon nanotubes. Phys. Rev Lett 95, 236403-07 (2005).

[20] Sternfeld, T., Saunders, M., Cross, R. J. and Rabinovitz, M. The inside story of fullerene anions: A He-3 NMR aromaticity probe. Ang. Chemie, Int. Ed., 42, 3136-3139 (2003).

[21] submitted (August 2008).

[22] Chen, J., and Dong, J. Electronic properties of peapods: effects of fullerene rotation and different type of tubes. J. Phys.: Cond. Matter. 16, 1401-1408 (2004).

[23] Matsuda, K., Maniwa, Y. and Kataura, H. Highly rotational C60 dynamics inside single-walled carbon nanotubes: NMR observations Phys. Rev. B. 77, 075421 (2008).

[24] Wågberg, T., et al.13C NMR on intercalated 2-D polymerised C60 and modified peapods. AIP Conf. Proc. 723, 238-41 (2004).

[25] Marques, M. A. L., d'Avezac, M. and Mauri, F. Magnetic response and NMR spectra of carbon nanotubes from ab initio calculations. Phys. Rev. B. 73, 125433 (2006).

[26] Latil, S., Henrard, L., Bac, C. G., Bernier, P. and Rubio, A. 13C NMR chemical shift of single-wall carbon nanotubes. Phys. Rev. Lett. 86, 3160-3163 (2001).

[27] Bachilo, S. M., et al. Structure-assigned optical spectra of single-walled carbon nanotubes. Science 298, 2361 (2002).

[28] Schlapbach, L. and Züttel, A. Hydrogen-Storage materials for mobile applications. Nature 414, 353-358 (2001).

[29] Yang, F. H., Lachawiec, Jr., A. J. and Yang, R. Y. Adsorption of Spillover Hydrogen Atoms on Single-Wall Carbon Nanotubes. J. Phys. Chem. B, 110, 6236 -6244, (2006).

[30] Kim, Y., et al. High-purity diamagnetic single-wall carbon nanotube buckypaper. Chemical Mater. 19, 2982-2986 (2007).

Chapter 7

New NMR strategies to study carbon nanotubes

The local magnetic properties of the one dimensional inner space of the nanotubes are investigated using ^{13}C nuclear magnetic resonance spectroscopy of encapsulated fullerene molecules inside single walled carbon nanotubes. Isotope engineering and magnetically purified nanotubes have been advantageously used on our study to discriminate between the different diamagnetic and paramagnetic shifts of the resonances. Ring currents originating from the π electrons circulating in the nanotube, are found to actively screen the applied magnetic field by -36.9 ppm. Defects and holes in the nanotube walls cancel this screening locally. At high magnetic fields, the modifications of the NMR resonances of the molecules from free to encapsulated can be exploited to determine some structural characteristics of the surrounding nanotubes.

Understanding, tailoring and exploiting the properties of single wall carbon nanotubes (SWNTs) have received major interests since their discovery [1, 2, 3, 4]. In addition to their one dimensional properties, SWNTs have another remarkable characteristic regarding to their inner space where unique experiments can be performed in a physically and chemically inert nanospace. Hence, SWNTs can be used as a template to study the properties of confined materials which could be drastically different from their bulk properties [5]. In addition to fundamental interest, the inner space in SWNTs can be used for various applications. Example of applica-

tions are gas storage of the next generation of synthetic fuel [6, 7]. In biology, they can be used as nano needles to deliver drug to a specific location without destroying cells [8]. A 1D wire of transition metal encapsulated in SWNTs was suggested as an advanced memory device or as a conducting wire needed for high density magnetic storage[9]. For both, the fundamental point of view and for potential applications, it is necessary to study local magnetic properties of SWNTs. Nuclear Magnetic Resonance (NMR) spectroscopy is an excellent tool for this purpose. Recently, NMR computations using ab-initio calculation and classical magnetic theory have been used to study the local magnetic properties of encapsulated species [10, 11, 12]. Chemical shifts of the nuclei encapsulated inside SWNTs were predicted to shift diamagnetically in the range from 10 to 25 ppm. Experimentally, it is a challenge to measure this effect since high resolution NMR conditions, highly purified SWNTs samples and isotope engineering are all together necessary to circumvent broadenings and overlapping of the NMR resonance lines. In the experiments discussed here, we investigated the case study of SWNTs filled with C_{60} fullerenes, a carbon allotrope well know as 'peapods' which was discovered by Luzzi and coworkers[13, 14].

Peapods samples meant for NMR measurements, were prepared from SWNTs with 1% natural abundance in ^{13}C. As received PII-SWNTs from Carbon Solution, Inc. were purified using the novel magnetic filtration method[15, 16]. Purified SWNTs materials (30 mg) and 25% ^{13}C enriched fullerenes (20 mg) were out-gassed in a dynamic vacuum of 10^{-9} Bar for one hour at 650^oC and 300^oC, respectively. The quartz tube containing the SWNTs and fullerene materials was sealed and annealed at 650^oC for 10 hours in order for the fullerenes to fill the interiors of the SWNTs. After the filling step, the resulting peapods materials were post-annealed in a dynamic vacuum at 650^oC for an hour to remove the non-encapsulated fullerenes.
X-ray diffraction (copper Kα with a wavelength of 1.54 Å) was used to assess the filling efficiency of the fullerenes into the SWNTs. The micro structures of peapods were examined using a JOEL 2010 transmission electron microscope at 80 keV to avoid electron beam damage. High resolution ^{13}C Magic Angle Spinning NMR experiments were carried out using Bruker and Tecmag spectrometers at magnetic fields of 4.7 T and 9.4 T operating at Larmor frequencies of 50.3 MHz and 100.6 MHz, respectively. Experiments were performed under qualitative and quantitative conditions with respect to the NMR relaxation times.

Figure 7.1 presents the ^{13}C MAS NMR spectra of the magnetically purified SWNTs and the peapods samples at spinning rates about 10 kHz. The spectrum presented in Figure 7.1 a) of the purified SWNTs is characterized by one sp^2 resonance at 118.8 ppm in agreement with previous reports[17]. Its line-width is interpreted in terms of a distribution of chemical shifts related to different chiralities and diameters of the SWNTs. The spectrum of the peapods sample at 4.7 T, displayed in Figure 7.1 c) shows two resonances labelled α at 148.2 ppm and β at 111.3 ppm where the latter is splitted at higher field (9.4 T) into β_1 at 113.4 ppm and β_2 at 110.6 ppm, as shown in Figure 7.1 d). Based on TEM and XRD measurements, a minimum of 70% C_{60} filling ratio was found in our samples. Hence, taking into account the ^{13}C isotope enrichment, a contribution of 16% from the nanotubes to the total NMR signal was estimated. According to the observed line-positions and line-widths, the rest of the signal was attributed to encapsulated C_{60}. No residual non-encapsulated C_{60} was detected at 143.6 ppm. To go further in the interpretation of our data, we propose a model for the fitting of the NMR line-shape, based on the diamagnetic shieldings from ring currents circulating on the SWNTs envelop which have been reported in recent theoretical works [10, 12, 11]. We suggest the following scenario : a major part of the encapsulated C_{60} molecules of β-type is experiencing a diamagnetic shielding in agreement with the literature and a minor part of α-type in the vicinity of defects or holes in the SWNTs is not magnetically screened [18]; leading to a splitting $\Delta = \delta_\alpha - \delta_\beta$. A schematic respresentation of the peapods with the C_{60} -α and -β assignments is presented in Figure 7.2. One expects also to have C_{60} molecules in intermediate situations giving contributions to the NMR signal between these two extreme line-shifts. The best fit of our experimental data, presented in Figure 7.1 b), was achieved fixing a Lorentzian line for SWNTs at 118.8 ppm and 16% of the total intensity and using a distribution of line-shifts between δ_α and δ_β according the Equations 7.1 and 7.2.

$$\Lambda(s) = \delta_\beta + \Delta\left(1 + \frac{2}{\pi}\arctan\left(\eta\left(s - s_0\right)\right)\right) \tag{7.1}$$

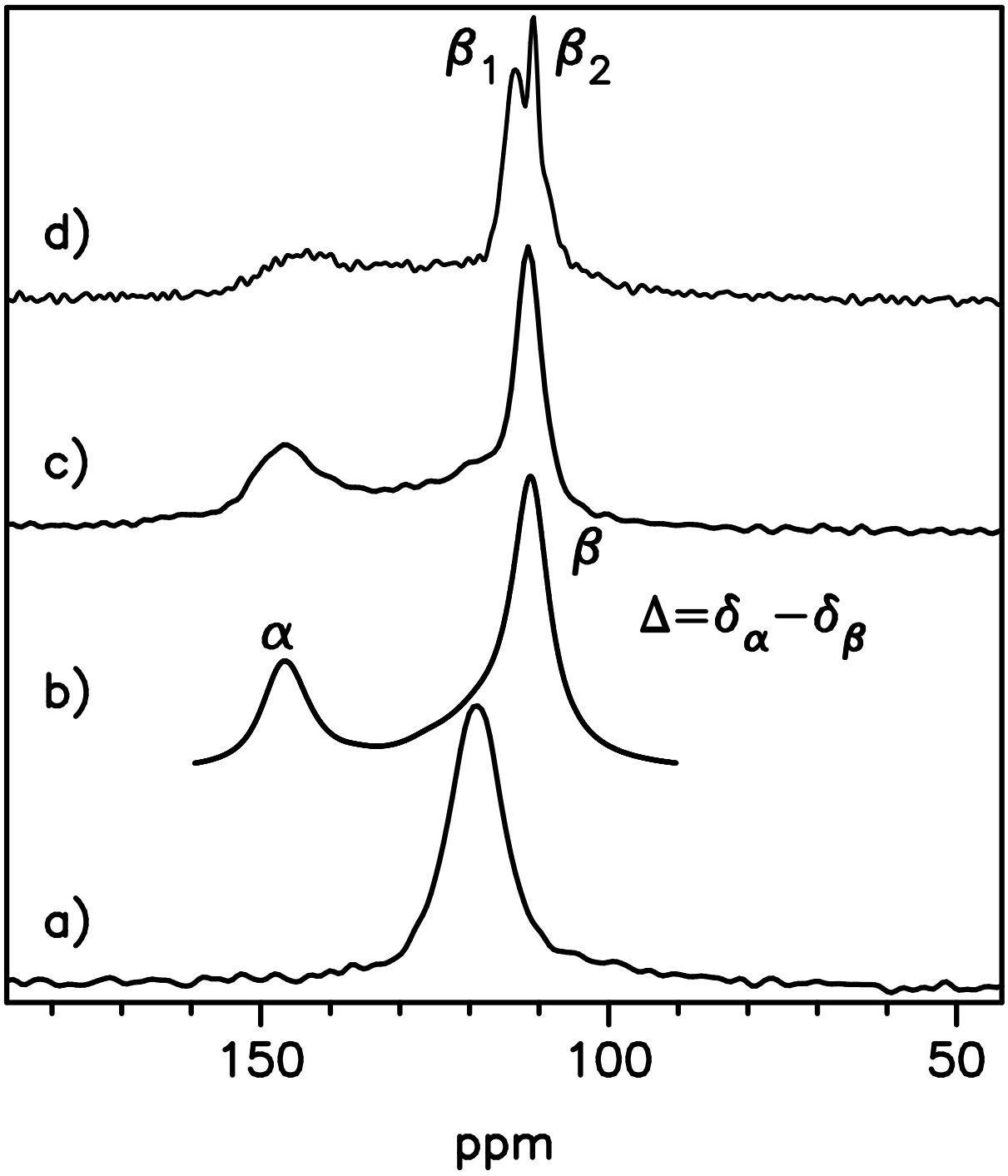

Figure 7.1: High resolution ^{13}C MAS NMR spectra at a spinning rate about 10 kHz at room temperature, a) magnetically purified SWNTs, b) fit of peapods spectrum presented in c) at 50.3 MHz and d) at 100.6 MHz. α and β corresponds to the two inequivalent C_{60} situations inside the SWNTs. The doublet β_1 and β_2 is resolved at high magnetic fields and correspond to two different diamagnetic screenings from the SWNTs.

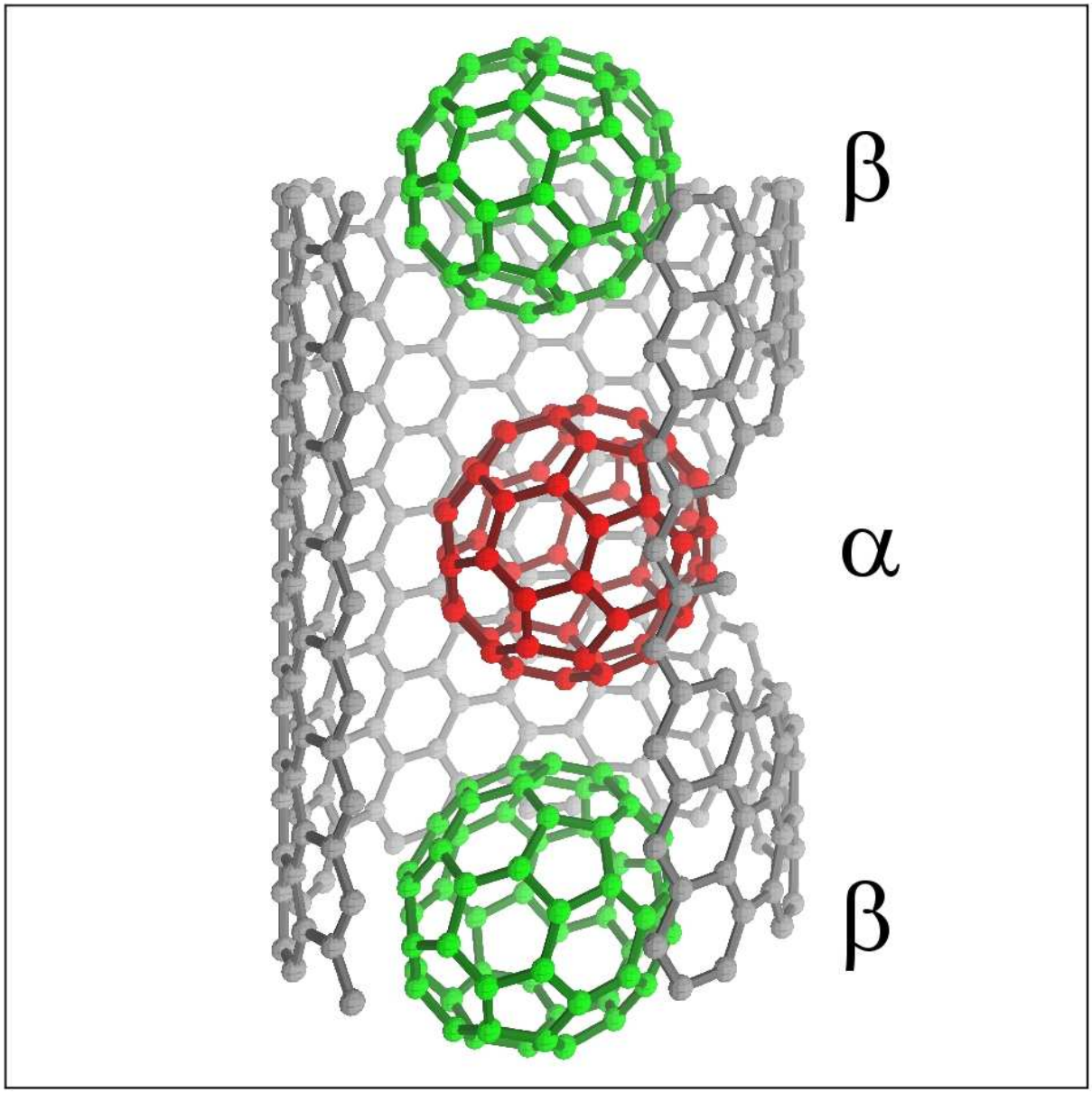

Figure 7.2: Schematic representation of a peapod made of a (10,10) nanotube with a hole on the right and three encapsulated C_{60} in the situations : α (red) next to the defect and β (green) diamagnetically screened by the π electrons circulating on the SWNTs. For clarify of the illustration, the carbons from the nanotube in the forefront are not represented.

with $s_0 \in [-L, +L]$, the NMR line-shape reads

$$I(\delta) = I_0 \int_{-L}^{+L} \frac{1}{\pi} \frac{\sigma}{(\delta - \Lambda(s))^2 + \sigma^2} ds. \tag{7.2}$$

The ratios between the quantities of α and β molecules can be obtained from $I_\alpha = (L - s_0)/2L$ and $I_\beta = (L + s_0)/2L$, respectively. η is sensitive to the transition between the situations α and β and σ is the Lorentzian half-width. The following parameters could be extracted from the fit of the data presented in Figure 7.1, $\Delta = -36.9\ ppm$, $\delta_\alpha = 148.2\ ppm$, $I_\beta = 32\%$, $\delta_\beta = 111.3\ ppm$ and $I_\beta = 68\%$. Our results fully support the recent theoretical predictions on the change in the chemical shift of encapsulated molecules arising from ring currents circulating in the nanotube [10, 12, 11].

We turn now to the interpretation of the spectrum recorded at higher magnetic field, displayed in Figure 7.1 d). The β contribution is splitted into β_1 and β_2 by 2.8 ppm. This doublet was expected at higher magnetic fields but never observed experimentally [10, 12, 11]. This feature indicates two inequivalent C_{60} molecules certainly attributed to two different magnetic behavior of the encapsulating SWNTs. In our case, two different diamagnetic screenings can be invoked to interpret the experiments, the case β_2 corresponding to the larger effect. According to recent theoretical studies, a significant difference in the behaviors of armchair and zizag nanotubes is expected [10, 12, 11]. From an experimental point of view, further NMR experiments are under progress in order to enlighten these details.

Using the novel-magnetically purified SWNTs and 25% ^{13}C enriched fullerenes, the local magnetic property of SWNTs and peapods were investigated using NMR spectroscopy. We demonstrated experimentally, that encapsulated fullerenes experience an averaged diamagnetic shielding of -36.9 ppm due to the ring currents produced by the π electrons circulating on the SWNTs. This diamagnetic shielding is canceled by paramagnetic currents at defects on the walls of SWNTs. In addition, the NMR experiments at high magnetic fields reveal a doublet in the β line, suggesting two different magnetic behaviors of the SWNTs related to their characteristics like the chirality. Our findings open a new route to develop NMR strategies to investigate the magnetic properties of nanotubes and their derivatives by using encapsulated molecules as

nano-probes. Further experiments utilizing He^3 NMR are under progress.

Bibliography

[1] S. Iijima, and T. Ichihashi, Nature 363, 603 (1993).

[2] S. J. Tans, M. H. Devoret, R. J. A. Groeneveld, and C. Dekker, Na ture 394, 761 (1998).

[3] H. Ishii, H. Kataura, H. Shiozawa, H. Yoshioka, H. Otsubo, Y. Ta kayama, T. Miyahara, S. Suzuki, Y. Achiba, M. Nakatake, T. Narimura, M. Higashiguchi, K.Shimada, H. Namatame, and M. Taniguchi, Nature 426, 540 (2003).

[4] A. Javey, J. Guo, Q. Wang, M. Lundstrom, and H. Dai, Nature 424, 654 (2003).

[5] M. M. Calbi, M. W. Cole, S. M. Gatica, M. J. Bojan, and G. Stan, Rev. Mod. Phys. 73, 857 (2001).

[6] A. C. Dillon, K. M. Jones, T. A. Bekkedahl, C. H. Kiang, D. S. Bethune, and M. J. Heben, Nature 386, 377 (1997).

[7] L. Schlapbach, and A. Z:uttel, Nature 414, 353 (2001).

[8] A. Bianco, K. Kostarelos, and M. Prato, Curr. Opin. Chem. Biol. 9, 674 (2005).

[9] Y. F. Li, R. Hatakeyama, T. Kaneko, T. Izumida, T. Okada, and T. Ka to, Appl. Phys. Lett. 89, 083117 (2006)

[10] M. A. L. Marques, M. d'Avezac, F. Mauri, Phys. Rev. B. 2006, 73, 125433.

[11] N. A. Besley and A. Noble, J. Chem. Phys. 128, 101102 (2008)

[12] E. Zurek, C. J. Pickard and J. Autschbach, J. Phys. Chem. C , 2008, 112, 9267-9271.

[13] D. J. Hornbaker, S. -J. Khang, S. Misra, B. W. Smith, A. T. Johnson, E. J. Mele, D. E. Luzzi, A. Yazdani, Science 2002, 295, 828.

[14] B. W. Smith, M. Monthioux, D. E. Luzzi, Nature 1998, 396, 323.

[15] Y. Kim, D. E. Luzzi, J. Phys. Chem. B. 2005, 109, 16636.

[16] Y. Kim, O. N. Torrens, J. M. Kikkawa, E. Abou-Hamad, C. Goze-Bac, D. E. Luzzi, Chem. Mater. 2007, 19(12), 2982.

[17] C. Goze-Bac, S. Latil, P. Lauginie, V. Jourdain, J. Conard, L. Duclaux, A. Rubio and P. Bernier, Carbon 40, 1825 (2002).

[18] F. López-Urías, J. A. Rodríguez-Manzo, E. Muñoz-Sandoval, M. Terrones, H. Terrones, Opt. Mater. 2006. 29, 110.

Conclusion and Perspectives

NMR studies of carbon nanotubes and derivatives

During the last years, important results on the electronic, dynamical and magnetic properties of carbon nanotubes and derivatives have been obtained in our group in collaboration with researchers working on the synthesis and modelization. Up to now, only few groups have been using our approach based on Nuclear Magnetic Resonance, since the experiments face two types of problems. First, the quantity and quality of the samples should fit the constrain of NMR experiments, second isotopic engineering is necessary to discriminate between the different NMR resonances. Today, the improving control of the quality of the synthesis and the possibility to produce non-magnetic samples are expected to stimulate the community to look at the potential of NMR in nanotubes and its derivatives. In the future, with the help of our collaborators, we are going to focus on the modifications of carbon nanostructures with functionalization, intercalation and encapsulation of molecules and their potential applications.

Research Project

nanoNMRI

Micro and nano probes for the near field detection of radio frequencies from nuclear spins : NMR and MRI applications to living sciences

Nuclear Magnetic Resonance (NMR) and Magnetic Resonance Imaging (MRI) are heavily used spectroscopies in biochemistry, agronomy, biology and diagnosis in medicine. They are based on the detection of radio-frequencies (RF) originating from polarized nuclear spins. This project concerns a new strategy to detect these RF in the near field of the object of interest and to evaluate this new technique to the study of living systems. In the light of these potential developments, one expect unprecedented spatial, time and spectral resolutions leading to accurate understanding of physical, chemical and biological interplays existing in an ensemble or individual living cells. Our approach is based on the scaling down of the RF antenna in a first step to micrometer with the use of micro cantilever and in a second step by taking advantage of the exceptional mechanical and electronic properties of one carbon nanotube (NT) at the end of a microcoaxial tip. Hyperlocalyzed NMR spectroscopy will be possible from nuclear spins located around the tiny antenna. With the help of an accurate control of the positioning of the RF probe, MRI will be performed to sub micronic scales by collecting spectral information like lineshifts, line intensities, relaxations... in correlation with the displacements. The detection of hyperlocalized NMR signals from living systems will be of great interest to better understand the biological, physical and chemical mechanisms opening new route for diagnosis and therapeutic treatments. In the present project, the development of a micro/nano NMR probe will improve the sensitivity and the time-space resolution of the measured parameters in order to study the

localization, the occurrence and/or disappearance of biological markers involved in physiological or pathophysiological phenomena.

Colloborators

- Pr. Michel Zanca CHU Gui de Chauliac Biophysics Department
- Eric Nativel et Pascal Falgayrettes, Nanosolo IES
- Paul Stein, University Odense, Danmark
- Nadia Bertin, INRA Avignon
- Manuel Gaviria et Monica Cappelini, Neureva Montpellier
- Angel Rubio, University San Sebastian, Spain

Selected publications